An-Najah National University

Faculty of Graduate Studies

Design Unified Power Flow Compensator to Solve Power Quality for Maithaloon - Jenin's Medium Voltage Network

By

Bara' A. H. Dweikat

Supervisor

Dr. Kamel Saleh

This Thesis Is Submitted in Partial Fulfilment of The Requirements for The Degree of Master of Electrical Power Engineering, Faculty of Graduate Studies, An-Najah National University, Nablus, Palestine

2020

Design Unified power flow compensator to solve Power Quality for Maithaloon - Jenin's Medium Voltage Network

By

Bara' Ayman Dweikat

This thesis was defended successfully on 10/12/2020and approved by:

Committee members	Signature
Dr. Kamel S. Saleh	……………………………
Dr. Maher Khammash	……………………………
Dr. Jaser A Sa'ed	……………………………

Dedication

I dedicate this work to my father and mother, who have always been the main reason for me to complete my educational career and a source of encouragement and hope. To my brothers and sisters and their children, to my friends, to dear family and relatives, to my colleagues in the Northern Electricity Distribution Company, to my distinguished teacher, Dr. Kamel Subhi, to the souls of the martyrs of our great people and our brave prisoners in the prisons of the occupation.

Acknowledgments

I would like to thank Almighty God for giving me the strength, courage and the ability to complete this research. I would also wish to appreciate my supervisor Prof. Kamel Saleh for his invaluable support, advice, help and time. I would like to thank Northern Electrical Distribution Company (Nedco) for helping me in this master's course.

I would like to thank An Najah National University School of Engineering and IT specially the Electrical Engineering Department staff and colleagues for informative discussions and input accorded to me.

Finally, I would like to extend my deepest gratitude to those closest to me; my Father Ayman Dweikat and Mum, Shadia Dweikat. Many thanks for their inestimable support.

الإقرار

أنا الموقع أدناه مقدم الرسالة التي تحمل عنوان:

Design Unified power flow compensator to solve Power Quality for Maithaloon - Jenin's Medium Voltage Network

أقر أن ما اشتملت عليه هذه الرسالة هو نتاج جهدي الخاص باستثناء ما تمت الإشارة إليه حيثما ورد، وان هذه الرسالة كاملة، أو أي جزء منها لم يقدم من قبل لنيل أي درجة أو لقب علمي أو بحثي لدى أي مؤسسة تعليمية أو بحثية أخرى.

Declaration

The work provided in this thesis unless otherwise referenced is the researcher's work, and has not been submitted elsewhere for any other degree or qualification.

Student Name:	**اسم الطالب:**
Signature:	**التوقيع:**
Date:	**التاريخ:**

Table of Contents

LIST OF FIGURES

LIST OF TABLES

LIST OF APPENDICES

LIST OF ABBREVIATIONS AND ACRONYMS

DG	Distributed Generation
UPFC	Unified Power Flow Compensator
AC	Alternating Current
IEEE	Institute of Electrical and Electronics Engineers
IEC	The International Electrotechnical Commission
OHL	Overhead transmission line

SLD	Single Line Diagram
FFT	Fast Fourier Transform
STATCOM	Static Synchronous Compensator
THD	Total harmonic distortion
SVC	Static VAR compensator
MV	Medium Voltage level
LV	Low Voltage level
KVA	Apparent power (Kilo Volt Ampere)
RMS	Root Mean Square
PF	Power Factor
PV	Photovoltaic System
PQ	Power Quality
DC	Direct Current
FACTS	Flexible Alternating Current Transmission System
ACSR	Aluminum conductor steel-reinforced cable
CU	Cupper
TR	Transformer
KV	Kilo Volt
TCSC	Thyristor controlled series capacitor
SSSC	static synchronous series compensator
TL	Transmission Line
PWM	Pulse width modulation
ABC	Aerial Bundled ABC Cable
GIS	Geographic Information System

Design Unified Power Flow Compensator to Solve Power Quality for Maithaloon - Jenin's Medium Voltage Network

By

Bara' Ayman Dweikat

Supervisor

Dr. Kamel Saleh

Abstract

The increasing of nonlinear loads leads to evaluate the harmonics generated from devices because they can harm the quality of power systems.

In the distribution system, harmonics cause many problems such as voltage distortions, increasing of line current which will cause additional losses, overloading and overheating, failure of some electrical equipment as transformers, capacitors, and motors. Moreover, harmonics may cause interfering with telecommunication lines. This research will be done on real grid feed Maithaloon area which has a lot of nonlinear loads like water pumps, stone crushers, concrete factory and many other non-liner loads, also many of distributed generators interconnected with the grid. The Maithaloon electrical grid (Jenin-Palestine) grid fed from Israeli Electrical Company at the far end of long distribution transmission line operated at 33 kV and have rated capacity of about 5 MVA, the penetration due to the DG's connected either on MV or LV side on the grid is very high (about 45-50%) compared to the standard recommendations. The field measurements of the current at medium voltage side show a high and un acceptable THD level varies between (26- 46%).

The research based on FACTS devices specially the UPFC which designed and integrated to the real model of Maithaloon electrical grid and operated as adaptive device in MATLAB simulation model to eliminate the harmonics, improve the voltage levels and reduce the electrical losses. The design of UPFC built using the multilevel inverter technique and the

controllers used the vector control theory (d-q method), and the DC source either renewable, capacitor banks or batteries.

The results after the operating the UPFC show a huge improvement on the voltage levels (from 29kV to 34.5 kV) in addition to a good improvement on THD (8-9%). Moreover, the reduction on the losses in the network was considered and calculated in details.

Chapter One

Introduction

1.1 Background :

An electrical power system is a very complicated interconnected network comprising of numerous generators, transmission lines, variety of loads and transformers. The term Flexible Alternating Current Transmission System (FACTS) devices describes a wide range of high voltage, large power electronic converters that can increase the flexibility of power systems to enhance AC system controllability, stability and increase power transfer capability and improve power quality. Demand for power and ensuing development of the modern power system has led to an increasing complexity in the study of power systems, presenting new challenges to power system stability, and in particular, to the aspects of transient stability and small-signal stability. Power quality problems specially the electrical losses and voltage variations affect the grid widely and reduce the line flow and customer complains. FACTS devices stabilize transmission systems with increased transfer capability, losses reduction, power quality improvement and reduced risk of line trips. Other benefits attributed to FACTS devices are additional energy sales due to increased transmission capability, reduce energy losses and wheeling charges due to increased transmission capability and because of the delay in investment of high voltage transmission lines or even new power generation facilities.

The major problem in power system is upholding steady acceptable system parameters like bus voltage, reactive power and active power under normal operating and anomalous conditions. Harmonics in power grid is one of the most issues affect the electrical equipment by shorten their life time. Also, the drop voltage and fast voltage variation are important point in power quality of the grid. In past, the filters and voltage regulators used widely to solve some of power quality problems, the slow behavior of these devices led to use the FACTS devices since its operated as an active compensator and operate dynamically in all conditions. UPFC for instance, is very versatile FACTS controller.

1.2 Problem Statement:

Due to the load increase, power electronics drivers and converters, also, the availability of distributed generators the power utilities are looking for ways to maximize the utilization of their existing transmission systems, reducing the losses and increasing the profit. Controlling the power flow in the transmission lines is an important issue in planning and operating of power system. The harmonics injected from load cause many problems in power system and affect all the physical parameters and phenoniums of the electrical systems like drop voltage, skin effect, corona effect, dielectric stress losses on transformers, transmission lines and protection relays.

FACTS can be applied at these instances to avert all the effects of the harmonics and improve voltage regulation, control the phase angle, the voltage magnitude at chosen buses and/or line impedances of transmission system.

1.3 Motivation:

This research is motivated by the growing use of FACTS to automate and optimize power grids enabling improve power quality, mitigate dynamic sensitivities and reduce chances of system collapse under severe disturbances. Placement of FACTS is achievable and the research in this area has been widely done. The research is also inspired by difficulties in power quality issues in Maithaloon area since the Total harmonic distortions on current varies between (26- 46) % on Medium voltage transmission lines and the voltage drop and variations are large. Because of the compensation behavior of the UPDC, it will improve the power quality increase the Utility revenue.

1.4 Objectives:

1.4.1 General Objective

The main objective of this research was to investigate impacts of incorporating FACTS devices specially the UPFC in a real power network on harmonic and voltage stability enhancement using an exact real model to the grid with and without FACTS devices.

1.4.2 Specific Objective

- To design UPFC to compensate and operate as active filter to eliminate the harmonics and improve voltage levels

- To model the real electrical grid and build the exact electrical and SLD diagrams
- To Integrate the UPFC with Grid in many operation modes and find the best location
- Improve the quality of power system and check if the power quality parameters become within standards
- The research will be based on the MATLAB/SIMULINK program.

1.5 Thesis Outline:

Chapter One: outlines brief introduction of the problem to be solved, background, proposed approach, and contributions of the research. The rest four parts are:

Chapter two: Introduction of Load flow with harmonics and DG. And UPFC

Chapter Three: Electrical Grids Modulation and analysis

Chapter Four: Unified Power Flow Compensator (UPFC)

Chapter Five: Compensation Scenarios.

Chapter Six: Results and standard verifications

Chapter Seven: Conclusion

Chapter Two

Electrical Load flow with harmonics, DG. And UPFC

2.1 Introduction:

In a power system, the electrical power flows from the generating planets toward the loads through transmission lines and other electrical equipment on the grid. The flowing of electrical power (active and reactive power) is known as load flow or power flow. The load flow analysis is very important tool based on intelligent algorithms used for planning, estimating and finding the steady-state operation of a power system. Power flow studies provide an organized mathematical approach to find out the bus voltages (kV)), phase angles, power factor (PF.), current (A), active (kW) and reactive power (kVAR) flows through different branches, generators, transformer stations, and load in steady-state conditions. The power system is modelled by an electrical circuit that consists of power sources either traditional or distributed, transmission lines, and a distribution grid. The modulation circuit is called a single line diagram [1].

The results derived from the load flow analysis comprise the voltages of loads buses in magnitudes and phase angle, the reactive powers and voltage phase angles at source buses, the real and reactive power passing the transmission lines [2]. The resulting equations in terms of power are the power flow equations they are non-linear and solved using the iterative techniques using numerical methods.

For the past times, many numerical analysis techniques have been applied for solving the load flow analysis and obtain accurate results. The most well-known iterative methods are the Gauss-Seidel, the Newton-Rapson, and Fast Decoupled method [3]. Also, with the industrial revolution and society development, the power system increase, and the dimension of the load flow equation will increase to several thousand. So, at sometimes numerical mathematical methods cannot converge to a correct solution. Thus, power system engineers have to find more reliable and accurate methods that lead to face many problems in the power industry especially determining which method is most suitable for a power system analysis. In power flow analysis, the best method to use must have a high degree accuracy and faster solution. Hand calculations are good for a finding of the operating characteristics of small electrical circuits but the need to reach accurate calculations of load flow or short circuits analyses will be impractical without using computer software. The power engineers used digital computers to calculate load flow in the mid-1950s. There have been many various methods used for load flow analysis. The development of these methods based on the basic requirement of load flow analysis such as convergence, computing efficiency, memory, convenience, and flexibility of the implementation [5-9]. Nowadays, the new modern computers are widespread, all kinds of power system studies, including load flow, can now be carried out easily [7]. The numerical method can be modelled to find the solutions using computers, so there is a need to know which of these methods is faster and more reliable in load flow analysis.

This part of the research will compare the numerical methods: Gauss-Seidel, Newton-Raphson, and Fast Decoupled methods use for load flow analysis; then will apply using one of them on research.

2.1.1 Bus Classifications

The bus is a node in which one or many types of electrical equipment (transmission lines, loads, and generators) are connected. In a power grid study, each bus has its voltage magnitude (|V|), voltage phase angle (δ), active power (P), and reactive power (Q) [4] [5]. The load flow algorithms must have two of these bus quantities and the rest found through the solution of equation [6]. So, the buses are categorized depending on the known quantities which are specified previously. Buses are divided into three categories as shown in Table 1.

2.1.2 Slack Bus

This bus is considered as the reference and first energized bus in the power system to achieve the stability condition of power in the grid since the voltage |V| and phase angle (δ) are set previously and must supply the required is P and Q. The slack is usually the largest generating station that can be regulated to meet whatever is required to ensure power balance [5].

2.1.3 Generator (PV) Bus

This is a voltage-controlled bus. The bus is connected to a generator unit in which the output power generated can be controlled by adjusting the prime mover and the voltage by adjusting the excitation of the generator. Often, limits are given to the values of the reactive power because of the characteristics of the individual machine. The known variable in this bus is P and |V| and the unknown is Q and δ [7] [5].

2.1.4 Load (PQ) Bus

This bus represents the loads and customers in the power system and it can be found from historical data, real measurements, or forecast. The known variable for this bus is P and Q and the unknown variable is |V| and δ [7] [5].

Table 2-1 Classification of Electrical Buses

Bus Type	Real Power	Reactive Power	Voltage	Phase angle
Slack Bus	Unknown	Unknown	Known	Known
Generator (PV) Bus	Known	Unknown	known	Unknown
Load Bus	Known	Known	Unknown	Unknown

2.2 Power/Load Flow Analysis:

The first step to do the load flow analysis is to calculate the Y-bus admittance matrix using the electrical parameters of the transmission lines and transformer input data. The nodal equation for a power system network using Y bus written as follows:

$$I = YBus*V \tag{1}$$

The nodal equation can be written in a generalized form for an n bus system.

$$I_i = \sum_{j=1}^{n} Y_{ij} V_j \text{ for } n = 1,2,3, n \tag{2}$$

The complex power delivered to bus$i$ is:

$$P_i + jQ_i = V_i I_i^* \tag{3}$$

$$I_i = \frac{P_i - jQ_i}{V^*} \tag{4}$$

Substituting for Ii in terms of Pi& Qi, the equation gives:

$$\frac{P_i - jQ_i}{V^*} = V \sum_{j=1}^{n} Y_{ij} - \sum_{j=1}^{n} Y_{ij} V_{ij} \quad , J \neq i \tag{5}$$

The power flow equation uses the iterative methods to find load flow results and estimates the problems. So, in this research a short review for the general form of Newton Raphson load flow, have to be done since, the research will be based on it for the load flow study.

2.2.1 Newton-Raphson Method

The technique named referring to Isaac Newton and Joseph Raphson. The method was created in the late 1960s [3]. It is considered an iterative method that estimate a group of non-linear simultaneous equations to a set of linear simultaneous equations using Taylor's series expansion and the terms are limited to the first approximation. It is the most iterative method used for the power system load flow since its convergence characteristics are relatively more powerful compared to other processes and the reliability of this approach is comparatively good since it can solve cases that lead to divergence with other popular processes [9]. If the assumed value is near the solution, then the result is obtained very quickly, but if the assumed value is farther away from the solution then the method may take longer to converge [5]. The admittance matrix is used to write equations for currents entering a power system. Equation (2) is expressed in a polar form, in which J includes bus $\imath$

$$I\imath = \sum_{J=1}^{n} |Y\imath J||V\imath| < \theta\imath J + \delta J \tag{12}$$

The real and reactive power at bus $\imath$ is

$$P\imath - JQ\imath = V\imath^{*}\, I\imath \tag{13}$$

Substituting for Ii in Equation (12) from Equation (13)

$$P\imath - JQ\imath = |V\imath| < -\delta\imath \sum_{J=1}^{n} |Y\imath J||VJ| < \delta\imath J + \delta\imath \tag{14}$$

The real and imaginary parts are separated:

$$P\imath = \sum_{J=1}^{n} |V\imath||VJ||Y\imath J|\cos(\theta\imath J - \delta\imath + \delta J) \tag{15}$$

$$Q_I = \sum_{J=1}^{n} |V_I||V_J||Y_{IJ}|\sin(\theta_{IJ} - \delta_I + \delta_J) \tag{16}$$

The above Equation (15) and (16) constitute a set of non-linear algebraic equations in terms of |V| in per unit and δ in radians. Equation (15) and (16) are expanded in Taylor's series about the initial estimate and neglecting all higher-order terms, the following set of linear equations are obtained.

$$\begin{bmatrix} \Delta P_2^{(k)} \\ \vdots \\ \Delta P_n^{(k)} \\ \hline \Delta Q_2^{(K)} \\ \vdots \\ \Delta Q_n^{(k)} \end{bmatrix} = \left[\begin{array}{ccc|ccc} \frac{\partial P_2^{(k)}}{\partial \delta_2} & \cdots & \frac{\partial P_2^{(k)}}{\partial \delta_n} & \frac{\partial P_2^{(k)}}{\partial |V_2|} & \cdots & \frac{\partial P_2^{(k)}}{\partial |V_n|} \\ \vdots & \ddots & \vdots & \vdots & \ddots & \vdots \\ \frac{\partial P_n^{(k)}}{\partial \delta_2} & \cdots & \frac{\partial P_n^{(k)}}{\partial \delta_n} & \frac{\partial P_n^{(k)}}{\partial |V_2|} & \cdots & \frac{\partial P_n^{(k)}}{\partial |V_n|} \\ \hline \frac{\partial Q_2^{(K)}}{\partial \delta_2} & \cdots & \frac{\partial Q_2^{(K)}}{\partial \delta_n} & \frac{\partial Q_2^{(K)}}{\partial |V_2|} & \cdots & \frac{\partial Q_2^{(K)}}{\partial |V_n|} \\ \vdots & \ddots & \vdots & \vdots & \ddots & \vdots \\ \frac{\partial Q_n^{(K)}}{\partial \delta_2} & \cdots & \frac{\partial Q_n^{(K)}}{\partial \delta_n} & \frac{\partial Q_n^{(K)}}{\partial |V_2|} & \cdots & \frac{\partial Q_n^{(K)}}{\partial |V_n|} \end{array}\right] \begin{bmatrix} \Delta P_2^{(k)} \\ \vdots \\ \Delta P_n^{(k)} \\ \hline \Delta Q_2^{(K)} \\ \vdots \\ \Delta Q_n^{(k)} \end{bmatrix}$$

In the above equation, the element of the slack bus variable voltage magnitude and angle are omitted because they are already known. The element of the Jacobian matrix is obtained after partial derivatives of Equations (15) and (16) are expressed which gives a linearized relationship between small changes in voltage magnitude and voltage angle. The equation can be written in matrix form as

$$\begin{bmatrix} \Delta P \\ \Delta Q \end{bmatrix} = \begin{bmatrix} J_1 & J_3 \\ J_2 & J_4 \end{bmatrix} \begin{bmatrix} \Delta \delta \\ \Delta |V| \end{bmatrix}$$

J1, J2, J3, J4 are the elements of the Jacobian matrix.

The difference between the schedule and calculated values known as power residuals for the terms $\Delta P_i^k$and $\Delta Q_i^k$is represented as:

$$\Delta P_i^K = P_i^{ref.} - P_i^k \quad (17)$$

$$\Delta Q_i^K = Q_i^{ref.} - Q_i^k$$

The new estimates for bus voltage are:

$$\delta^{k+1} = \delta_i^k + \Delta\delta_i^k \quad (18)$$

$$|V^{k+1}| = |V_i^k| + \Delta|V_i^k|$$

2.2.2 Power Flow Model for the UPFC

2.2.2.1 Basic Operation of UPFC

The basic operation of the UPDC will discuss deeply in CHAPTER 4, but in short, the equivalent circuit consisting of two coordinated synchronous voltage sources should represent the UPFC adequately for the purpose of fundamental frequency steady-state analysis. The figure 2-1, shows the equivalent circuit of the UPFC.

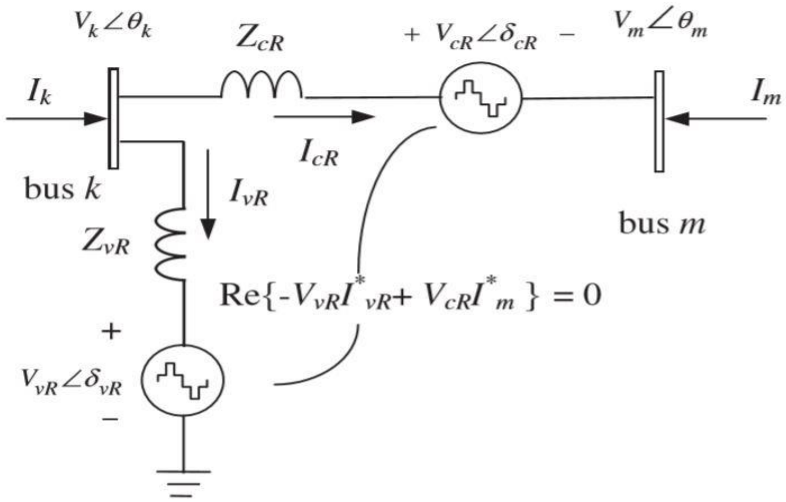

Figure 2-1:Unified power flow controller equivalent circuit

The UPFC voltage sources are:

$$E_{\nu R} = V_{\nu R}(\cos\delta_{\nu R} + j\sin\delta_{\nu R}) \tag{19}$$

$$E_{cR} = V_{cR}(\cos\delta_{cR} + j\sin\delta_{cR}) \tag{20}$$

Where,

$V_{\nu R}$ and $\delta_{\nu R}$ are the controllable magnitude ($V_{\nu Rmin}<V_{\nu R}<V_{\nu Rmax}$) and the phase angle

(0 < $\delta_{\nu R}$< 2π) of the voltage source representing the shunt converter.

The magnitude V_{cR} and phase angle δ_{cR} of the voltage source representing the series converter are controlled between limits ($V_{cRmin}<V_{cR}<V_{cRmax}$) and (0 < δ_{cR}< 2π) , respectively.

The phase angle of the series-injected voltage determines the mode of power flow control. If δ_{cR} is in phase with the nodal voltage angle θ_k , the UPFC regulates the terminal voltage. If δ_{cR} is in quadrature with respect to

θ_k ,it controls active power flow, acting as a phase shifter. If δ_{cR} is in quadrature with the line current angle then it controls active power flow, acting as a variable series compensator. At any other value of δ_{cR} the UPFC operates as a combination of voltage regulator, variable series compensator, and phase shifter. The magnitude of the series-injected voltage determines the amount of power flow to be controlled.

2.2.2.2 UPFC model for power flow

Based on the equivalent circuit shown in Figure 2-1, and Equations (19) and (20), the active and reactive power equations are [8] at Bus k,

$$\begin{aligned} P_k = {} & V_k^2 G_{kk} + V_k V_m[G_{km}\cos(\theta_k - \theta_m) + B_{km}\sin(\theta_k - \theta_m)] \\ & + V_k V_{cR}[G_{km}\cos(\theta_k - \delta_{cR}) + B_{km}\sin(\theta_k - \delta_{cR})] \\ & + V_k V_{vR}[G_{vR}\cos(\theta_k - \delta_{vR}) + B_{vR}\sin(\theta_k - \delta_{vR})], \end{aligned} \tag{21}$$

$$\begin{aligned} Q_k = {} & -V_k^2 B_{kk} + V_k V_m[G_{km}\sin(\theta_k - \theta_m) - B_{km}\cos(\theta_k - \theta_m)] \\ & + V_k V_{cR}[G_{km}\sin(\theta_k - \delta_{cR}) - B_{km}\cos(\theta_k - \delta_{cR})] \\ & + V_k V_{vR}[G_{vR}\sin(\theta_k - \delta_{vR}) - B_{vR}\cos(\theta_k - \delta_{vR})]; \end{aligned} \tag{22}$$

At bus m:

$$\begin{aligned} P_m = {} & V_m^2 G_{mm} + V_m V_k[G_{mk}\cos(\theta_m - \theta_k) + B_{mk}\sin(\theta_m - \theta_k)] \\ & + V_m V_{cR}[G_{mm}\cos(\theta_m - \delta_{cR}) + B_{mm}\sin(\theta_m - \delta_{cR})], \end{aligned} \tag{23}$$

$$\begin{aligned} Q_m = {} & -V_m^2 B_{mm} + V_m V_k[G_{mk}\sin(\theta_m - \theta_k) - B_{mk}\cos(\theta_m - \theta_k)] \\ & + V_m V_{cR}[G_{mm}\sin(\theta_m - \delta_{cR}) - B_{mm}\cos(\theta_m - \delta_{cR})]; \end{aligned} \tag{24}$$

series converter:

$$P_{cR} = V_{cR}^2 G_{mm} + V_{cR} V_k \left[G_{km} \cos(\delta_{cR} - \theta_k) + B_{km} \sin(\delta_{cR} - \theta_k)\right] \\ + V_{cR} V_m [G_{mm} \cos(\delta_{cR} - \theta_m) + B_{mm} \sin(\delta_{cR} - \theta_m)], \quad (25)$$

$$Q_{cR} = -V_{cR}^2 B_{mm} + V_{cR} V_k [G_{km} \sin(\delta_{cR} - \theta_k) - B_{km} \cos(\delta_{cR} - \theta_k)] \\ + V_{cR} V_m [G_{mm} \sin(\delta_{cR} - \theta_m) - B_{mm} \cos(\delta_{cR} - \theta_m)]; \quad (26)$$

shunt converter:

$$P_{vR} = -V_{vR}^2 G_{vR} + V_{vR} V_k [G_{vR} \cos(\delta_{vR} - \theta_k) + B_{vR} \sin(\delta_{vR} - \theta_k)] \quad (27)$$

$$Q_{vR} = V_{vR}^2 B_{vR} + V_{vR} V_k [G_{vR} \sin(\delta_{vR} - \theta_k) - B_{vR} \cos(\delta_{vR} - \theta_k)] \quad (28)$$

Assuming loss-less converter valves, the active power supplied to the shunt converter, $P_{\nu R}$, equals the active power demanded by the series converter, P_{cR} ; that is,

$$P_{\nu R} + P_{cR} = 0 \quad (29)$$

Furthermore, if the coupling transformers are assumed to contain no resistance then the active power at bus k matches the active power at bus m. Accordingly,

$$P_{\nu R} + P_{cR} = P_m + P_k = 0 \quad (30)$$

The UPFC power equations, in linearised form, are combined with those of the AC network. For the case when the UPFC controls the following parameters:

(1) voltage magnitude at the shunt converter terminal (bus k)

(2) active power flow from bus m to bus k

(3) reactive power injected at bus m, and taking bus m to be a PQ bus, the linearised system of equations is as follows:

$$\begin{bmatrix} \Delta P_k \\ \Delta P_m \\ \Delta Q_k \\ \Delta Q_m \\ \Delta P_{mk} \\ \Delta Q_{mk} \\ \Delta P_{bb} \end{bmatrix} = \begin{bmatrix} \frac{\partial P_k}{\partial \theta_k} & \frac{\partial P_k}{\partial \theta_m} & \frac{\partial P_k}{\partial V_{vR}} V_{vR} & \frac{\partial P_k}{\partial V_m} V_m & \frac{\partial P_k}{\partial \delta_{cR}} & \frac{\partial P_k}{\partial V_{cR}} V_{cR} & \frac{\partial P_k}{\partial \delta_{vR}} \\ \frac{\partial P_m}{\partial \theta_k} & \frac{\partial P_m}{\partial \theta_m} & 0 & \frac{\partial P_m}{\partial V_m} V_m & \frac{\partial P_m}{\partial \delta_{cR}} & \frac{\partial P_m}{\partial V_{cR}} V_{cR} & 0 \\ \frac{\partial Q_k}{\partial \theta_k} & \frac{\partial Q_k}{\partial \theta_m} & \frac{\partial Q_k}{\partial V_{vR}} V_{vR} & \frac{\partial Q_k}{\partial V_m} V_m & \frac{\partial Q_k}{\partial \delta_{cR}} & \frac{\partial Q_k}{\partial V_{cR}} V_{cR} & \frac{\partial Q_k}{\partial \delta_{vR}} \\ \frac{\partial Q_m}{\partial \theta_k} & \frac{\partial Q_m}{\partial \theta_m} & 0 & \frac{\partial Q_m}{\partial V_m} V_m & \frac{\partial Q_m}{\partial \delta_{cR}} & \frac{\partial Q_m}{\partial V_{cR}} V_{cR} & 0 \\ \frac{\partial P_{mk}}{\partial \theta_k} & \frac{\partial P_{mk}}{\partial \theta_m} & 0 & \frac{\partial P_{mk}}{\partial V_m} V_m & \frac{\partial P_{mk}}{\partial \delta_{cR}} & \frac{\partial P_{mk}}{\partial V_{cR}} V_{cR} & 0 \\ \frac{\partial Q_{mk}}{\partial \theta_k} & \frac{\partial Q_{mk}}{\partial \theta_m} & 0 & \frac{\partial Q_{mk}}{\partial V_m} V_m & \frac{\partial Q_{mk}}{\partial \delta_{cR}} & \frac{\partial Q_{mk}}{\partial V_{cR}} V_{cR} & 0 \\ \frac{\partial P_{bb}}{\partial \theta_k} & \frac{\partial P_{bb}}{\partial \theta_m} & \frac{\partial P_{bb}}{\partial V_{vR}} V_{vR} & \frac{\partial P_{bb}}{\partial V_m} V_m & \frac{\partial P_{bb}}{\partial \delta_{cR}} & \frac{\partial P_{bb}}{\partial V_{cR}} V_{cR} & \frac{\partial P_{bb}}{\partial \delta_{vR}} \end{bmatrix} \begin{bmatrix} \Delta \theta_k \\ \Delta \theta_m \\ \frac{\Delta V_{vR}}{V_{vR}} \\ \frac{\Delta V_m}{V_m} \\ \Delta \delta_{cR} \\ \frac{\Delta V_{cR}}{V_{cR}} \\ \Delta \delta_{vR} \end{bmatrix} \quad (31)$$

Where ΔP_{bb} is the power mismatch given by Equation (29), If voltage control at bus k is deactivated, the third column of Equation (31) is replaced by partial derivatives of the bus and UPFC mismatch powers with respect to the bus voltage magnitude V_k . Moreover, the voltage magnitude increment of the shunt source, $\Delta V_{\nu R}/V_{\nu R}$ is replaced by the voltage magnitude increment at bus k, $\Delta V_k/V_k$.

If both buses, k and m, are PQ the linearised system of equations is as follows:

$$\begin{bmatrix} \Delta P_k \\ \Delta P_m \\ \Delta Q_k \\ \Delta Q_m \\ \Delta P_{mk} \\ \Delta Q_{mk} \\ \Delta P_{bb} \end{bmatrix} = \begin{bmatrix} \frac{\partial P_k}{\partial \theta_k} & \frac{\partial P_k}{\partial \theta_m} & \frac{\partial P_k}{\partial V_k} V_k & \frac{\partial P_k}{\partial V_m} V_m & \frac{\partial P_k}{\partial \delta_{cR}} & \frac{\partial P_k}{\partial V_{cR}} V_{cR} & \frac{\partial P_k}{\partial \delta_{vR}} \\ \frac{\partial P_m}{\partial \theta_k} & \frac{\partial P_m}{\partial \theta_m} & \frac{\partial P_m}{\partial V_k} V_k & \frac{\partial P_m}{\partial V_m} V_m & \frac{\partial P_m}{\partial \delta_{cR}} & \frac{\partial P_m}{\partial V_{cR}} V_{cR} & 0 \\ \frac{\partial Q_k}{\partial \theta_k} & \frac{\partial Q_k}{\partial \theta_m} & \frac{\partial Q_k}{\partial V_k} V_k & \frac{\partial Q_k}{\partial V_m} V_m & \frac{\partial Q_k}{\partial \delta_{cR}} & \frac{\partial Q_k}{\partial V_{cR}} V_{cR} & \frac{\partial Q_k}{\partial \delta_{vR}} \\ \frac{\partial Q_m}{\partial \theta_k} & \frac{\partial Q_m}{\partial \theta_m} & \frac{\partial Q_m}{\partial V_k} V_k & \frac{\partial Q_m}{\partial V_m} V_m & \frac{\partial Q_m}{\partial \delta_{cR}} & \frac{\partial Q_m}{\partial V_{cR}} V_{cR} & 0 \\ \frac{\partial P_{mk}}{\partial \theta_k} & \frac{\partial P_{mk}}{\partial \theta_m} & \frac{\partial P_{mk}}{\partial V_k} V_k & \frac{\partial P_{mk}}{\partial V_m} V_m & \frac{\partial P_{mk}}{\partial \delta_{cR}} & \frac{\partial P_{mk}}{\partial V_{cR}} V_{cR} & 0 \\ \frac{\partial Q_{mk}}{\partial \theta_k} & \frac{\partial Q_{mk}}{\partial \theta_m} & \frac{\partial Q_{mk}}{\partial V_k} V_k & \frac{\partial Q_{mk}}{\partial V_m} V_m & \frac{\partial Q_{mk}}{\partial \delta_{cR}} & \frac{\partial Q_{mk}}{\partial V_{cR}} V_{cR} & 0 \\ \frac{\partial P_{bb}}{\partial \theta_k} & \frac{\partial P_{bb}}{\partial \theta_m} & \frac{\partial P_{bb}}{\partial V_k} V_k & \frac{\partial P_{bb}}{\partial V_m} V_m & \frac{\partial P_{bb}}{\partial \delta_{cR}} & \frac{\partial P_{bb}}{\partial V_{cR}} V_{cR} & \frac{\partial P_{bb}}{\partial \delta_{vR}} \end{bmatrix} \begin{bmatrix} \Delta \theta_k \\ \Delta \theta_m \\ \frac{\Delta V_k}{V_k} \\ \frac{\Delta V_m}{V_m} \\ \Delta \delta_{cR} \\ \frac{\Delta V_{cR}}{V_{cR}} \\ \Delta \delta_{vR} \end{bmatrix} \quad (32)$$

In this case, $V_{\nu R}$ is maintained at a fixed value within prescribed limits, ($V_{\nu Rmin}<V_{\nu R}<V_{\nu Rmax}$).

2.3 The Behaviour of Harmonics and Their Effect on Power System Equipment:

The Harmonics have a major effect on the most effective equipment in the electrical grid especially the transmission lines, transformers, and protective relays. The harmonics generated due to the non-linear loads fed from the electrical network and some distributed generators make a disturbance and create harmonics on the current waveform.

2.3.1 Harmonics Effect on Transmission Lines

The Harmonics affect the transmission systems in various ways, it increases the skin effect since this electrical effect depends on the frequency and AC resistance increases. Also, the power losses, voltage drop will increase and the power transmission capacity will decrease because the harmonics will generate current component other than the fundamental to follow through.

The harmonics in transmission lines will increase the dielectric stress on the cables and, it will increase the Corona effect since the harmonics increase the peak-peak voltage.

2.3.2 Harmonics Effect on Transformers

The Losses of the transformers are generally the excitation (no load) losses, impedance losses, and stray losses. The stray losses are part of the load losses, and it is appeared due to the effect of the magnetic flux on the clamps, tank, and other components of the transformer [13]. So, the stray losses are categorized according to its source to winding stray loss or loss and losses from the other components of the transformer (P_{OSL}). The winding stray losses include the winding conductor strand eddy current loss and the losses due to circulating current appears in the transformer in many conditions all these losses are considered to constitute winding eddy-current loss (P_{EC}). The equation 25 summarize the total losses of the transformer.

$$P_{LL} = P + P_{EC} + P_{OSL} \tag{33}$$

Where,

P_{LL}: is the Load loss (Watt).

P: is the I^2R losses.

P_{EC}: Eddy current losses in the winding.

P_{OSL}: The other stray losses.

2.3.2.1 Harmonic Current effect on I^2R losses.

When the load current increased because of the harmonic component, the winding losses (I^2R) will increase.

2.3.2.2 Harmonic Current Effect on Winding eddy-Current loss

The eddy-current losses (P_{EC}) appear in Winding due to the magnetic flux which is proportional to the square of the load current and approximately proportional to the square of frequency [13]. So, this characteristic of supplying non-linear load will cause more winding loss and abnormal winding temperature rise and hottest spot temperatures.

2.3.2.3 Harmonic Current Effect on Other Stray Losses

The other stray losses (P_{OSL}) in the clamps, tank, and other transformer accessories will increase proportionally to the square of load current because of the magnetic flux and not as the rate of the winding eddy-losses. Studies and researches shown that the eddy-current losses in bus bars, connections, and structural parts increase by a harmonic exponent factor of 0.8 or less [13].

2.3.2.4 Harmonic _ DC Component of load Current

The harmonic load current usually has a small DC component which will increase the transformer loss, magnetizing current, and increase the sound level of the transformer [13].

2.3.2.5 Harmonic Effect on top-Liquid gas

The liquid immersed transformers, the top-liquid rise (θ_{TO}) will increase as the total load losses increase due to harmonic loading. Unlike dry-type transformers, the other stray loss (P_{OSL}) must be considered, since these losses also affect the top-liquid rise [13].

2.3.3 Harmonics Effect on Protection Relays

There are many types of protection relays used to protect the power system equipment. The distance relay usually used to protect the transmission lines and, it operates by measure the line voltage and current to find the impedance and compare it with previously stored value [14].

Much researches are done to check the effect of harmonics on the distance relay, and they found that the distance relay will react improperly and sense faults at zones other than the desired ones. Which will distribute the distance protection selectivity also, showing that the fault location and the fault resistance were affecting the impedance seen by the distance relay [15].In General, the effect of harmonics on distance is directly proportional to the harmonic's current intensity and inversely proportional to line length [14].

2.3.4 Summary of Electrical Losses Calculation Due to Harmonics.

2.3.4.1 Transformer Losses Due to Harmonic (Calculation Method) [13]

Because the transformers are operating under harmonic load conditions the overheating of the windings will accrue frequently, so it is important to consider total losses of the transformers sine the loss density in the windings on a per-unit basis (base current is rated current and base loss density is the I^2R loss density at rated current). The equation 25 is applied for the rated conditions and can be rewritten to be as in equation 26:

$$P_{LL_R}(pu) = 1 + P_{EC_R}(pu) + P_{OSL_R} \tag{34}$$

Where,

$P_{LL\_R}\ (PU)$: is the per-unit load loss under rated conditions

$P_{EC_R}(pu)$: is the per-unit winding eddy-current loss under rated conditions

$P_{OSL_R}(PU)$: is the per-unit other stray loss under rated conditions

The eddy-current losses due to the non-sinusoidal load currents expressed as in the following equation 27.

$$P_{EC} = P_{EC_R} \sum_{h=1}^{h=h_{max.}} (\frac{I_h}{I_R})^2 h^2 \tag{35}$$

Where,

P_{EC}: is the winding eddy-current loss (watts)

P_{EC_R}: is the winding eddy-current loss under rated conditions (watts)

h: is the harmonic order

$h_{max.}$: is the highest significant harmonic number

I_h: is the RMS current at harmonic h (amperes)

I_R: is the RMS fundamental current underrated frequency and rated load conditions (amperes)

The I^2R at rated conditions is one per-unit, but for the no sinusoidal load current the RMS current found using the following equation 2-28.

$$I(pu) = \sqrt{\sum_{h=1}^{h=h_{max}} I_h^2(pu)} \tag{36}$$

2.3.4.2 Transformer Harmonic Loss Factor (K_ factor)

The Loss (K) factor is a number that used to determine the capabilities of a transformer in supplying power to a load. F_{HL} is a proportionality factor applied to the winding eddy losses, which represents the effective RMS heating as a result of the harmonic load current. F_{HL} is the ratio of the total winding eddy-current losses due to the harmonics, P_{EC}, to the winding eddy current losses at the power frequency, when no harmonic currents exist (P_{EC_O}). This definition in equation form is as follows in equation 29.

$$F_{HL} = \frac{P_{EC}}{P_{EC_O}} = \frac{\sum_{h=1}^{h=h_{max}} I_h^2\, h^2}{\sum_{j=1}^{h=h_{max}} I_h^2} \tag{37}$$

2.3.4.3 Transmission Line Loses Due to Harmonics (Calculation Method)

The harmonic affects the transmission lines and influences the physical behavior of them. Since the harmonics accrue on several frequencies this will influence the skin effect nature of the transmission line because it depends on the frequencies which will lead to an increase in the AC resistance.

The harmonics mean following current on frequency multiple of the fundamental which means the losses of the conductors increase and can be found using equation 30.

$$P_{Loss_{TL}} = \sum_{h=1}^{h=n} I_n^2 R_n \tag{38}$$

The dielectric stress and corona effect of the transmission lines will increase due to the harmonic since it increases the peak-to-peak voltage.

2.4 UPFC and Harmonics Mitigation :

Referring to the ordinary equations for calculating the power and based on Fourier series, a non-sinusoidal voltage or current can be presented as the sum of sinusoidal components at different frequencies. The product of voltage and current components provides the active power. Since the integral of some terms with different frequencies are zero, so the active power equation is as follow:

$$P_\iota = \sum_{\iota}^{\infty} V_\iota I_\iota \cos\theta_\iota \tag{39}$$

Where V_ι and I_ι are the voltage and current at the ι^{th} harmonic, respectively, and θ_ι is the angle between the voltage and current at the same frequency. Equation (39) expresses the active power at different frequency components are independent. Based on this fact, a shunt converter in UPFC can absorb the active power in one frequency and generates output power in another frequency. [12]So, when the harmonic current follow through the transmission line the UPFC can absorb it easily and operate to mitigate it. CHAPTER 4 will illustrate deeply the elimination of harmonics using the UPFC.

Chapter Three

Electrical Grids Modulation and analysis

3.1 Electrical Grids Modulation and Analysis:

Modern-day in Palestine power systems are heavily stressed because of the growing demand for electricity and the lack of energy resources since all electrical grids feed from Israeli electrical company (IEC) and there are no generation stations to feed the loads. So, there is a huge difference between the supply and demand for electricity. Power shortages occur due to the increasing population, improved living standards, and huge commercial projects such as factories, water pumps, and stone crushers. A solution for these problems is to increase the power delivered from the IEC or establish new distributed generation units and decrease power losses. Any increase in power generation demands new transmission lines, substations and environmental effects have to be created which require high capital investments and natural pollution, as the result, many investors take the responsibility to build Photovoltaic solar farms to support the electrical grid. Although the existing transmission networks operate near their rated capacity, yet there is some flexibility in increasing the power handling capacity of the existing transmissions lines. May the use of Flexible AC transmission systems (FACTS) are power electronic-based semiconductor devices that will enhance the power handling capability of the transmission lines. This research will be based on the Unified Power flow compensator (UPFC) to improve the power quality, decrease the electrical losses, enhance the voltage profile, and eliminate the harmonics of the grid. Also, the research will have done using the real electrical network of Maithaloon.

3.1.1 Maithaloon Electrical Grid

This real grid is one of the networks operated by Nedco and covers many villages (Maithaloon, Siris, Al Juideda, Ser). The Grid has 38 distribution transformers,21,5 Km OHL ACSR with cross-section varies between (70-95mm), and cupper underground cables of about 3.6Km with a cross-section area of 50 mm, also the grid connection point has rated capacity of 5 MVA, and 1.4MWp PV farm.

To Model, this grid the real data of all equipment Transformers, OHL, Cables, Loads, and PV systems shall be exact as in reality. So, the modeling of the grid-based in the following steps:

3.1.2 Find the Exact Location for all the Electrical Components.

All electrical components were set on the exact coordinates with unique code for each element and set on maps, Figure 2-1, Show the locations. Appendix (1).

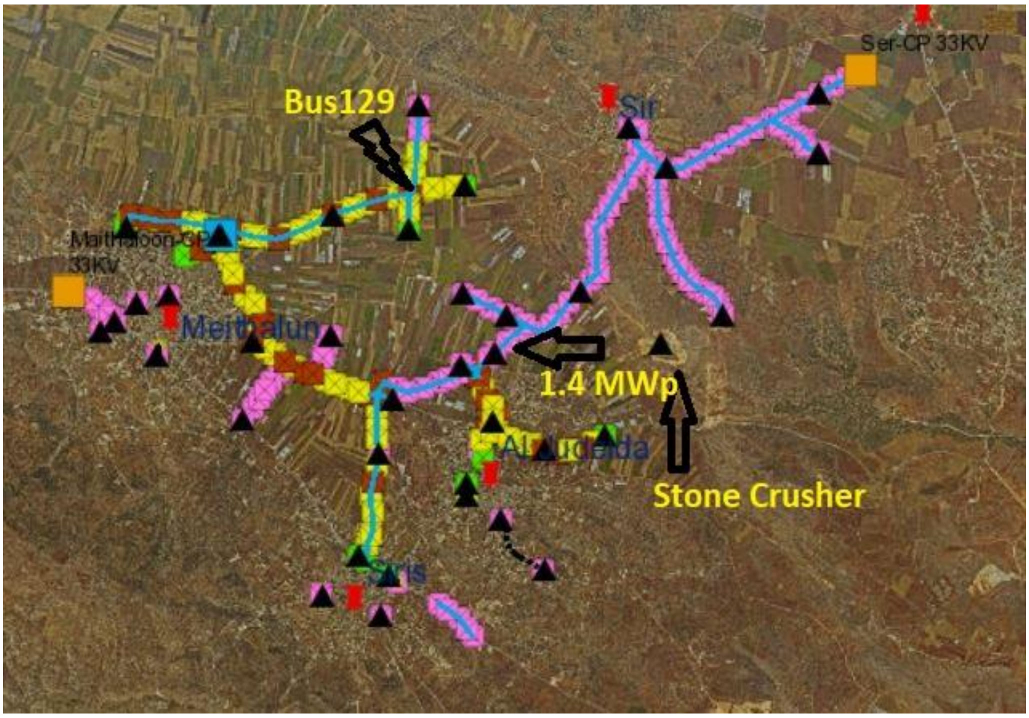

***Figure 3-1**: Electrical Equipment Locations*

3.1.3 Extract the Exact Length of the Cables and OHL.

The underground cables and the overhead transmission lines (OHL) in the grid are one of the types mentioned in Table 2-2 [16]:

Table 3-1 Types of Cables and OHL

Cable Type	DC Resistance per phase R'(20°C) in Ohm/km	Reactance X' in Ohm/km
ACSR 70	0.413	0.331
ACSR 95	0.2992	0.311
3*(1*50mm),36KV, CU	0.387	0.203786

After classifying the types of cables and OHL as in reality the physical parameter for each one calculated for the cable length and parameters and

IDs, Table 2-3, shows the brief data for the cables and OHL and the detailed parameter in Appendix (2).

Table 3-2 Detailed Data for Cables and OHL

Cable ID	Cable Type	Length	DC Resistance per phase R'(20°C) in Ohm/km	Reactance X' in Ohm/km	Cable Resistance Ohm	Cable Reactance Ohm
JT0008-JT0001	ACSR 70	460	0.413	0.331	0.18998	0.15226
JT0001-JT0642	3*(1*50mm),36KV, CU	440	0.387	0.203786	0.17028	0.08966584
JD0001-JT0641	3*(1*50mm),36KV, CU	270	0.387	0.203786	0.10449	0.05502222

3.1.4 Check the Transformer Name Plates

To model the grid correctly the detailed parameters of the transformers must be checked, so all transformers nameplates captured and mentioned briefly in Table 2-4 and detailed data in Appendix (3). All transformers operated on a voltage level of 33/0.4 kV. [16]

Table 3-3 Transformers Name Plate Data

TR ID	Capacity	Impedance	Number of taps	Nominal Tap position	Load losses (KW)	No-load losses (KW)	No-load current (%)	Vector Croup
JD0056	630 KVA	5	5	3	5	1.15	0.429	DYN11
JD0142	630 KVA	4.5	7	4	5	1.15	0.429	DYN11
JD0144	630 KVA	4	7	5	5	1.15	0.429	DYN11

3.1.5 Draw a Single Line Diagram (SLD) to Represent the Grid.

The SLD is the simplified description for representing electrical equipment's of the power system and the way of connection. Also, the modelling algorithms and software based on SLD, to build the mathematical matrixes and do the analysis. Figure 2-2, shows the SLD built

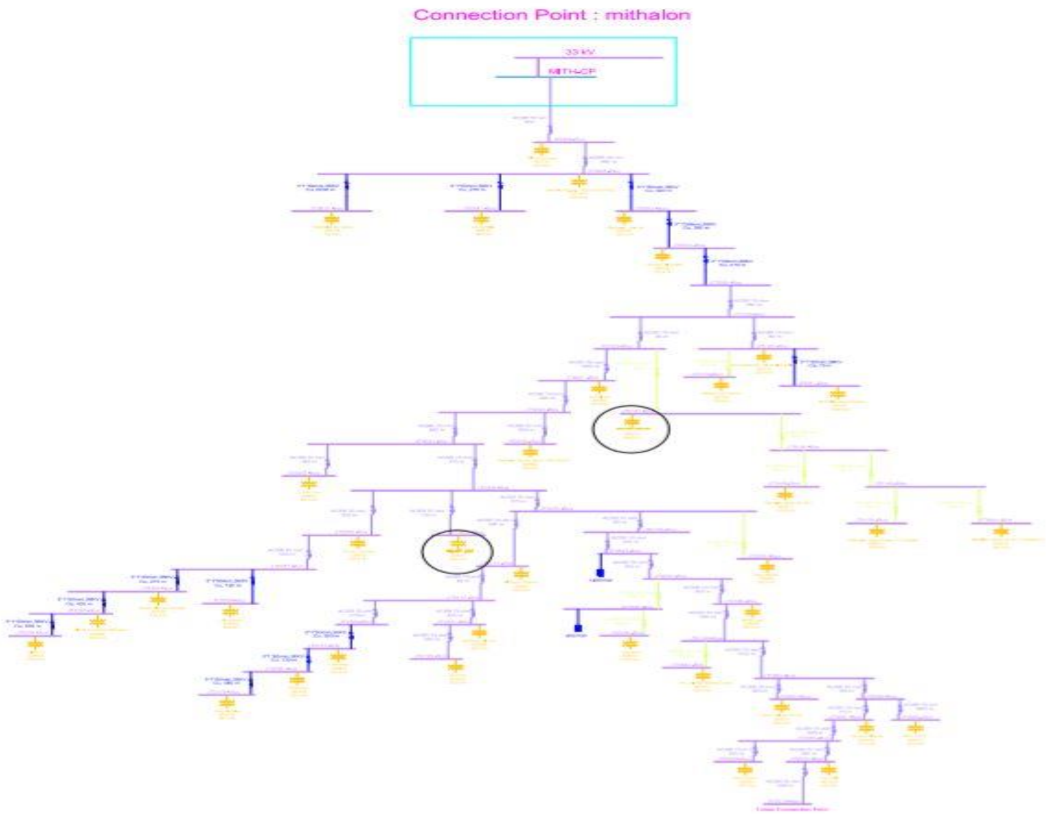

Figure 3-2: Maithaloon SLD

for Maithaloon electrical grid. Appendix (4) shows the drawing in deep details.

3.1.6 Estimate the Loads of the Transformers Depending on the Transformer Load Factor

The load measured for each transformer at low voltage side for long period of time. The average load factor for the transformers was about 40% and instantaneous power factor varies widely depending on load conditions but the average accumulative power factor is about 97%. So, the approximated loads for each transformer found referred to the last load assumption and Table 2-5, show the exact rated capacity of the transformer with its approximated loads

Table 3-4 . Load estimation of the Transformers

TR ID	Rated Capacity	Load Factor	Power Factor	Real Power	Reactive Power
JD0138	400	0.4	0.97	155.2	38.8967865
JD0139	400	0.4	0.97	155.2	38.8967865
JD0140	160	0.4	0.97	62.08	15.5587146
JD0141	250	0.4	0.97	97	24.31049156
JD0142	630	0.4	0.97	244.44	61.26243874
JD0015	250	0.4	0.97	97	24.31049156
JD0014	400	0.4	0.97	155.2	38.8967865
JD0016	160	0.4	0.97	62.08	15.5587146
JD0011	250	0.4	0.97	97	24.31049156
JD0012	250	0.4	0.97	97	24.31049156
JD0013	250	0.4	0.97	97	24.31049156
JD0002	250	0.4	0.97	97	24.31049156
JD0003	400	0.4	0.97	155.2	38.8967865

JD0053	400	0.4	0.97	155.2	38.8967865
JD0054	250	0.4	0.97	97	24.31049156
JD0005	400	0.4	0.97	155.2	38.8967865
JD0004	100	0.4	0.97	38.8	9.724196625
JD0006	160	0.4	0.97	62.08	15.5587146
JD0056	630	0.4	0.97	244.44	61.26243874
JD0010	400	0.4	0.97	155.2	38.8967865
JD0144	630	0.4	0.97	244.44	61.26243874
JD0019	400	0.4	0.97	155.2	38.8967865
JD0017	160	0.4	0.97	62.08	15.5587146
JD0018	100	0.4	0.97	38.8	9.724196625
ND0061	100	0.4	0.97	38.8	9.724196625
JD0020	250	0.4	0.97	97	24.31049156
JD0008	400	0.4	0.97	155.2	38.8967865
JD0009	250	0.4	0.97	97	24.31049156
JD0052	400	0.4	0.97	155.2	38.8967865
JD0062	250	0.4	0.97	97	24.31049156
JD0063	630	0.4	0.97	244.44	61.26243874
JD0001	250	0.4	0.97	97	24.31049156
JD0007	400	0.4	0.97	155.2	38.8967865
JD0055	630	0.4	0.97	244.44	61.26243874
JD0054	250	0.4	0.97	97	24.31049156
JT0059	250	0.4	0.97	97	24.31049156

3.1.7 The PV Farm Modulation

In this research the PV farm of 1.4 MWp, considered as current source operate at rated conditions without any variations. The effect of harmonics generated from the solar inverters neglected because the inverter type test shows small effect of harmonics generated from the inverter at any load condition. Appendix (5), shows the detailed inverter type test.

3.1.8 Build the Model on MATLAB

From the SLD of Maithaloon and the detailed electrical parameters of transmission lines, transformers and the load approximation, the electrical model of the grid built referring to the equipment and coding algorithm of Nedco. Also, the sources of harmonics, Photovoltaic were modelled and the measuring and sensing devices connected to some buses to evaluate the load flow results.

In MATLAN/SIMULINK, there are blocks represent the electrical equipment's such transmission lines, transformers, power sources, measuring devices but all these blocks need to be configured referring to the real parameters. The figure 2-3 below shows the modelled grid on MATLAB/SIMULINK.

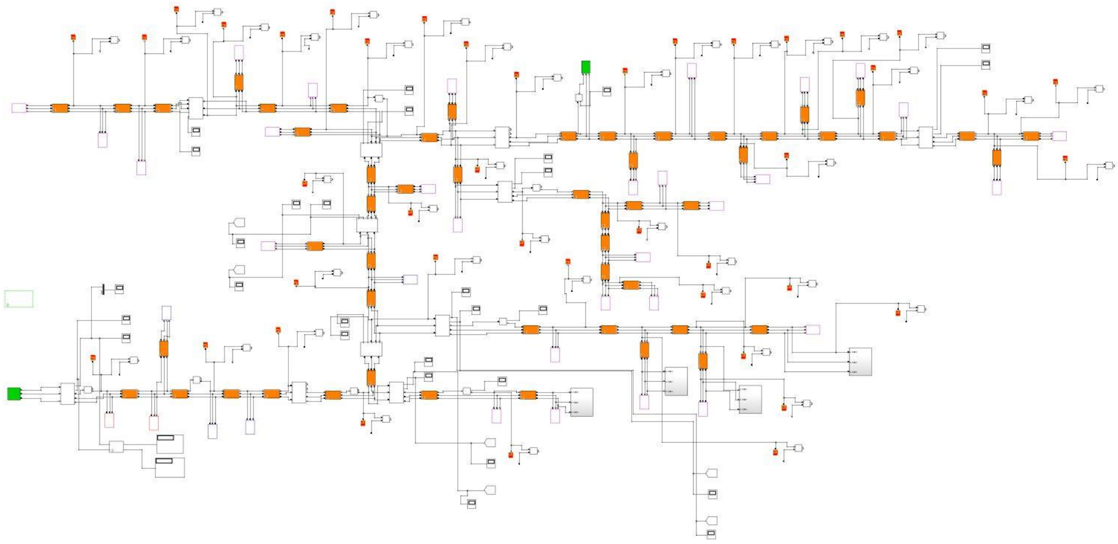

Figure 3-3: MATLAB Real Grid Model

Measure the Real Parameters (Voltages, Currents, Harmonics)

In reality, the energy analyzer connected to bus 29 (operated on 33 KV), to read the real measurements of voltage, current, harmonics and power factor with time frame of 5 minutes between the measured values. The measurements used to draw the power profiles for voltage, current, power factor and, current. The detailed real measurements mentioned briefly in Appendix (6).

3.1.9 The measured Voltage Profile.

The measured voltage profile at Bus 29, not far from the connection point, shows that the voltage varies between (30 to 33) kV and there are unbalanced voltage profiles and fast variation which affect the power quality of the grid shown in Figure 2-5.

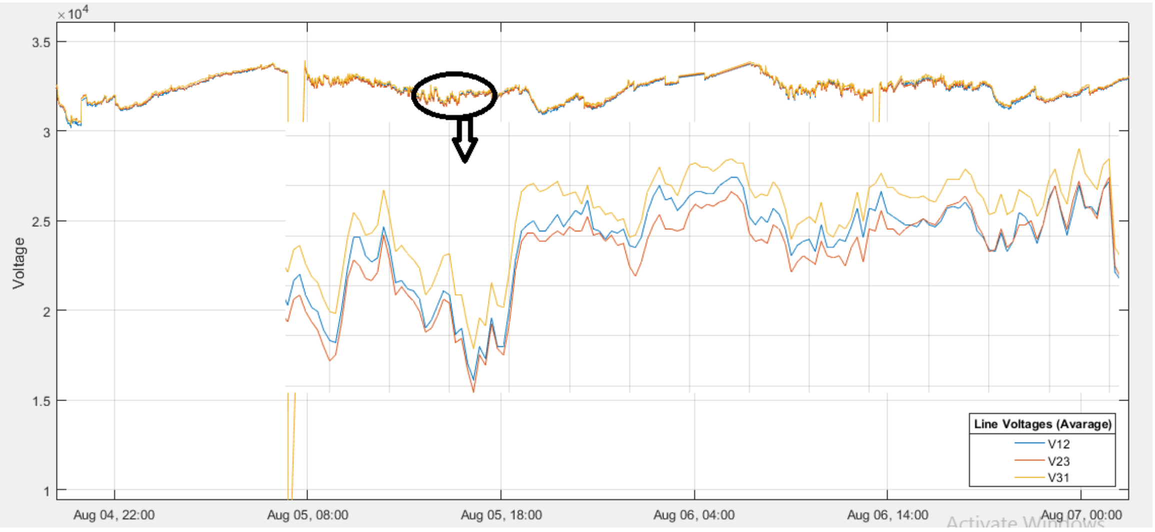

Figure 3-4. The measured voltage profile at Bus 29_Maithaloon Grid

3.1.10 Measured Harmonic Profiles for may days

The total harmonic distortion profile indicates that the grid suffers from highly nonlinear loads which cause THD varies between 20% and 46% on 33kV. And this will affect the electrical losses, voltage drop and other power quality indicators. The figure 2-5, shows the harmonic measured profile on Maithaloon electrical grid. The table 2-6, summarise the measured component of the current other than the fundamental and the total harmonic distortion values on each phase.

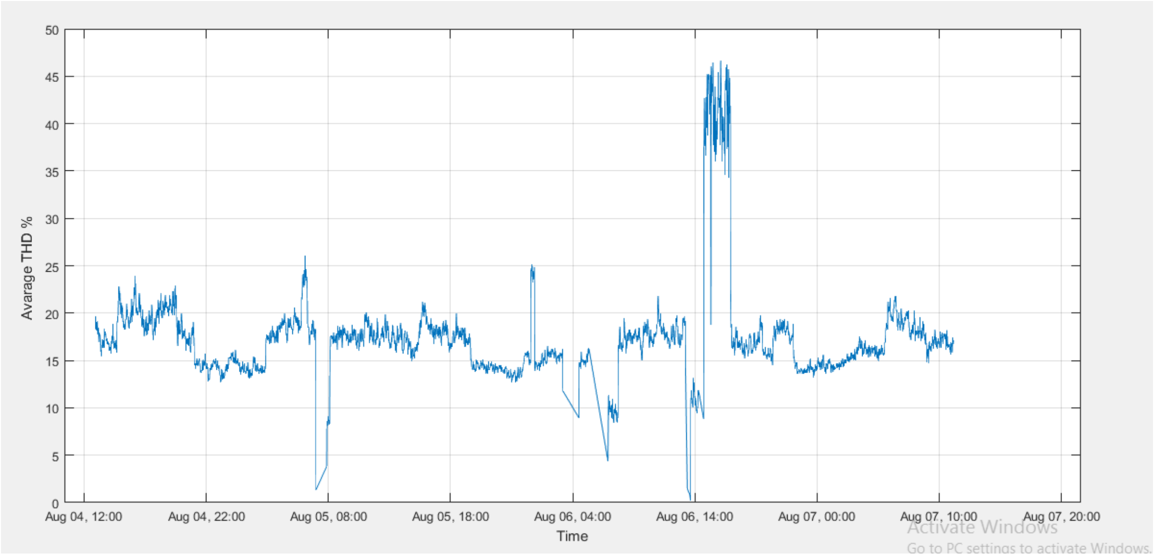

Figure 3-5.The measured Harmonic Distortion at Bus 29_Maithaloon Grid

3-5. The Maximum and Average Measured of Current Component Other Than Fundemental

	Phase	**2nd**	**3rd**	**4th**	**5th**	**6th**	**7th**	**8th**	**9th**	**10th**	**11th**	**THD%**
Max	R	0.166	0.488	0.103	1.424	0.062	0.86	0.038	0.187	0.028	0.246	46.7
Avg.		0.134	0.255	0.079	1.148	0.039	0.663	0.027	0.124	0.020	0.184	17.5
Max	S	0.236	0.491	0.105	1.749	0.058	0.728	0.036	0.168	0.025	0.308	46.1
Avg.		0.185	0.280	0.076	1.458	0.040	0.532	0.017	0.132	0.017	0.246	19.9
Max	T	0.158	0.497	0.092	1.698	0.060	0.836	0.041	0.191	0.028	0.217	51.4
Avg.		0.103	0.233	0.038	1.430	0.035	0.608	0.026	0.131	0.016	0.158	21.8

3.1.11 Measured Power Factor Profile

The power factor profile measured at bus 29 shown in Figure 2-7. From the Profile it seems that there is variation in the instantaneous power factor and vary rapidly reoffering to load and distributed generation conditions.

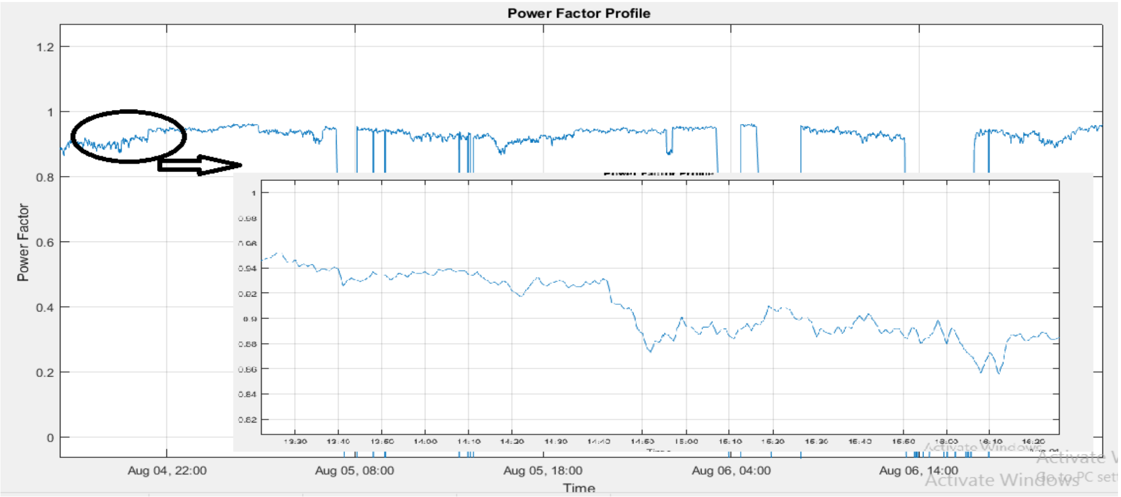

Figure 3-6.The Measured Power Factor Profile at Bus 29_Maithaloon Grid

3.1.12 The Measured Current Profile.

The current profile at bus 29 of Maithaloon grid figure 2-8, shows that the current injected from this bus is highly distorted and vary rapidly.

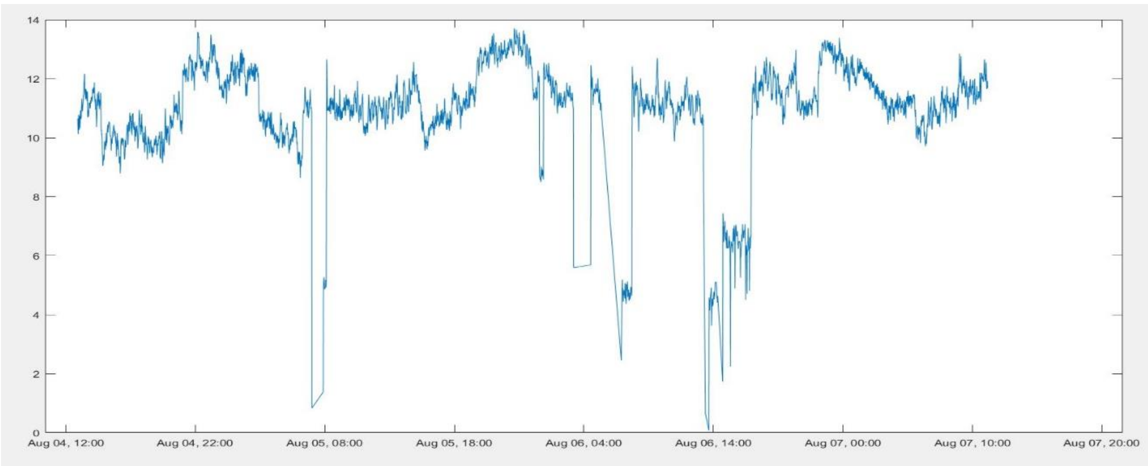

Figure 3-7. The Measured Current Profile at BUs_29- Maithaloon Grid

3.1.13 Modelling of Harmonic Source

The measurements reading of harmonics done on the Medium-voltage line of Maithaloon. In MATLAB/SIMULINK the source of the harmonics modeled as current sources parallel for each phase, Figure 2-9 shows the MATLAB model of Harmonics.

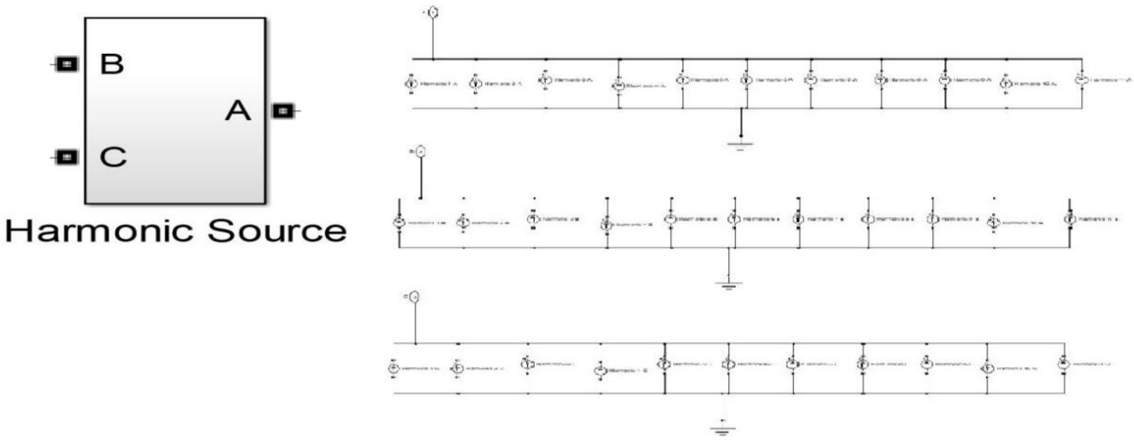

Figure 3-8. Modelling of Harmonic Source

Chapter Four

Unified Power Flow Compensator (UPFC)

4.1 Introduction:

Nowadays and due to the nonlinear loads and distributed generation the idea of smart power systems comes to the front and based on power electronics, information systems, and communications to improve the control, reliability and, the power quality of the grid with optimal use of resources. Flexible alternating current transmission system (FACTS) incorporates power electronic-based controllers to enhance controllability and increase power transfer capability. FACTS controllers are very useful in smart power systems to successfully integrate the increased shares of variable renewable energy sources.

The compensating devices are two types: the synchronous machines and the Flexible Alternating current transmission systems (FACTS). The synchronous compensator is a synchronous motor operate no load to compensate the grid with reactive power and improve the power factor, but unfortunately these devices has slow dynamic behavior and their response always requires seconds to do the function. Nowadays, the modern power electronic devices allow the power system engineers to design devices with fast time response (in cycles) which will improve the static and dynamic operation of the power system. So, in power systems, FACTS are usually use to regulate the transmission lines, and increase their utilization, improve the dynamic and stability of the grid, also it increases the quality of supply for the sensitive loads [17].

FACTS divided to three group's dependents on their switching techniques: mechanically (i.e. Phase shift transformer), Thyristors and Fast switching devices (IGBT's, MCT's, GTO's) [18].

The FACTS devise which are used for controlling and enhancing the power system are:

- The first-generation devices
- Static Var Compensator (SVC)
- Thyristor controlled series capacitor (TCSC)
- Thyristor controlled phase shifter
- The second-generation devices
- Static synchronous compensator (STATCOM)
- Static Synchronous series Compensator (SSSC)
- Unified Power flow controller (UPFC)

In short, the most promising device in the FACTS concept has the ability to adjust three control parameters:

- The bus voltage
- Transmission line reactance
- Phase angle between two buses in the Grid
- Control the static and dynamic operation of TL.
- Power Quality improvement.

4.2 UPFC Technology and Controller Topology:

4.2.1 Technology

The UPFC consists of one shunt and one series converter that share a back-to-back common direct current (dc) link provided by a dc storage capacitor, battery, or another fixed dc source, as shown in Fig.9. These two converters are switching voltage source converters having semiconductor devices with turn-off capability.

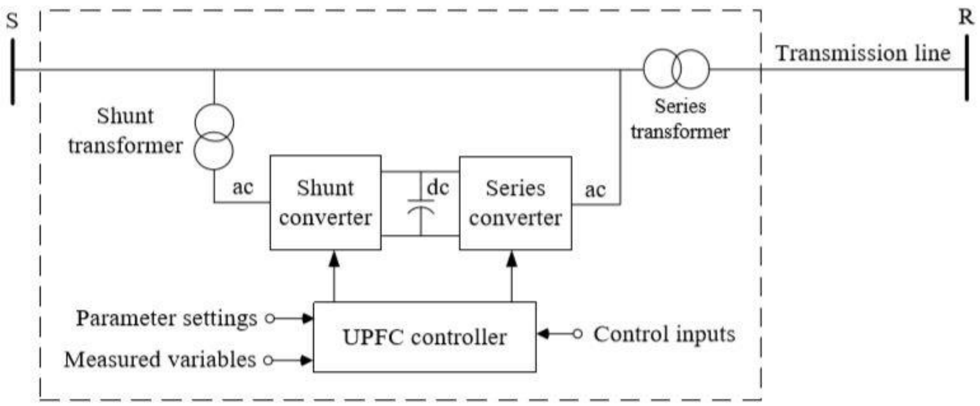

Figure 4-1 Structure of UPFC

The series converter controls the active and reactive power of the transmission line by injecting an AC voltage with a controllable magnitude and phase angle. The shunt converter supplies or absorbs the active power required by the series converter. Moreover, the shunt converter can supply or absorb reactive power, thus providing shunt reactive power compensation.

4.2.2 Converter Topologies

The main topologies of the UPFC converter can be categorized into two categories, the first is the multi-pulse converters, and the other is multi-level converters. For a given power, the multi-pulse converter has better total harmonic distortion but higher transformer complexity than the multi-level converter. Multi-level converters for UPFC are classified as:1) multipoint-clamped converters (MPC) or diode-clamped converters [19]; 2) chain converters or cascade converters [20], [21]; and 3) nested-cell converters or flying capacitor converters [22].

4.2.3 Application

The Applications of UPFC in transmission systems include: 1) power flow control and congestion management [23]; 2) reactive power compensation and control [24]; 3) voltage control [25]; 4) power transfer capability enhancement [26]; 5) power loss reduction [27]; 6) load curtailment reduction [28]; 7) power quality improvement ; 8) power system reliability enhancement; 9) harmonic mitigation ; 10) improvement of transient stability; 11) damping inter-area and intra-area oscillations ; 12) damping of sub-synchronous resonance.

The UPFC is also used in power distribution systems, where it is sometimes called distribution-UPFC (D-UPFC). The applications of D-UPFC include voltage control of distribution system when voltage sags and swells occur [29]; line loss minimization in loop distribution systems [30];

and voltage regulation in all nodes with simultaneous line loss minimization in loop distribution systems [30].

4.2.4 UPFC Operational Modes and Simulation Models

The UPFC can operate in different modes to support the electrical grid with many operational scenarios either in a steady-state or dynamic. In the case of steady-state modes, the UPFC has models to represent the Power flow, optimal power flow (OPF), and steady-state harmonic model. Also, there are needs to understand the interactions between the grid and the UPFC so the dynamic models are necessary especially the small-signal dynamic model, transient stability models, fault analysis models, and the dynamic harmonic models [31].

4.2.5 Control Methods

To control the operation of the UPFC, many approaches operate to force the system to provide the needed results and improve the grid power quality.

Linear and linearized control methods are the simplest technique and usually use the PI controller which tuned around the operation point and almost give accurate results.

As the need for using highly technical and fast controllers to operate and track the grid situation an advanced control method developed such as

- **The decoupled controller** for the real and reactive power through the transmission line using PWM [32], this technique allows the controller to operate under unbalanced conditions [33].

- **Vector control** is like a decoupled method since it ensures the independent control of power and reactive power [34].
- **Preventive Control**, which allows a predictive control scheme for UPFC and provides better transient performance in comparison with decoupled control [35] which improves the static and dynamic behavior of the controller.
- **Coordinated Control**, used to enhance the small-signal stability of the UPFC and to avoid excessive instability of the UPFC dc-link capacitor voltage during transient conditions [36].
- **Sliding Mode Control**, it is an advanced nonlinear direct power control, based on sliding mode control theory, is proposed for UPFC with a matrix converter (vector switching converter) [37].
- **Robust Control**, the controller will improve power system stability [38].
- **Adaptive Control**, this method is used to improve the transient stability in the conventional PI controller of UPFC, by adding a self-tuning controller.
- **Hybrid Control**, a combined linear and nonlinear control strategy for UPFC helps improve transient stability [39]. An advanced control, which combines phase angle control and cross-coupling control, achieves quick response of active and reactive power without power fluctuations, as well as improved transient performance [40].
- Intelligent Control, such as Neural Network (NN), Fuzzy Logic, Genetic Algorithm (GA), and Particle Swarm Optimization (PSO).

4.3 Operating Principals of UPFC and Harmonics Mitigation:

4.3.1 Operating principals:

The power circuit of the three-phase UPFC system is shown in Figure 3-2. The Active Power Filter (APF) is using a 27-level asymmetrical inverter. Each phase of this inverter consists of three H-bridges supplied by three independent DC sources. The series inverter is coupled to the transmission line via a series transformer, and the shunt coupled to bus i directly. The shunt inverter reacts as normal STATCOM and can generate or absorb reactive and active power.

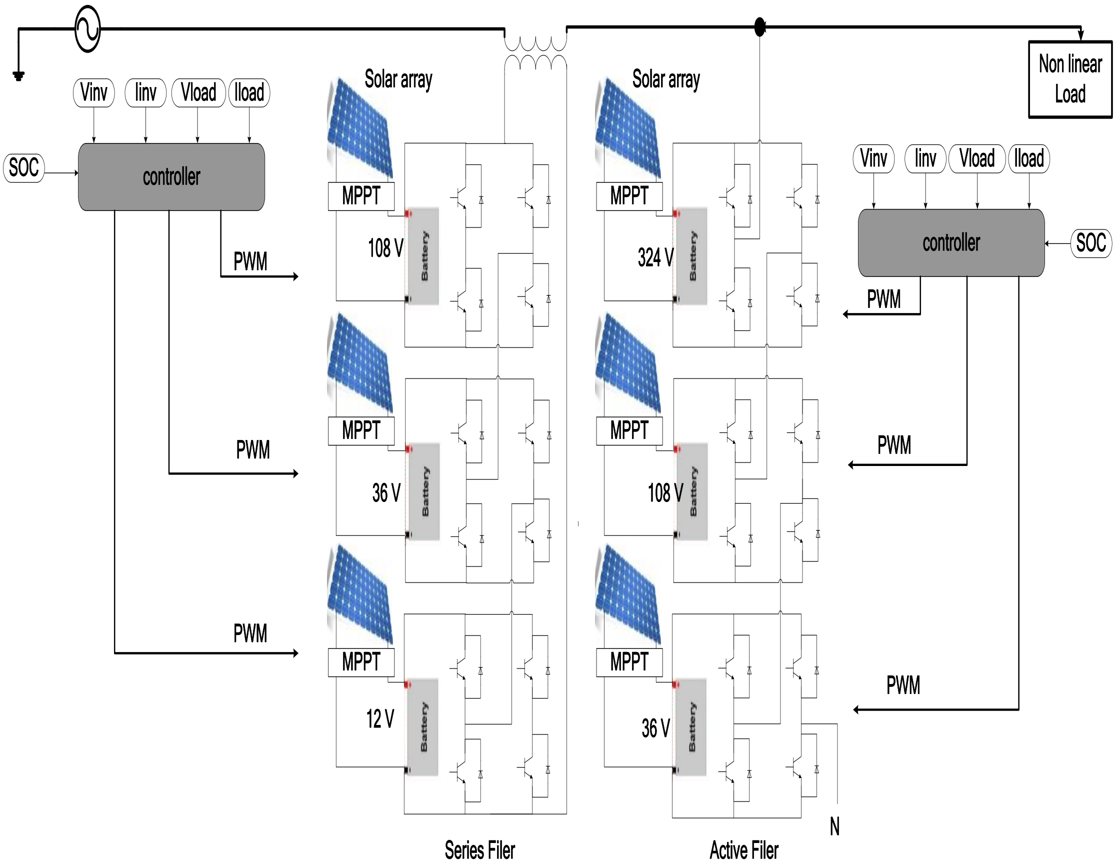

Figure 4-2. Operating principle of UPFC

4.3.2 UPFC as Harmonic Mitigator

The UPFC can operate to extract the harmonics and start to operate as harmonic mitigator. In this research the controller of UPFC have to extract the harmonics then generate signals to compensate the grid.

4.3.2.1 Extraction of the Harmonic Currents.

The reference signal which will lead any controller extracted using the time or frequency domain. The time domain is a simple instantaneous estimation used to generate reference signal from distorted signal and, in power system the signals will be voltage or current.

4.3.2.2 Instantaneous Active and Reactive Power Theory (p-q).

The (p-q) theory used to separate the fundamental and other components of non-linear load in power system. The three phase systems without zero sequence can be expressed as:

$$X_a + X_b + X_c = 0 \qquad (31)$$

A matrix as in equation (32) can be created to transform from a-b-c to α-β-0 system as shown below:

$$\begin{bmatrix} vo \\ v\alpha \\ v\beta \end{bmatrix} = \sqrt{2}/\sqrt{3} \begin{bmatrix} 1/\sqrt{2} & 1/\sqrt{2} & 1/\sqrt{2} \\ 1 & -1/2 & -1/2 \\ 0 & \sqrt{3}/2 & -\sqrt{3}/2 \end{bmatrix} \begin{bmatrix} va \\ vb \\ vc \end{bmatrix} \qquad (32)$$

$$\begin{bmatrix} io \\ i\alpha \\ i\beta \end{bmatrix} = \sqrt{2}/\sqrt{3} \begin{bmatrix} 1/\sqrt{2} & 1/\sqrt{2} & 1/\sqrt{2} \\ 1 & -1/2 & -1/2 \\ 0 & \sqrt{3}/2 & -\sqrt{3}/2 \end{bmatrix} \begin{bmatrix} ia \\ ib \\ ic \end{bmatrix} \tag{33}$$

The theory depends on the transformation from the 3-phase system (a-b-c) to the 0-α-β system.

$$\begin{bmatrix} ia \\ ib \\ ic \end{bmatrix} = \sqrt{2}/\sqrt{3} \begin{bmatrix} 1/\sqrt{2} & 1 & 0 \\ 1/\sqrt{2} & -1/2 & \sqrt{3}/2 \\ 1/\sqrt{2} & -1/2 & -\sqrt{3}/2 \end{bmatrix} \begin{bmatrix} io \\ i\alpha \\ i\beta \end{bmatrix} \tag{34}$$

From equation (32) and (33) a new relation can be driven as following:

$$i_N = i_a + i_b + i_c = \sqrt{3}\ i_0 \tag{35}$$

The power can be defined as following:

$$\begin{bmatrix} po \\ p\alpha\beta \\ q\alpha\beta \end{bmatrix} = \begin{bmatrix} vo & 0 & 0 \\ 0 & v\alpha & v\beta \\ 0 & -v\beta & v\alpha \end{bmatrix} \begin{bmatrix} io \\ i\alpha \\ i\beta \end{bmatrix} \tag{36}$$

Where va, vb, vc and ia, ib, ic are phase voltages and currents.

po is the zero sequence (real instantaneous power).

$p\alpha\beta$ is the instantaneous real power.

$q\alpha\beta$ is the instantaneous imaginary power.

Equation (33) can be rewritten by using power and voltages instead of currents as following:

$$\begin{bmatrix} io \\ i\alpha \\ i\beta \end{bmatrix} = \ ^{1}/_{vov\alpha\beta^2} \begin{bmatrix} v\alpha\beta & 0 & 0 \\ 0 & vov\alpha & -vov\beta \\ 0 & vov\beta & vov\alpha \end{bmatrix} \begin{bmatrix} po \\ p\alpha\beta \\ q\alpha\beta \end{bmatrix} \quad (37)$$

Where

$$v\alpha\beta^2 = v\alpha^2 + v\beta^2 \quad (38)$$

There are power components which result.

$\overline{p0}$ = instantaneous power (Zero-sequence components).

$\widetilde{p0}$= alternated value of zero-sequence components.

$\overline{p}$= power component which is desired.

$\tilde{p}$= alternated value of the instantaneous real power.

$\overline{q}$= the imaginary instantaneous power.

$\tilde{q}$= the instantaneous imaginary power that belongs to the harmonic currents.

Only $\overline{p}$component is needed, and the filter will generate the others to get good power quality in the receiving current.

4.3.2.3 Instantaneous Active and Reactive Current Component (id-iq) method

The (d-q) current components are getting in this way to separate the fundamental from the other components. This method is chosen because is better for unbalance loads.

The transform is defined by the following equations:

$$\begin{bmatrix} \boldsymbol{id} \\ \boldsymbol{iq} \\ \boldsymbol{io} \end{bmatrix} = \tag{39}$$

$$\sqrt{\frac{3}{2}}\begin{bmatrix} \boldsymbol{cos\theta} & \mathbf{cos}(\boldsymbol{\theta} - \frac{\mathbf{2\pi}}{\mathbf{3}}) & \mathbf{cos}(\boldsymbol{\theta} + \frac{\mathbf{2\pi}}{\mathbf{3}}) \\ -\boldsymbol{sin\theta} & -\boldsymbol{sin\theta}(\boldsymbol{\theta} - \frac{\mathbf{2\pi}}{\mathbf{3}}) & -\boldsymbol{sin\theta}(\boldsymbol{\theta} + \frac{\mathbf{2\pi}}{\mathbf{3}}) \\ \mathbf{1}/\sqrt{\mathbf{2}} & \mathbf{1}/\sqrt{\mathbf{2}} & \mathbf{1}/\sqrt{\mathbf{2}} \end{bmatrix}\begin{bmatrix} \boldsymbol{ia} \\ \boldsymbol{ib} \\ \boldsymbol{ic} \end{bmatrix}$$

Where, θ is the angular position of the synchronous reference.

θ is a linear function of the fundamental frequency. The harmonic current component can be separated from the load currents using low pass filter. The load currents contain two components as following.

$$\boldsymbol{idl} = \widetilde{\boldsymbol{\imath ld}} + \overline{\boldsymbol{\imath ld}} \tag{40}$$

$$\boldsymbol{iql} = \widetilde{\mathbf{I}\boldsymbol{lq}} + \overline{\boldsymbol{\imath lq}} \tag{41}$$

$\overline{Ild}$and $\overline{\mathrm{I}lq}$are average termsand$\widetilde{Ild}$and $\widetilde{\mathrm{I}lq}$are oscillatory terms.

The following can be noticed:

So, (iql) is used to compensate the reactive power and improving the power factor and $(\widetilde{\imath ld})$to cancel harmonics.

The reference signal is:

$$\begin{bmatrix} \boldsymbol{ifd}^* \\ \boldsymbol{ifq}^* \end{bmatrix} = \begin{bmatrix} \widetilde{\boldsymbol{Ild}} \\ \boldsymbol{ilq} \end{bmatrix} \tag{42}$$

And by Inverse Park transform:

$$\begin{bmatrix} \boldsymbol{ifa} \\ \boldsymbol{ifb} \\ \boldsymbol{ifc} \end{bmatrix} = \frac{\sqrt{3}}{2}\begin{bmatrix} \boldsymbol{cos\theta} & -\boldsymbol{sin\theta} \\ \mathbf{cos}(\boldsymbol{\theta} - \frac{\mathbf{2\pi}}{\mathbf{3}}) & -\boldsymbol{sin\theta}(\boldsymbol{\theta} - \frac{\mathbf{2\pi}}{\mathbf{3}}) \\ \mathbf{cos}(\boldsymbol{\theta} + \frac{\mathbf{2\pi}}{\mathbf{3}}) & \boldsymbol{sin\theta}(\boldsymbol{\theta} + \frac{\mathbf{2\pi}}{\mathbf{3}}) \end{bmatrix}\begin{bmatrix} \boldsymbol{ifd}^* \\ \boldsymbol{ifq}^* \end{bmatrix} \tag{43}$$

To determine the angular position of the synchronous reference, a phase locked loop (PLL) can be used as shown in figure (2.1)

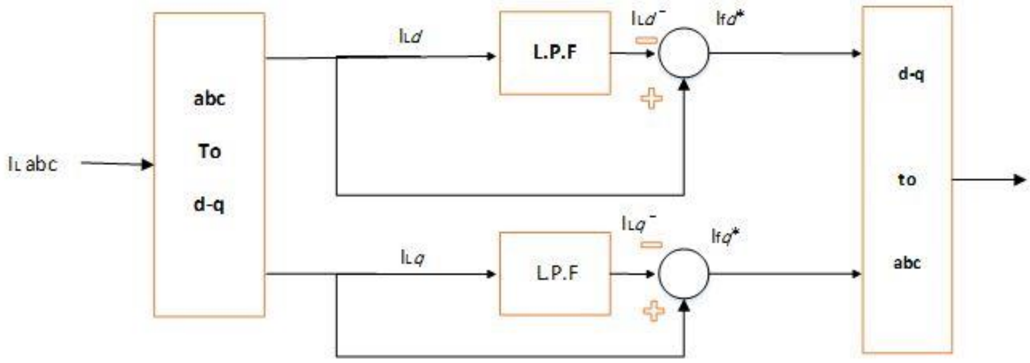

Figure 4-3.Reference current extraction with id-iq method.

4.4 Design the Controller of UPFC :

The Controller of the UPFC is based on the synchronous reference d-q method, the algorithm for this method mentioned in figure 3-5 [41].

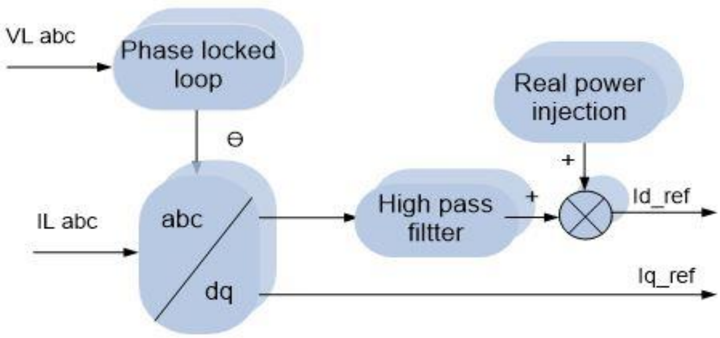

Figure 4-4. d-q method- the operational principle

The d-q method transforming the load current into the load voltage synchronous frame d-q frame. In this case, the current will have two components I_d and I_q. The I_d current is in the direction of the load voltage and so it is the real power current component. The I_q current will be perpendicular to the load voltage and hence it is the reactive power current component.

These d-q current components will have two components. The first component is the dc component that represents the fundamental component of the real and reactive components. The ac component represents the harmonics in the current.

4.5 Reference Voltage Calculation for Series Active Filter:

The instantaneous real and reactive method (PQ method) is adopted in this research to calculate the reference voltages for the series active filter [42]. This technique is illustrated in Figure 3-6.

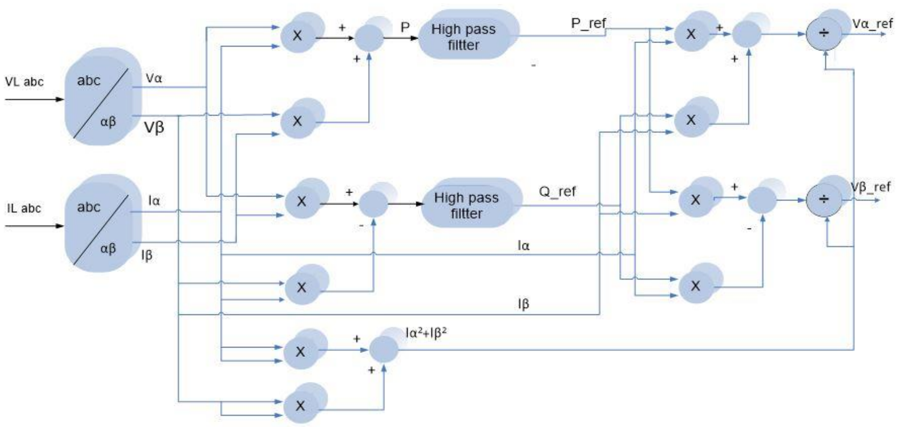

Figure 4-5. Principle of instantaneous active and reactive power theory (P-Q method)

4.6 Multi-level Inverter:

In this research a symmetric cascaded multi-level inverter was used. The three-phase inverter has three H-bridges connected in series and supplied by three independent DC source either photovoltaic arrays or Battery scaled in the power of three as shown in figure 3-6. This configuration of the multi-level inverter allows it to generate 27-level at the output of inverter instead of generating 7 levels when using symmetric sources. The output of each H-bridge is shown in figure 3-6 on voltage level of 0.4 kV then step-up the voltage level to reach 33 kV.

The switching frequency of the main H-bridge, which manages more than 80% of the total power, is the same frequency of the system (50 Hz). The frequency of the auxiliary H-Bridges is also low but increases as the voltage level of the inverter become lower in the chain.

The total harmonic distortion of the output waveform of the multilevel inverter is only 1.8% while it is in the case of using 2-level inverter is 5.4%. This low THD at the output of the multi-level helps to get rid of the need for any kind of filtering at the output of the active filter.

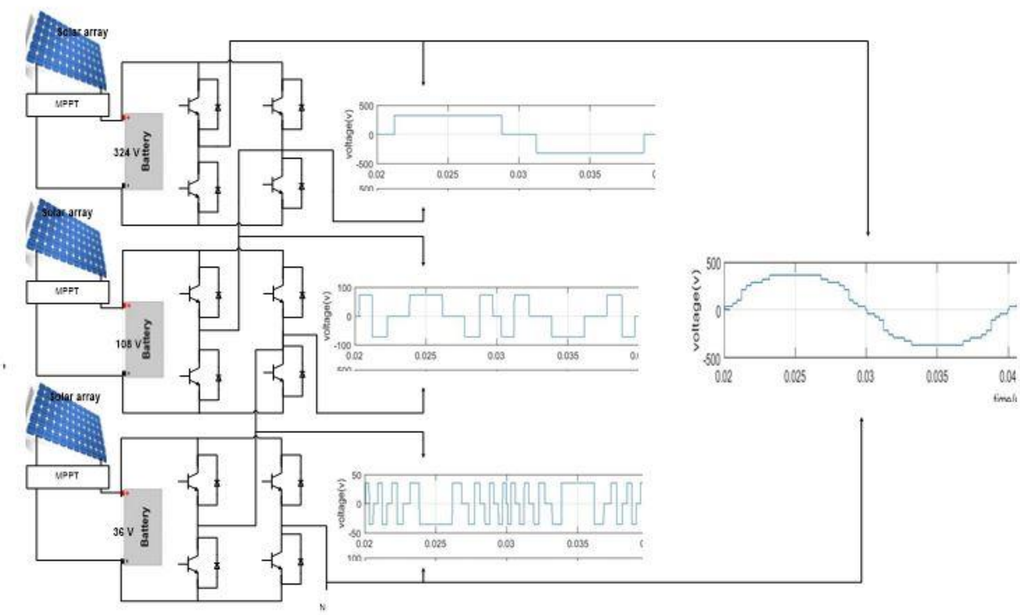

Figure 4-6. Asymmetric 27- level inverter

4.7 MATLAB Model of UPFC:

The MATLAB model UPFC developed on MATLAB/Simulink platform and built based on the original equation and representations of it. The figures below illustrate the block diagram and block components.

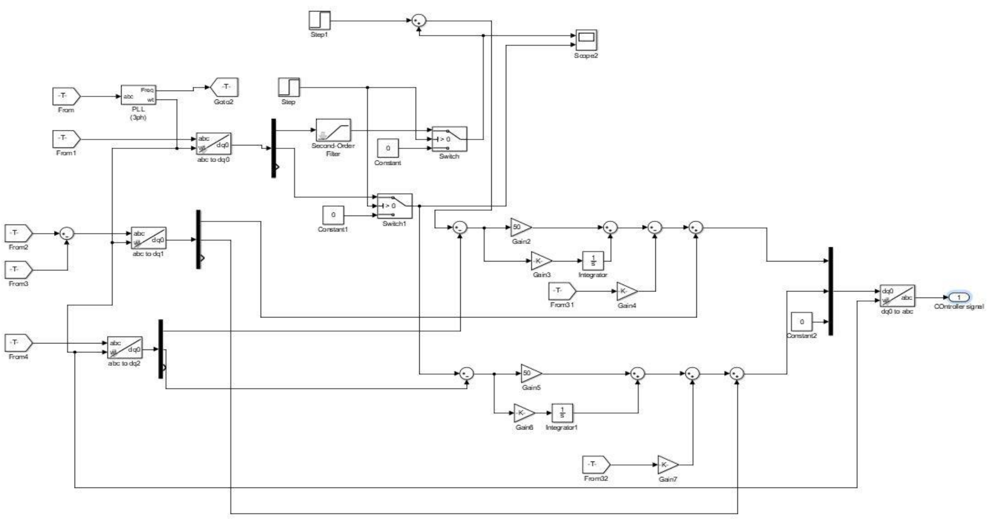

Figure 4-7. Control of Shunt inverter

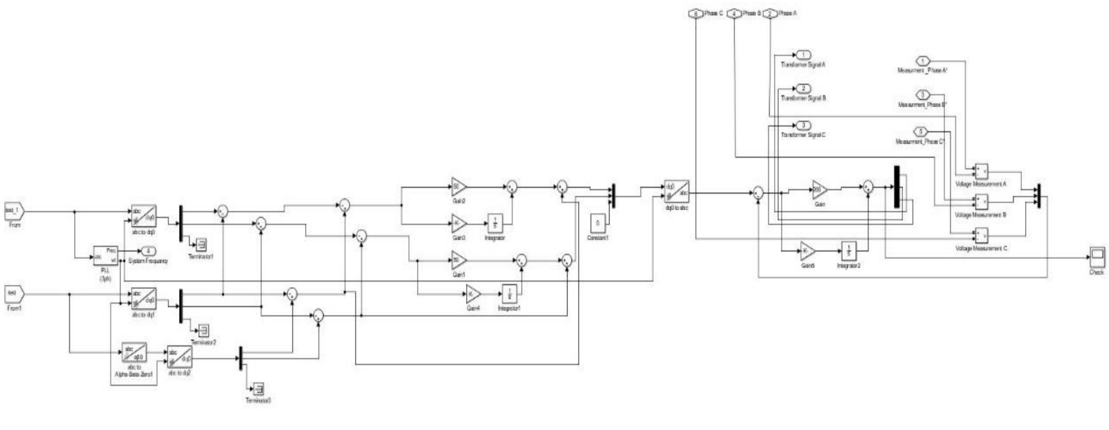

Figure 4-8. Control of Series inverter

4.8 Testing the Controller in Harmonic Elimination:

Figure 3-9. Below shows the source current before and post the operation of the UPFC. At t=0.4 s the active power filter starts working to mitigate the harmonics and the source current became pure sinusoidal. The total harmonic distortion (THD) was reduced from 18% to 0.4%. Then at t=0.7 s, the active power injection starts with 6 A current assistant as seen in Figure 3-9 and the total harmonic distortion remained very low (0.5%) during active power injection [41].

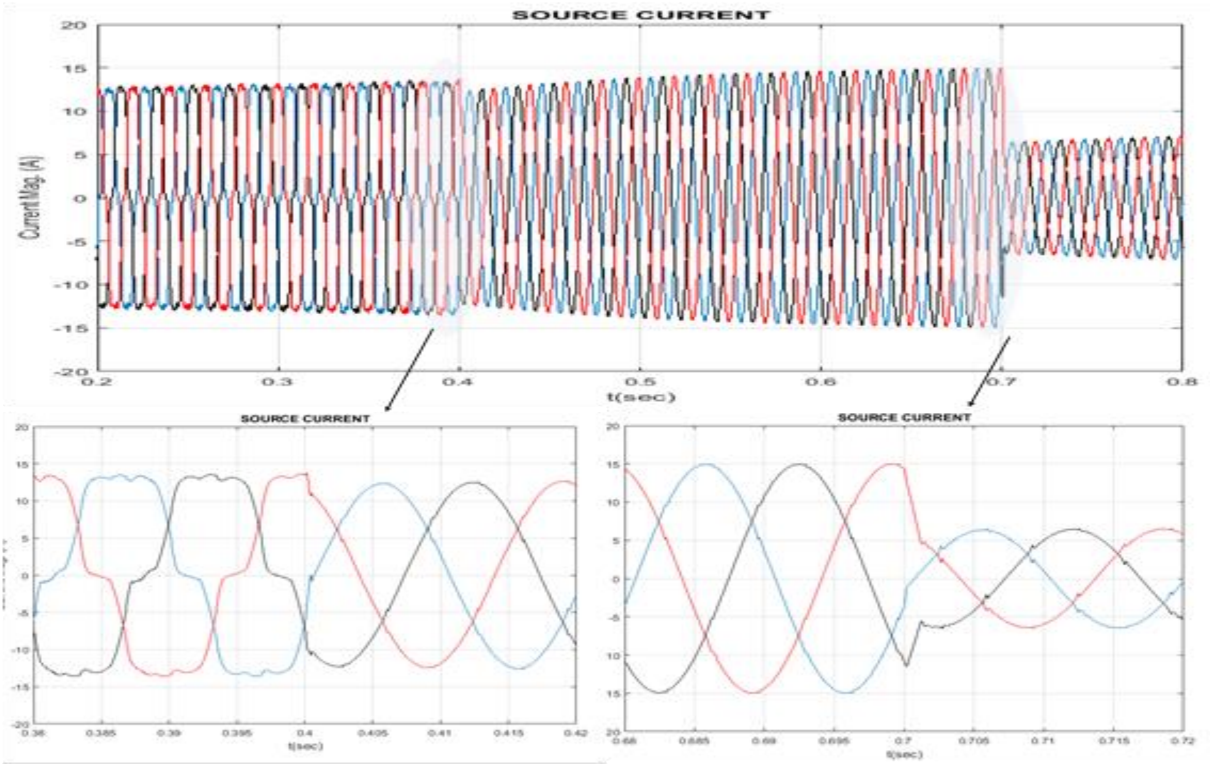

Figure 4-9. Source current before and after the compensation

Chapter Five

Compensation Scenarios

In the previous chapters of this thesis the modeling criteria of the grid, inverters, UPFC, and other parameters that may affect the electrical grid were illustrated deeply. This chapter will discuss the implementation of these models, analyze Maithaloon grid, using MATLAB/SIMULINK and show the results in many operational scenarios for the compensation system with different loading, location, one or many compensators, a fast variation of radiation and low voltage levels.

5.1 Maithaloon Real Grid:

As mentioned before the real grid of Maithaloon was modeled concerning the detailed physical and electrical parameters as in Chapter 2. In this section of the thesis, the model will simulate to check the electrical quality parameters then use the UPFC to improve the distorted signals.

5.1.1 Maithaloon Connection Point Electrical Parameters

Referring to Nedco Technical team The Connection Point of Maithaloon electrical parameters as shown in the table 5-1 [16]:

Table 5-1. Maithaloon Connection Point Electrical Specifications

Parameter	***Value***
Voltage Level (Rated/ Operational)	Rated 36 kV / Operational: 33 VK
Frequency	50 Hz
Short Circuit Level (MV_{sc})	96 MVA
$X/_R$ ratio	13
Power Factor (P.F)	Accumulative more than 90 %

5.1.2 Location of Harmonic Source and Test Buses

The Location of harmonic sources injected into the Maithaloon grid set referring to the real place in reality near the area of water pumps, stone crushers, and other nonlinear loads. To check the power quality conditions the Buses 129, 130, 141, and 206 set as test buses as shown in figure 5-1 .

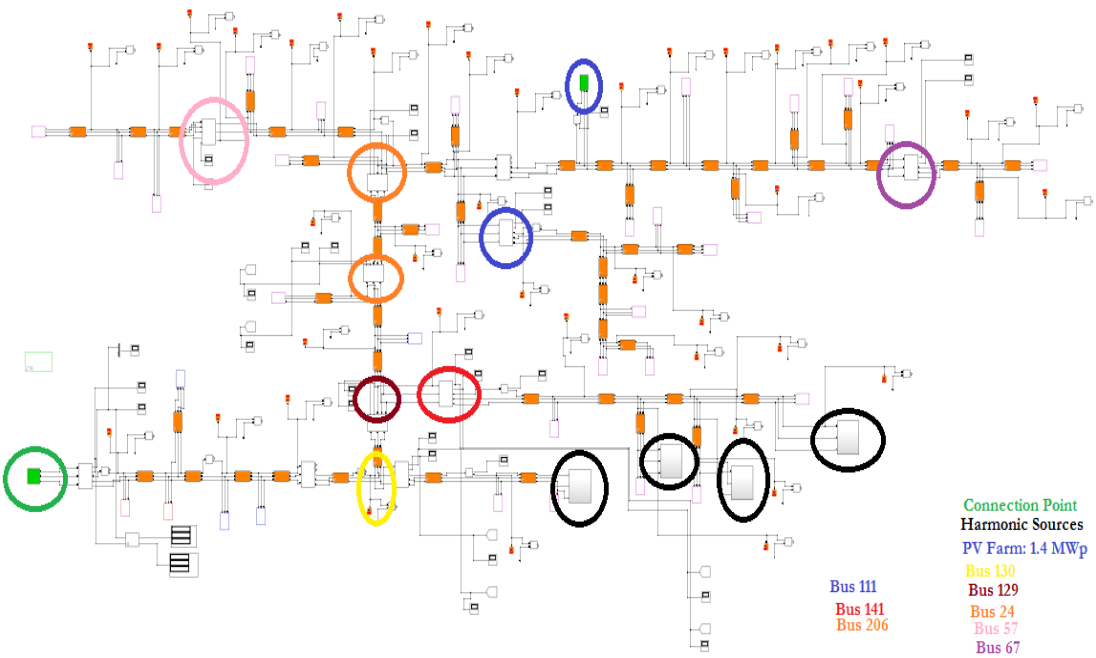

Figure 5-1. Real Grid Location of Harmonic Sources and Test Buses

5.2 Connection Point Voltage and Current Profile Before Compensation:

Voltage Profile:

The voltage profile figure 5-2, means that the Connection point at 33 kV and there is no large distortion on the source voltage signal.

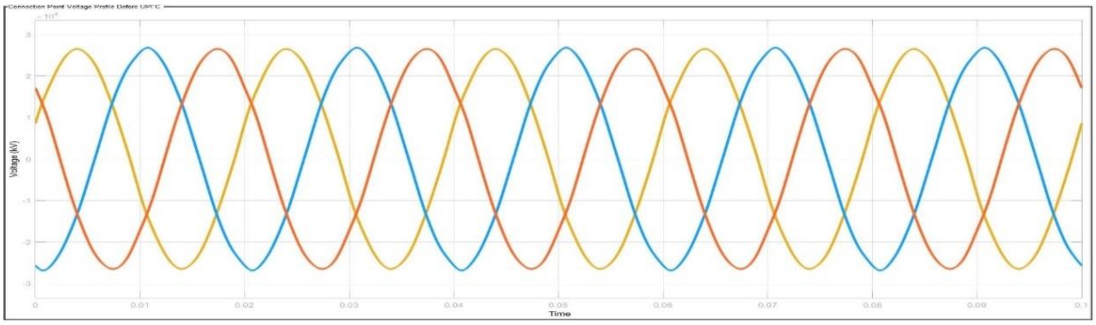

Figure 5-2.Connection Point Voltage Profile Before UPFC

Current Profile

The current profile figure5-3, mentions that the maximum Ampere consumed from the point (at the time of measurement) is about 97 A at 33 kV, and varies depending on the load behavior and PV generation. The THD of CP current is no more than 6%.

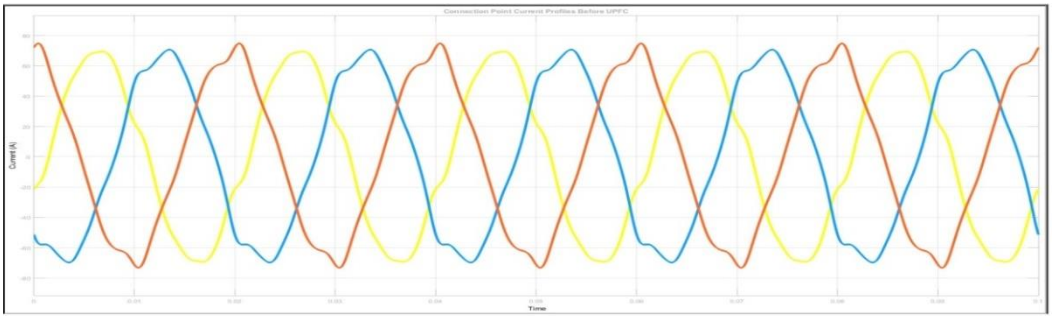

Figure 5-3.Connection Point Current Profiles before UPFC

5.2.1 Test Buses Voltage and Current Profiles

5.2.1.1 Bus 130 voltage and current Profile

The measurement of voltage profile in figure 5-4, taken before implementing the UPFC and The Distortion in the voltage signal (THD_v=12.74%).

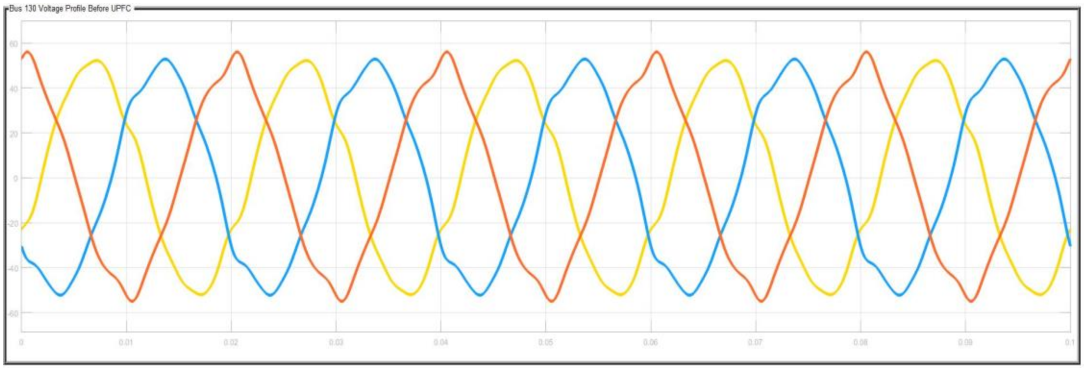

Figure 5.4 Bus 130 Voltage Profile before UPFC

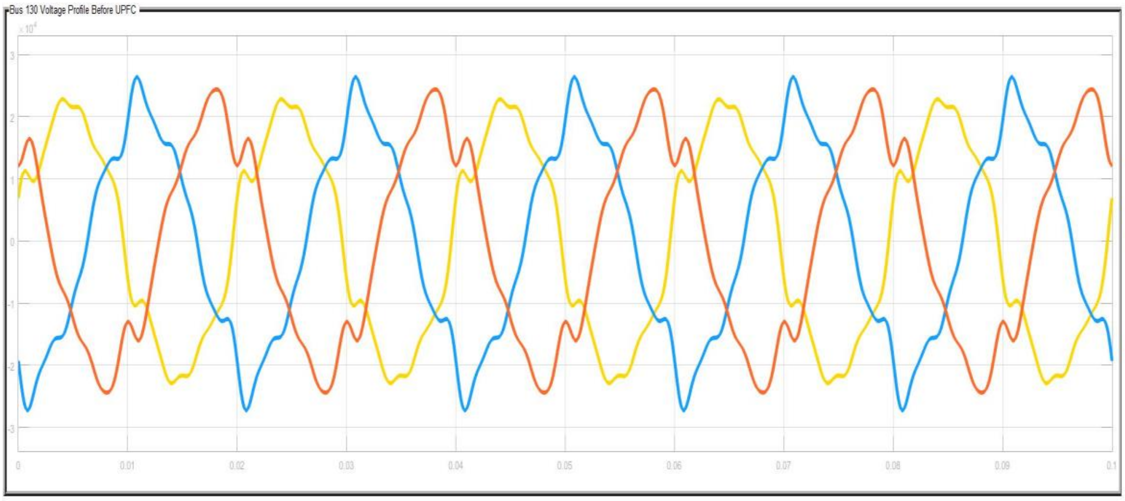

Figure 5-5. Bus 130 Current Profile before UPFC

The Total Harmonic Distortion (THD_i) at this bus reaches 48.96%, and the FFT analysis is shown in figure 5-6.

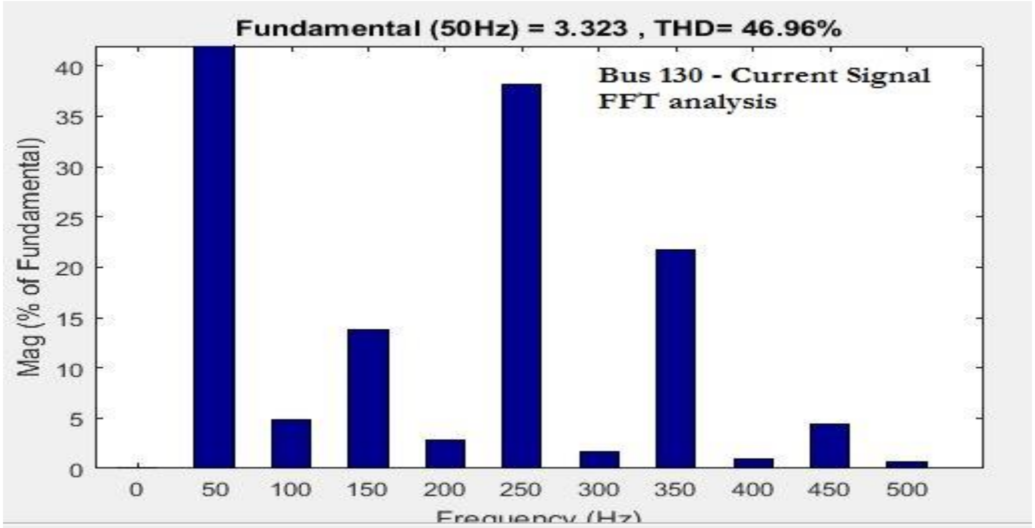

Figure 5-6.FFT analysis of Bus 130 Current signal

5.2.1.2 Bus 141 Voltage and Current Profile

These voltage measurements and profiles in figure 5-7, taken before implementing the UPFC and, the Distortion in the voltage signal THD_v= 13.01%.

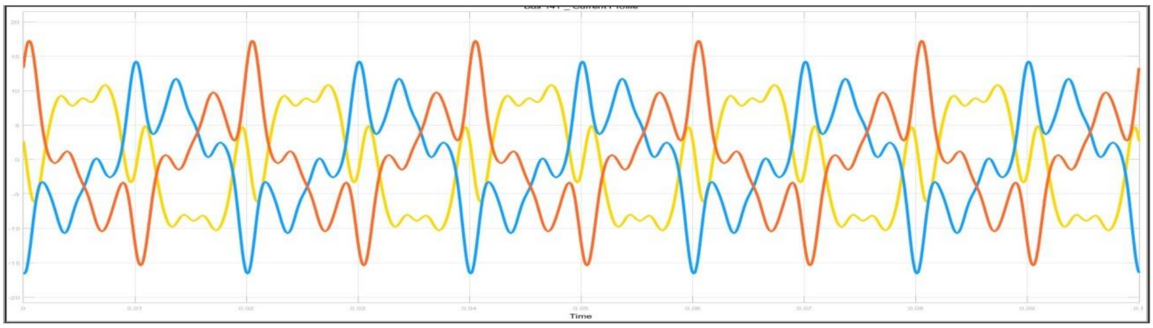

Figure 5-7.Bus 141_Voltage Profile before UPFC

The current measurement at the same bus mad the profile mentioned in figure 5-8.

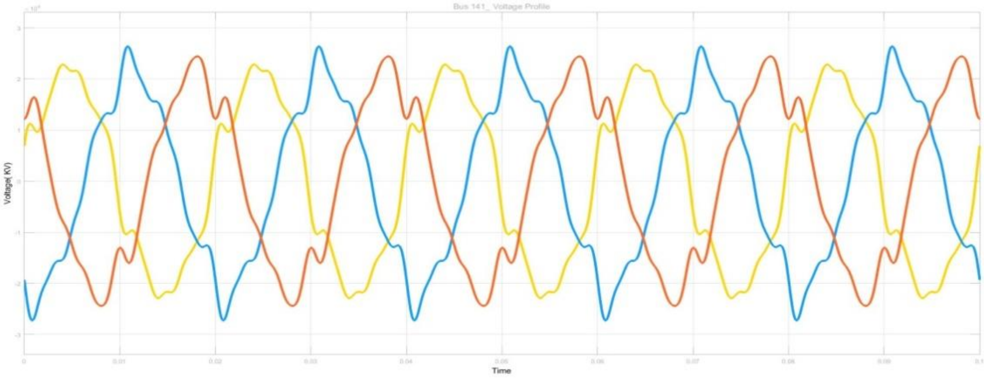

Figure 5-8.Bus 141_Current Profile before UPFC

The Harmonic distortion of the Current at Bus 141: THD_i=48.68%, and the FFT analysis as in figure 5-9.

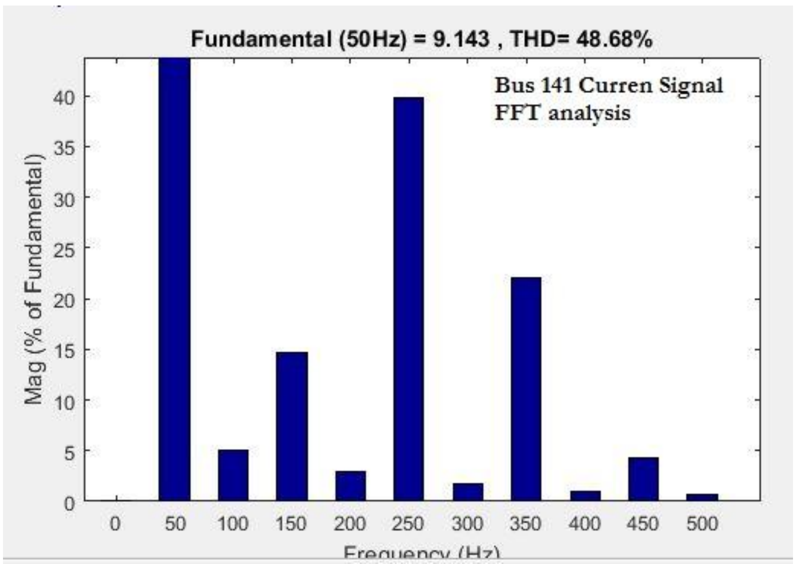

Figure 5-9.FFT analysis of Bus 141 Current signal

Bus 206 Voltage and Current Profiles

The voltage measurements drawn the profiles as shown in figure 5-10 which taken before implementing the UPFC. The Distortion in the voltage signal THD_v= 5.88%, and the Voltage level each this Bus is about 29.9 kV.

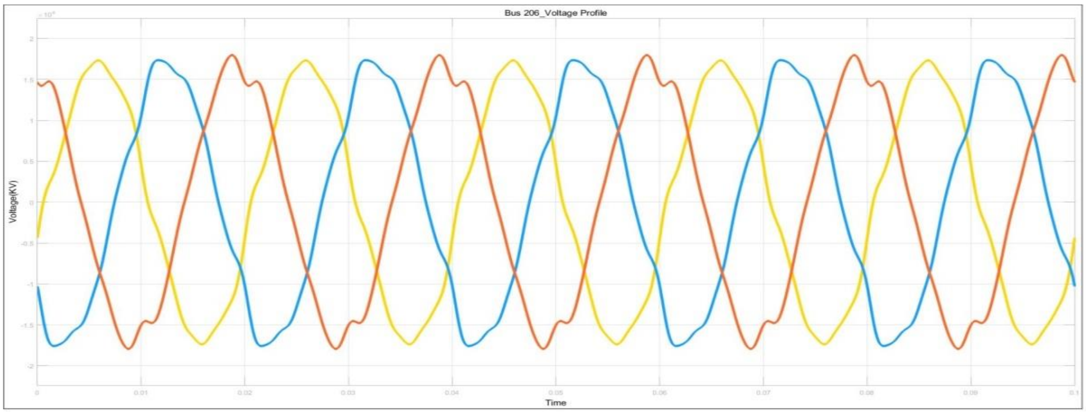

Figure 5-10. Bus 206 Voltage Profile before UPFC

The current profile at bus 206 as in figure 5-11.

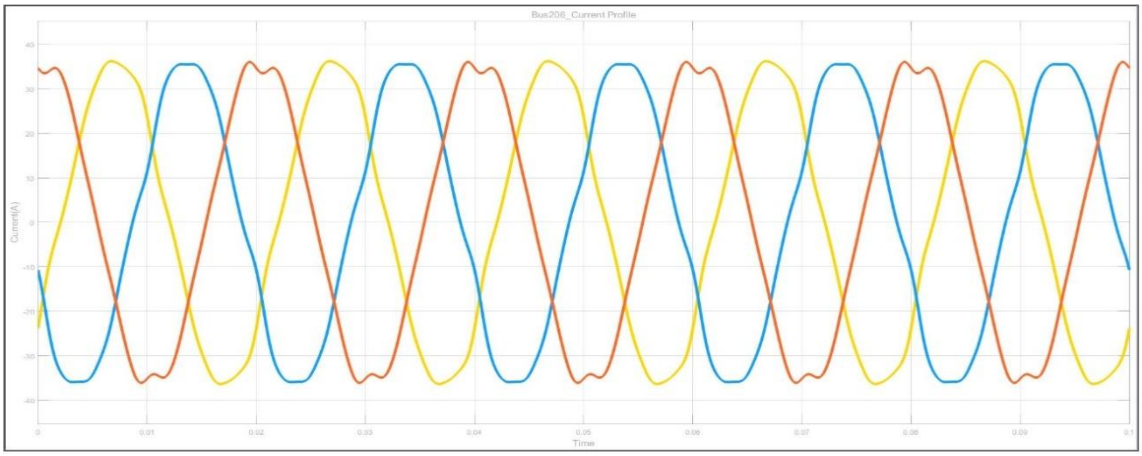

Figure 5-11. Bus 206 Current Profile before UPFC

Harmonic distortion of the Current at Bus 206: THD_i=4.24%, and the FFT analysis as in fig. 5-12.

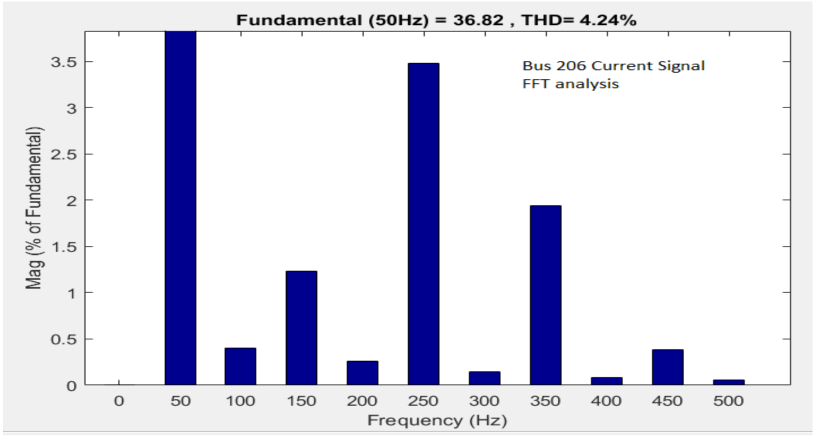

Figure 5-12.FFT analysis of Bus 206 Current signal

5.2.1.3 Bus 129 Current and Voltage Profiles

The voltage measurements drawn the profiles as shown in figure 5-13 which taken before implementing the UPFC.

The Distortion in the voltage signal THD_v= 13.1%.

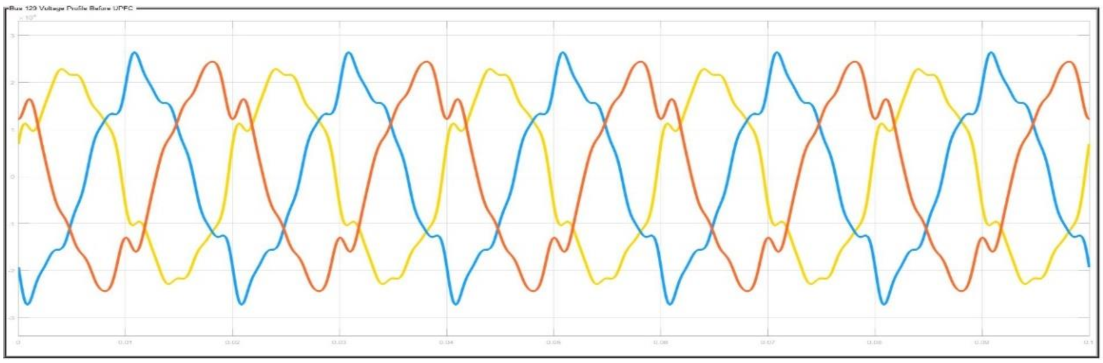

Figure 5-13.Bus 129 Voltage Profile before UPFC

The current profile at bus 206 as in figure5-14 and, the Harmonic distortion of the Current at Bus 129: THD_i=5.34%, and the FFT analysis as in fig. 5-15.

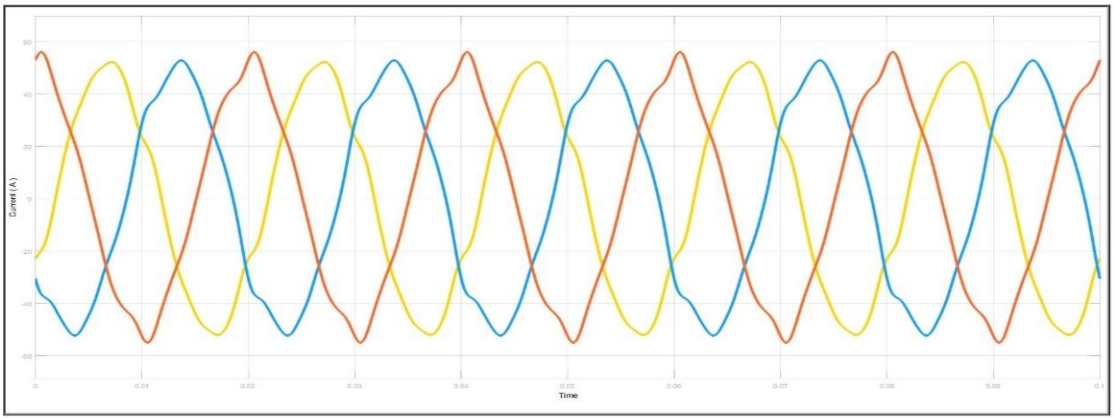

Figure 5-14.Bus 129 Current Profile before UPFC

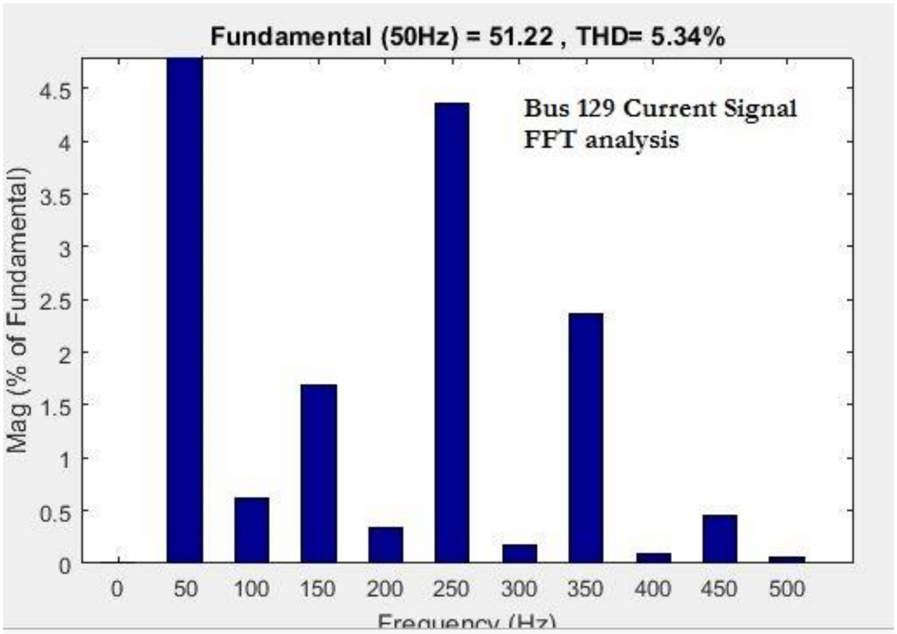

Figure 5-15.Bus 129 Current Signal FFT analysis

5.3 Summary of the Current and Voltage Profiles for Connection Point and Test Buses

Table 5-2.Maithaloon Grid Summary before UPFC

Bus ID	Bus Current	Bus Voltage	THD_i	THD_v
129			5.34%	13.1%
130			46.96%	12.74%
141			48.68%	13.01%
206			4.24%	5.88%
CP (Source)	97 A	33KV	5.96%	0.96%

5.4 Electrical Losses Due to the High Harmonic in the Medium Voltage Grid:

After Calculating the total losses from the harmonic on the Maithaloon MV grid with referring to the line impedance and the current flow due to each component of the harmonics on frequencies (100- 550) Hz, using equation 2-30, the table below summarizes the result.

Table 5-3. Maithaloon MV Grid Losses before UPFC

Total Losses (W)	79.40458967 W
W/Year	695584.2055 W
kWh/Year	695.5842055 kWh
Energy Price	0.32 Nis
Total Cost per Year	222.5869458 Nis
Maithaloon Grid Length	25.112 KM
Losses / KM/ Year	8.863768149 Nis

The effect of losses in the MV lines of the Maithaloon electrical network is not large because the operating voltage is 33 kV but there will be a huge effect on the transformer aging and losses (no and load losses) which will be explained later.

The Main effect of the high harmonic values can be seen on the low voltage side of the transformers (0.4KV side) the next test will show the number of losses of the LV side of one transformer.

5.4.1 Electrical Losses Due to the High Harmonic in the Low Voltage side of JD0142.

The JD0142 transformer has rated of 630 KVA and operate on 33/0.4 KV, the transformer has six feeders on its low voltage side which feed approximately 5000 m of (ABC 3*95mm2 +2*50mm2) cables. After measuring the exact loads on the secondary side and calculating the approximated losses due to the harmonics from (50-550) Hz and applying equation 2-30 the table below summarizes the results.

Table 5-4. Harmonic Losses on Low Voltage Feeders of JD0147

Total Losses (W)	818370.0026 W
W/Year	7168921223 W
kWh/Year	7168921.223 kW
Energy Price	0.32 Nis
Total Cost per Year	2294054.791 Nis
Maithaloon Grid Length	5000 M*
Losses /M/ Year	458.8109583 Nis

*the length of the low voltage grid estimated using GIS maps in Nedco centers.

5.4.2 Losses of Transformers Due to the High Harmonic of Low Voltage Grid.

According to the equations (2-25 to 2-29) the losses, and referring to the real measurements of loads and the detailed specific details of the transformer the losses on the transformer calculated in the following steps.

5.4.3 The Transformer technical Details

The 630 KVA transformer manufacturer data [43] summarized in the transformer test report and mentioned in the table below 5-5,

Table 5-5 630 KVA Transformer test report data

Item	**Description**
Primary Voltage	33000 Volt
Secondary Voltage	400 Volt
No. of taps and nominal tap	7 taps, nominal at 5
No-load Current (I_0%)	0.31%
Primary Resistance	12.150 Ohm
Secondary Resistance	0.750 m Ohm
Temperature (average winding rise)	55^0 C
Temperature (hottest-spot rise)	65^0 C
Load Losses (I^2R)	5530 W
No-load Losses	957 W
Rated Primary Current	11 A
Rated Secondary Current	909

5.4.3.1 The Real Measurements of the Transformer Loads

From the real measurements on the low voltage side of the transformer, the table 5-6 summarize the results and how far from the standard (IEC TR 61000-3-4:1998).

Table 5-6 Summary of the real Measurements on LV of transformer

Harmonic Number	Measured Data	Maximum Limit of MS 1555:2002(IEC TR 61000-3-4:1998)
1	367.7	
3	8.921	21.6
5	20.65	10.7
7	19.73	7.2
9	1.837	3.8
11	13.43	3.1
THD %	45.44%	25.72

5.5 Power Losses Calculations

Referring to the equations in chapter 2 and the equations which describe the load losses of the transformers under harmonic conditions.

- The total stray losses:

$$P_{TSL_R} = 5530 - 1.5\left(11^2 * 12.150 + 909^2 * \frac{0.750}{1000}\right) = 2395.2\ W$$

- The eddy current losses (P_{EC_R})

$$P_{EC_R} = 2395.2 * 0.4 = 958.08\ W$$

The value 0.4 taken from IEEE Std C57.110-2018- Table 14 “Estimate of distribution of total stray loss % for liquid immersed transformers”

- The Other Stray Losses

$$P_{OSL_R} = 2395.2 - 958.08 = 1437.12\,W$$

- The Harmonic Loss Factor due to the measured harmonics.

Table 5-7 Harmonic Loss and Stray loss factor calculations

h	I_h	I_h/I	$(I_h/I)^2$	h^2	$(I_h/I)^2 * h^2$	$h^{0.8}$	$(I_h/I)^2 * h^{0.8}$
1	367.7	0.404510451	0.163629	1	0.163628705	1	0.163628705
3	8.921	0.024261626	0.000589	9	0.005297639	2.408225	0.001417545
5	20.65	0.056159913	0.003154	25	0.078848396	3.623898	0.011429543
7	19.73	0.053657873	0.002879	49	0.141079201	4.743276	0.013656687
9	1.837	0.004995921	2.5E-05	81	0.002021697	5.799546	0.000144752
11	13.43	0.03652434	0.001334	121	0.161417321	6.809483	0.009084037
Total			0.171609		0.552292958		0.199361269

From the table above the Harmonic loss factor and harmonic factor for other stray loss calculated as below

$$F_{HL} = \frac{0.55229295}{0.171609} = 3.218$$

$$F_{HL_{STR}} = \frac{0.199361269}{0.171609} = 1.162$$

The total load losses of the transformer

$$P_{LL} = 5530 + 3.218 * 958.08 + 1.162 * 1437.12 = 10178.45\,W$$
$$= 10.178\,KW$$

5.6 Transformer Losses Due to Harmonic Load Current:

The table below summarizes the losses of the transformer due to the harmonics

Table 5-8 Summary of Transformer Losses due to harmonics

	Rated Losses	Losses due to harmonics
No Load	957 W	957 W
I^2R losses	5530 W	5530 W
Winding Losses	958.08 W	3083 W
Other Stray Losses	1437.12 W	1669.9 W
Total Losses	7925.2 W	10178.45 W

From the table above the losses of the transformer due to harmonics = 2253.2 W, so the harmonic on the secondary side of the transformer increases the losses by 28.5%.

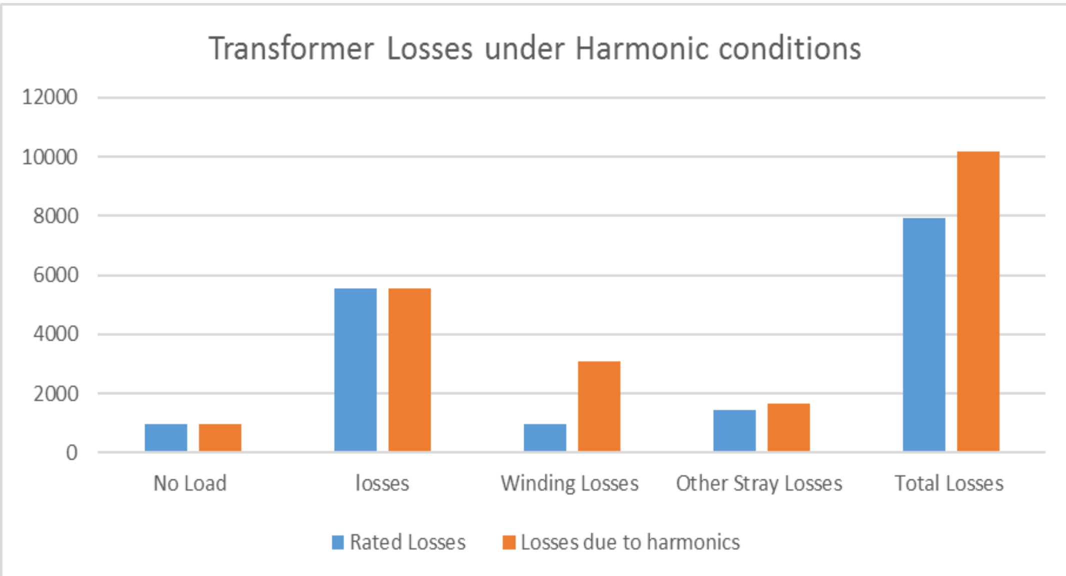

Figure 5-16 Summary of Transformer Losses due to harmonics

5.7 Location of UPFC and Test Buses:

The allocation of the UPFC was done several times and in different locations to assure the optimum operation of the grid, so many scenarios were done to reach the best case and better performance. The Proposed Locations of the UPFC and the test locations are shown in figure 5-17

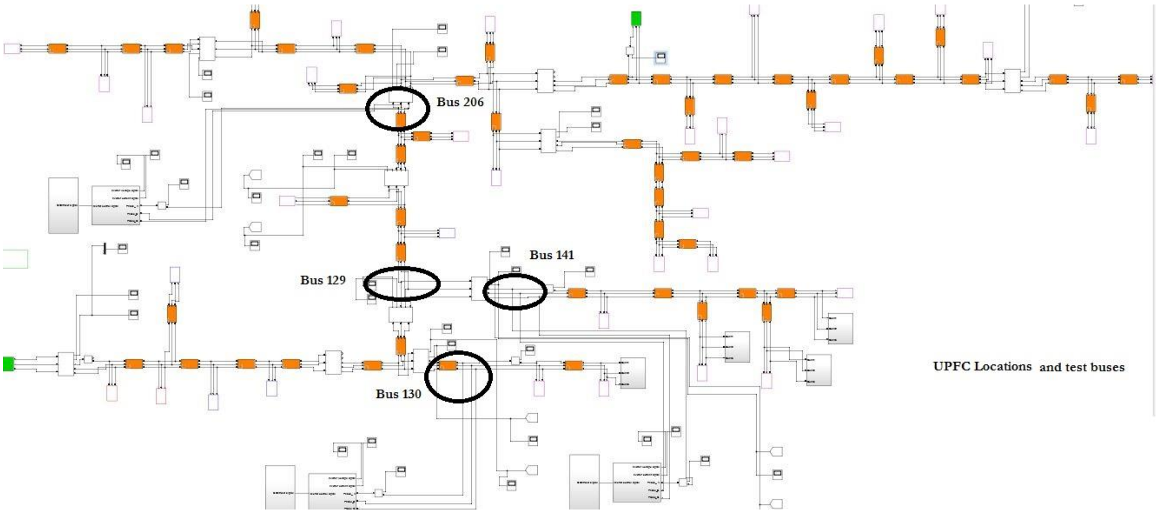

Figure 5-17. Location of UPFC and test buses

5.7.1 Operating the UPFC as STATCOM (harmonic filtering function)

On this test, the UPFC will operate like a harmonic filter to reach the best-operating conditions. And the test will be done on maximum current consumed from the connection point with maximum current, also the test will caried out on average load with average harmonic injected to grid.

5.7.2 The Scenario of Using Only one UPFC on Bus JT0141

In this case, the UPFC connected directly to the bus JT0141 to eliminate the generated harmonic forward this bus which is a highly distorted current wave as in fig.5-7, fig 5-8 for voltage and current respectively. On case of maximum load with maximum injected harmonics to the grid and after installing the UPFC the current wave form becomes as in fig. 5-18, and the voltages as in figure 5-19. The THD on current at this bus decreased from 48.68% before compensation to reach 3.36% on that bus. And the distortion on the voltage signal at this bus THD_v decreased from 13.01% to be 10.33%.

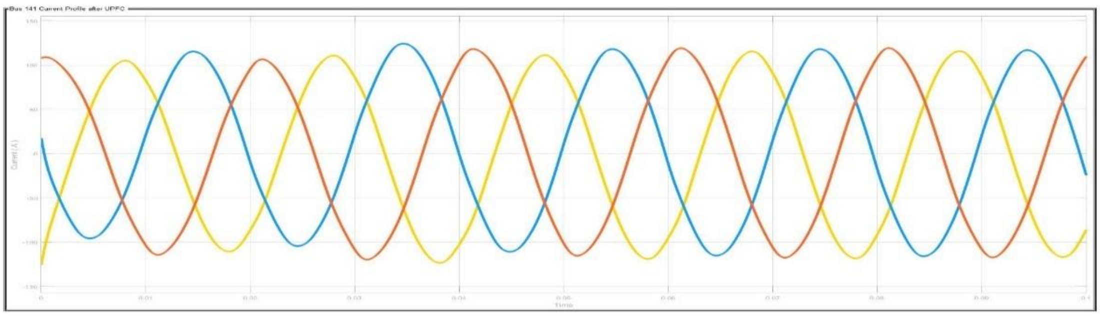

Figure 5-18. Current Profile at bus JT0141 after adding one UPFC as STATCOM

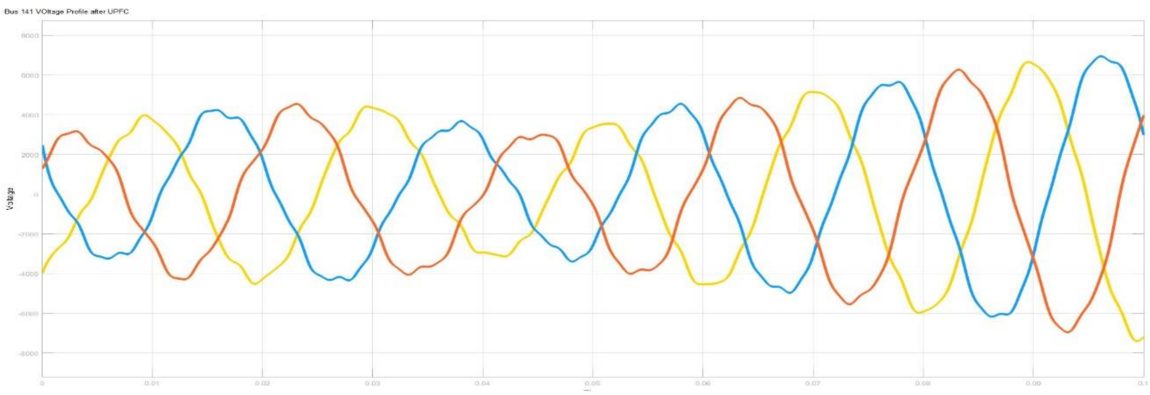

Figure 5-19.Voltage Profile at bus JT0141 after adding one UPFC as STATCOM

The Scenario of adding another UPFC on Bus JT0130

In this case, the UPFC connected directly to the bus JT0130 to eliminate the generated harmonic forward this bus which is a highly distorted current wave as in fig.5-4, fig 5-5 for voltage and current respectively. On case of maximum load with maximum injected harmonics to the grid and after installing the UPFC the current wave form becomes as in fig. 5-20, and the voltages as in figure 5-21. The THD on current at this bus decreased from 46.96 % before compensation to reach 5.91% on that bus. And the distortion on the voltage signal at this bus THD_v decreased from 12.74% to be 9.43%.

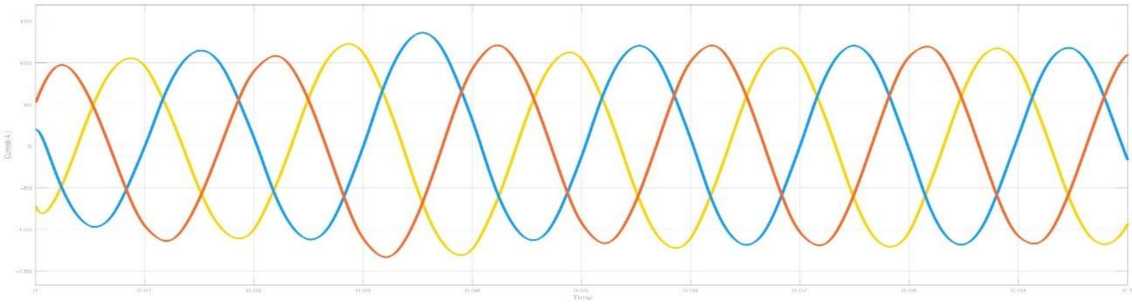

Figure 5-20.Current Profile at bus JT0130 after adding one UPFC as STATCOM

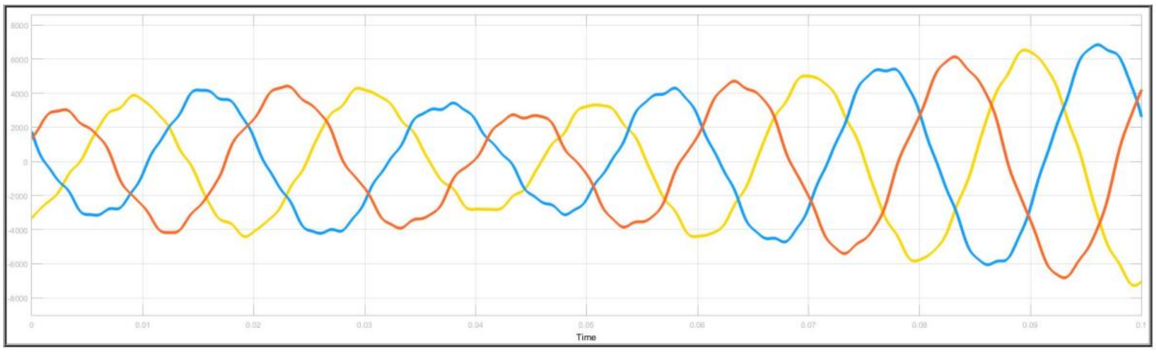

Figure 5-21.Voltage Profile at bus JT0130 after adding one UPFC as STATCOM

5.7.3 The Scenario of Adding Third UPFC on Bus JT0206

In this case, the UPFC connected directly to the bus JT0206 to eliminate the generated harmonic forward this bus which is a highly distorted current wave as in fig.5-10, fig 5-11 for voltage and current respectively. On case of maximum load with maximum injected harmonics to the grid and after installing the UPFC the current wave form becomes as in fig. 5-22, and the voltages as in figure 5-23. The THD on current at this bus decreased from 4.24 % before compensation to reach 1.84% on that bus. And the distortion on the voltage signal at this bus THD_v decreased to be 9.43%.

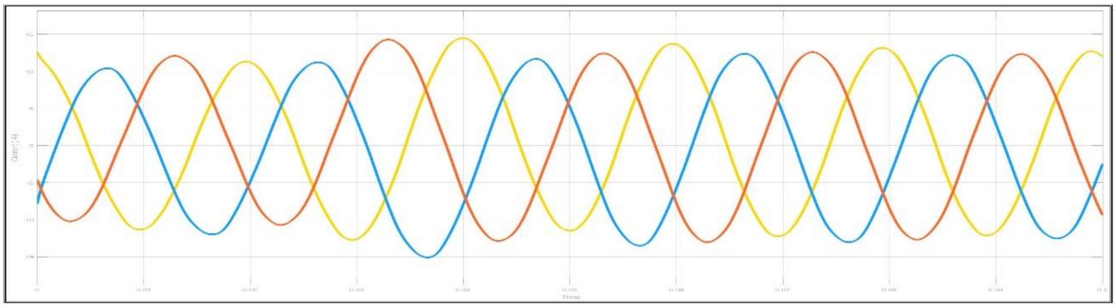

Figure 5-22.Current Profile at bus JT0206 after adding one UPFC as STATCOM

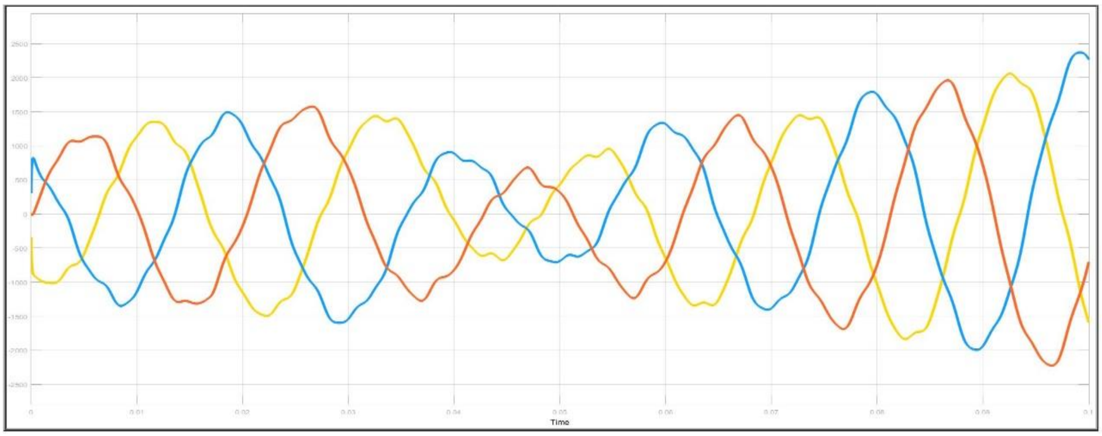

Figure 5-23.Voltage Profile at bus JT0206 after adding one UPFC as STATCOM

5.8 Summary of Operating the UPFC as STATCOM to Filtering the Harmonic of the Grid:

The total harmonic distortion on the tested buses decreased improved and be within the acceptable limits, the fig.5-24 shows the improvement of the THD_i after operating all the compensators together.

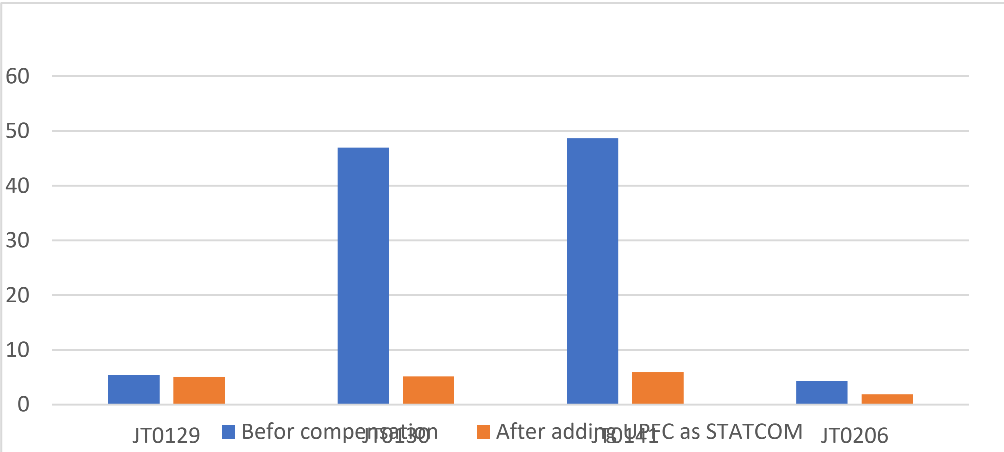

Figure 5-24.Improving the current THD after adding UPFC as STATCOM

The improvement on the voltages due to the harmonic elimination mentioned in the fig 5-25.

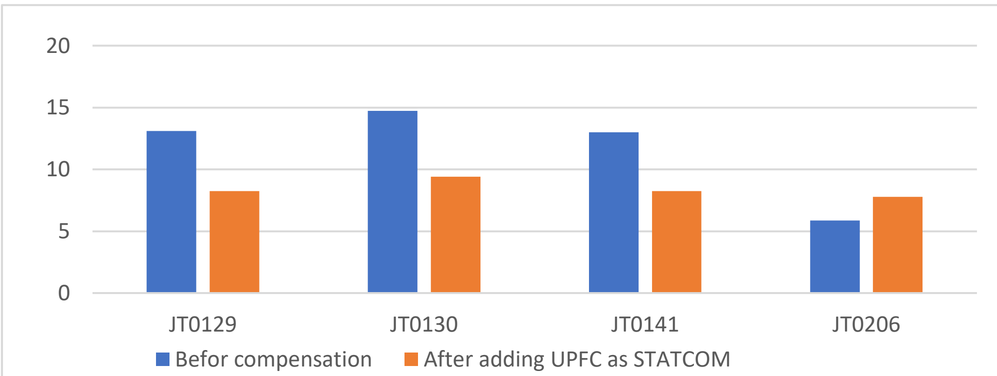

Figure 5-25.Improving the Voltage THD adding UPFC as STATCOM

In Summary, this operation mode eliminates the harmonics and improve the power quality of the current and voltage.

5.9 Adaptive Operation of the UPFC on Different Load Conditions:

In this case, the UPFC connected directly to the bus JT0141 to test the adaptive operation and eliminate the injected harmonic forward this bus. In this case the load reduced and the injected harmonics decreased (THD_ι= 33.93%) and the load current as shown in figure 5-26. Also, the voltage profile shown in fig.5-27.

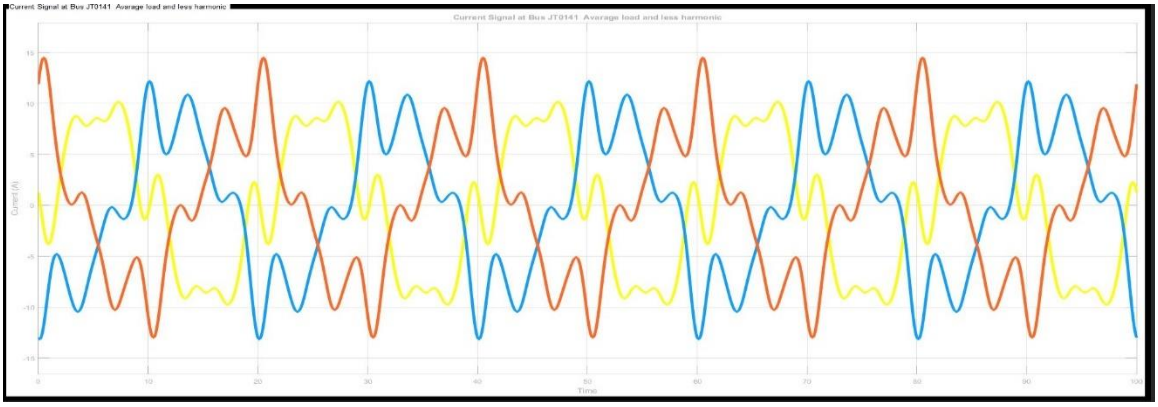

5-26. Current Waveform in case of low load with lower harmonic injection

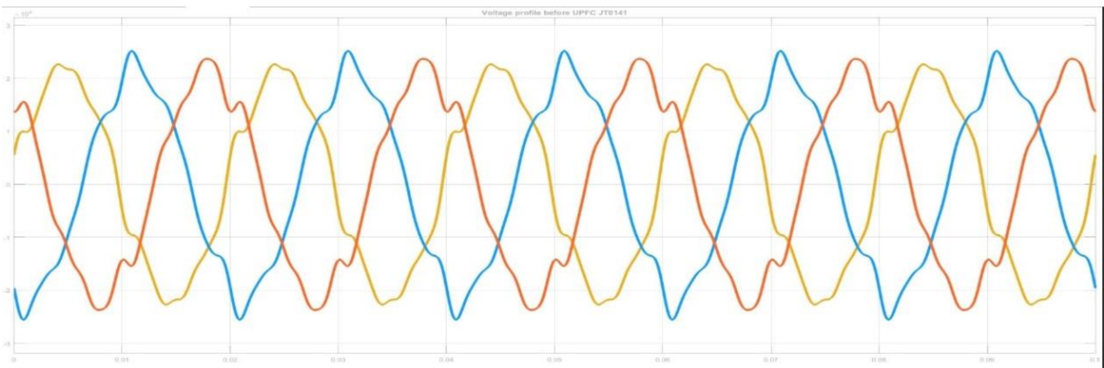

Figure 5-27. Voltage Waveform in case of load with lower harmonic injection

After installing the UPFC the current wave form becomes as in fig. 5-28, and the voltages as in figure 5-29. The THD on current at this bus decreased from 33.93% before compensation to reach 4.75% on that bus. And the distortion on the voltage signal at this bus THD_v decreased from 9.41% to be 4.71%.

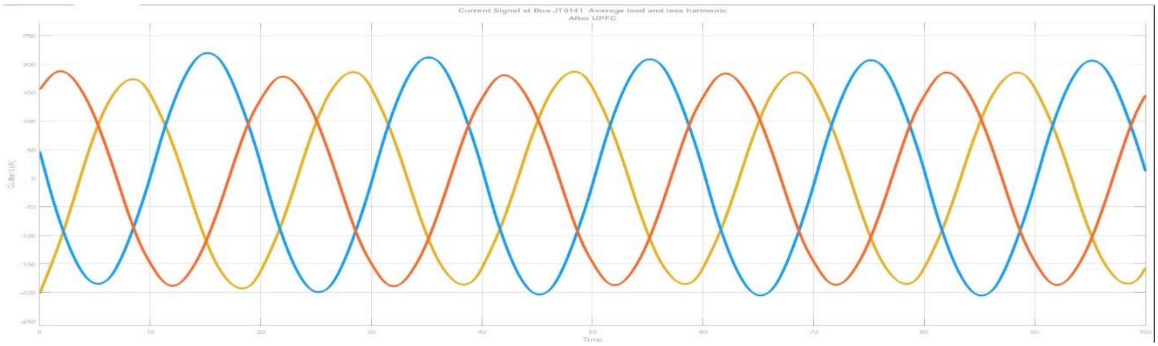

5-28. Current Signal After UPFC at but JT0141 low load

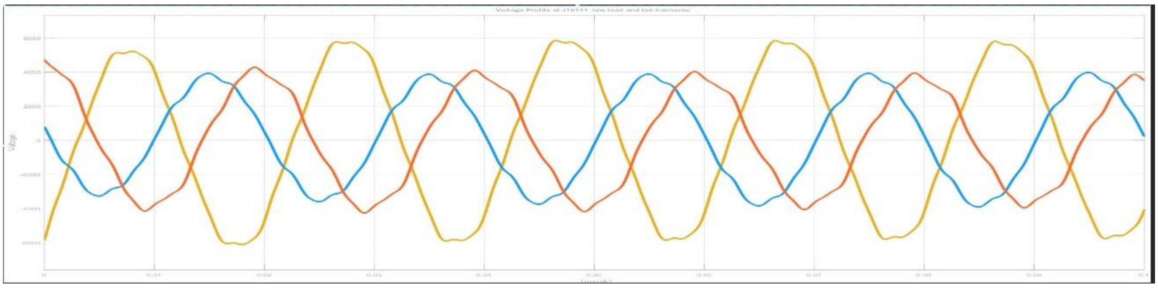

5-29.Voltage signal after UPFC at but JT0141 low load

In Summary, the UPFC operated as an active device since it can operate correctly on different operating scenarios and do the required tasks in mitigation the harmonics. The table summaries both operation cases.

Table 5-9. Operation Summary of UPFC on different load conditions at same bus (JT0141)

Condition	Load current On 33 kV	THD_i		THD_v	
		Before UPFC	**After UPFC**	**Before UPFC**	**After UPFC**
High load	About 12 A	48.68%	3.36%	13.01%	10.33%
Low load	About 8 A	33.93 %	4.75%	9.41%	4.71%

5.9.1 Operating the UPFC as Voltage Compensator

The Voltages in the grid around the normal operating voltage level (V_{LL}=33KV & V_{Ph}=19KV) except the buses after bus JT0206 the voltage drop to reach about ($V_{LL} = 28KV$ & $V_{Ph} = 19KV$) and need to install the compensation to improve the voltages.

5.9.2 The Location of the UPFC to Improve the Voltage Profiles

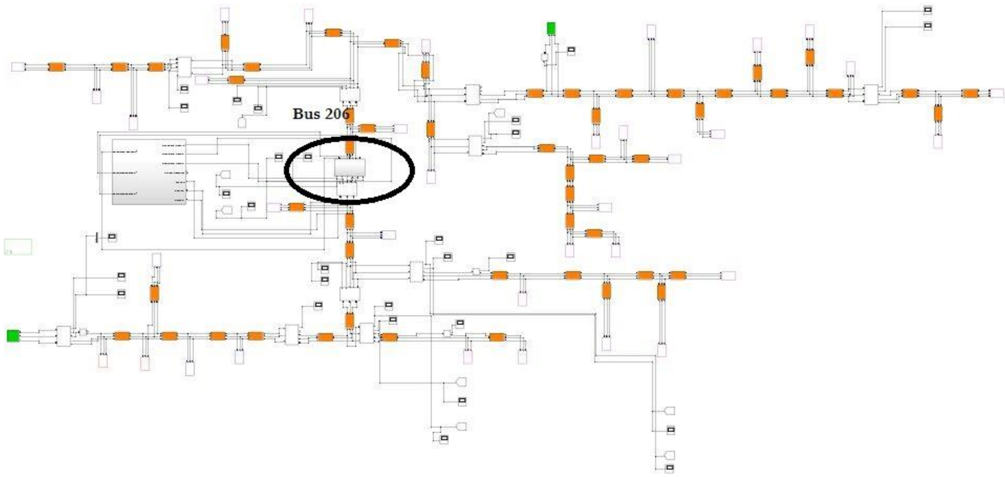

Figure 5-30. The Location of the UPFC in SVC mode.

5.9.3 MEffect of the Series Compensator on Bus JT0206

The voltages at this bus after adding the UPFC in SVC mode and the increase in voltage as shown in figure 5-31.

The voltage at this bus and the buses after JT0206 reached about $V_{LL} = 28KV$ & $V_{Ph} = 16KV$, so it is important to improve the voltages to get the needed voltages, the fig.5-31 show the voltages after improvement.

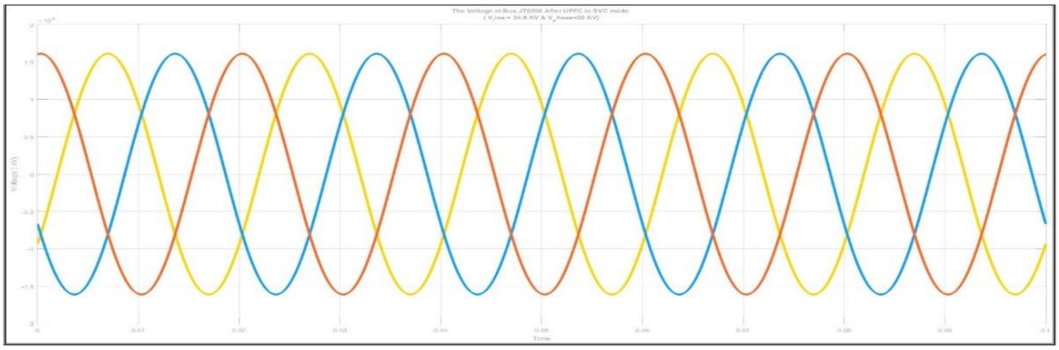

Figure 5-31.Voltage Profile at Bus JT0206 After UPFC in SVC mode

The voltages at bus JT0206 after UPFC becomes $V_{LL} = 34.6KV$ & $V_{Ph} = 20KV$, and the voltages reached the optimum voltages and can use the offload tap changers on the transformers to step down the voltages and reached 0.4KV at low voltage side.

Chapter Six

Results and standard verifications

The Power quality is a serious issue to deal with in electrical power systems because of its side effects on the electrical equipment of the grid. The most common causes of poor power quality can be broken down into four distinct areas: harmonic pollution, low power factor, load imbalances, and voltage variations. The bad quality of power increases the power losses of Transformers, transmission lines and decrease their estimated lifetime, Also, the poor power quality leads to bad effects on the protection coordination schema on power grids.

The harmonic pollution caused to be the nonlinear loads, power electronic drivers, and distributed generations. It leads to malfunction of many sensitive devices, elevators, digital systems, and other medical electrical equipment. In power grids the harmonics increase the transformer losses, oil temperature, increase the transmission lines losses, and the corona effect, also it affects the protection relays and forces them to operate unprobeable.

The large Voltage Variation in electrical grids caused by renewable sources, Photovoltaic, and wind turbines since they produce energy from uncontrolled energy sources. These sources cause voltage sag(dip) and swell(rise) in the voltage profiles. The flicker is a type of voltage variation and is made from the fast-current variation because of a lightning strike, arc furnace, and starting heavy load.

The low power factor is the relation between the active and reactive power delivered toward the loads. As the reactive power increase the real power and power factor decrease which increase the transmission lines losses, decrease their capability, and decrease the overall efficiency of the power grid. Also, the utilities have to pay penalties because of poor power factor.

The IEC61000 and the IEEE Standard 519-1992, are power quality standards which standardize and control the maximum permissible acceptable limits of each case of power quality issue.

6.1 Standards and Power Quality Codes:

6.1.1 Voltage Harmonic Limits According to IEEE 519-1992

Table 6-1. Voltage Limits IEE 519-1992

Bus Voltage at PCC	Individual Voltage Distortion (%)	Total Voltage Distortion THD (%)
69 KV and below	3	5.0
69.001KV through 161 KV	1.5	2.5
161.001 and above	1.0	1.5

6.1.2 Current Harmonic Limits (<69KV) According to IEEE 519-1992

Table 6-2 Current Harmonic Limits IEEE 519-1992

I_{SC}/I_L	< 11	$11 \leq h \leq 17$	$17 \leq h \leq 23$	$23 \leq h \leq 35$	$35 \leq h$	TDD
< 20	4.0	2.0	1.5	0.6	0.3	5.0
$20 < 50$	7.0	3.5	2.5	1.0	0.5	8.0
$50 < 100$	10.0	4.5	4.0	1.5	0.7	12.0
$100 < 1000$	12.0	5.5	5.0	2.0	1.0	15.0
> 1000	15.0	7.0	7.0	2.5	1.4	20.0

6.1.3 Steady-State Voltage quality performance level according IEEE Std 1250-2011 based on IEC 61000-4-30-2008.

Table 6-3.Steady-State Voltage quality performance

Power Quality category	***Planning Levels***
Voltage regulations	±5% of nominal for normal conditions
	±10% of nominal for normal conditions
Voltage unbalance	2% negative sequence
Voltage distortion	5% total harmonic distortion
	3% individual harmonic components
Voltage fluctuation/flicker	P_{st} less than 10
	Individual step changes less than 4%
Voltage frequency	±0.015 Hz

6.2 The Real Power Quality Measurements on the Real Grid:

As mentioned in table 2-2, the values of harmonic currents on each frequency from 100 up to 550 Hz, and figure 2-9, mentioned the harmonic profile measured on Maithaloon Grid. The maximum total harmonic distortion THD_i= 46%-54%.

The Voltage Profiles at PCC was good but at far distances and due to the high loads, the voltages decreased and become out of range and reached 28KV at sometimes.

6.3 The Results of Integrating The UPFC to Maithaloon Grid.

As discussed in chapter 5, the figures 5-26 and 5-27 summarized the effect of adding the UPFC on the harmonic distortion of the voltage and current. So, the effect of this improvement will decrease the electrical losses on the transmission lines and transformers.

Chapter Seven

Conclusion

The integration of UPFC on the Maithaloon electrical grid which has a poor quality of electrical source due to the high penetration of solar systems, water pump drivers, and other heavy loads, make a huge effect for improving the power quality and decreasing the technical losses in the transmission lines and transformers.

In a medium-voltage network (33 KV grid), the effect of integrating UPFC centrally to improve the harmonic on the transmission line was great with a small effect on losses due to the lower currents in these grids. The transformer losses due to the harmonics increased by about 28.5% which is a high value for the loaded transformers. On the low voltage test done to check the effect of the harmonics on the electrical losses the results show that the harmonics cause a huge effect on low voltage networks since the currents are high and the current components other than the harmonics increased, but on this grid the interconnection UPFC to make better effect it proposed to connect them distributed near the nonlinear loads.

The UPFC can operate in many conditions, power quality compensator, power factor improvement device, voltage balancing device, and any other need due to the flexibility of controlling the inverter and power storage devices.

References

[1] A. M. Khaskheli, . M. . A. Mahar, . A. S. Larik and S. . H. Bhellar, ***"Power Quality Improvement in Power System Network using Unified Power Flow Controller,"*** in *5th International Multi-Topic ICT Conference (IMTIC), IEEE, ISBN. 978-1-5386-6594-7* , 20 .9. 2018.

[2] Kothari, J. I and Nagrath, **Modern Power System Analysis**, New York, 2007.

[3] A. Keyhani, A. Abur and S. Hao, ***"Evaluation of Power Flow Techniques for Personal Computers,"*** *IEEE Trans- actions on Power Systems,* vol. 4, pp. 817-826.

[4] F. Milano, ***"Continuous Newton's Method for Power Flow Analysis,"*** *IEEE Transactions on Power Systems,* vol. 24, pp. 50-57, 2009.

[5] J. J. Grainger and W. D. Stevenson, ***"Power System Analysis,"*** *McGraw-Hill, New York,* 1994.

[6] H. W. Kabisama, **Electrical Power Engineering**, New York: McGraw-Hill.

[7] H. Hale and R. W. Goodrich, ***"Digital Computation or Power Flow—Some New Aspects,"*** *Power Apparatus and Systems,* vol. 78, no. Transactions of the American Institute of Electrical Engineers, pp. 919-923, 1959.

[8] G. M. Gilbert , D. E. Bouchard and A. Y. Chikhani, ***"A Comparison of Load Flow Analysis Using Dist Flow, Gauss-Seidel, and Optimal Load Flow Algorithms,"*** in *Proceedings of the IEEE Canadian Conference on Electrical and Computer Engineering*, Waterloo, Ontario, 24-28 May 1998.

[9] J. D. Glover and M. S. Sarma, **Power System Analysis and Design,** 3rd ed., Pacific Grove: Brooks/Cole, 2002.

[10] B. Stott and O. Alsac, ***"Fast Decoupled Load Flow,"*** *IEEE Transactions on Power Apparatus and Systems,* Vols. PAS-93, pp. 859-869, 1974.

[11] B. Stott, ***"Review of Load-Flow Calculation Methods,"*** *Proceedings of the IEEE,* vol. 62, pp. 916-929, 1974.

[12] I. A. Adejumobi, ***"Numerical Methods in Load Flow Analysis: An Application to Nigeria Grid System,"*** *International Journal of Electrical and Electronics Engineering (IJEEE),* vol. 3, 2014.

[13] IEEE std C57.110-2018, ***"IEEE Recommended Practice for Establishing Liquid-Immersed and Dry-Type Power and Distribution Transformer Capability When Supplying Nonsinusoidal Load Currents.".***

[14] M. A. Fathi, H. Y. Karim and . B. H. Hossam Alden , ***"Effect of harmonics on distance relay in short and medium transmission lines,"*** in *2016 Eighteenth International Middle East Power Systems Conference (MEPCON),* Cairo, Egypt , 2016.

[15] S. K. A., . A. M, K. R, A. s. Y, . A.-Q. Z. and . A.-B. M, ***"The Effect of the Harmonics, the Fault Location and the Fault Resistance on the Performance of the Impedance-Type Distance Relay,"*** *American Journal of Applied Sciences,* vol. 6, no. 4, pp. 788-796, 2009.

[16] *Ndco Team modelling of Grid parameters,* 2019.

[17] A. Kumar and A. Barik, ***"Power System Stability Using FACTS,"*** *IJMER,* vol. 1, no. 2,pp-666-672, 2018.

[18] S. Muthukrishnan and A. N. Kumar, ***"Comparison of Simulation and Experimental Results of UPFC used for Power Quality Improvement,"*** *International Journal of Computer and Electrical Engineering,* vol. 2, pp. 555-559, 2010.

[19] Y. Chen, B. Mwinyiwiwa, Z. Wolanski and B. T. Ooi, ***"Unified power flow controller (UPFC) based on chopper stabilized diode-clamped multilevel converters,"*** *IEEE Trans. Power Electron.,* vol. 15, no. 2, p. 258–267 , 2000.

[20] J. Wang and F. Z. Peng, ***"Unified power flow controller using the cascade multilevel inverter,"*** *IEEE Trans. Power Electron,* vol. 19, no. 4, p. 1077–1084 , 2004.

[21] F. Z. Peng, Y. Liu, S. Yang, S. Zhang, D. Gunasekaran and U. Karki, ***"Transformer-less unified power-flow controller using the cascade multilevel inverter,"*** *IEEE Trans. Power Electron,* vol. 31, no. 8, p. 5461–5472 , 2016.

[22] L. Xu and V. G. Agelidis, ***"Flying capacitor multilevel PWM***

converter based UPFC," *IEE Proc. Electr. Power Appl,* vol. 149, no. 4, p. 304–310 , 2002.

[23] L. Gyugyi, ***"Unified power-flow control concept for flexible AC transmission systems,"*** *IEE Proc. C,* vol. 139, no. 4, p. 323–331, 1992.

[24] C. D. Schauder, L. Gyugyi and M. R. Lund, ***"Operation of the unified power flow controller (UPFC) under practical constraints,"*** *IEEE Trans.Power Del.,* vol. 13, no. 2, p. 630–639, 1998.

[25] L. Gyugyi, C. D. Schauder, S. L. Williams, T. R. Rietman, D. R. Torgerson and A. Edris, ***"The unified power flow controller: A new approach to power transmission control,"*** *IEEE Trans. Power Del.,* vol. 10, no. 2, p. 1085–1097, 1995.

[26] J. Bian, D. G. Ramey, R. J. Nelson and A. Edris, ***"Astudy of equipment sizes and constraints for a unified power flow controller,"*** *IEEE Trans. Power Del.,* vol. 12, no. 3, p. 1385–1391, 1997.

[27] K. S. Verma, S. N. Singh and H. O. Gupta, ***"Location of unified power flow controller for congestion managment,"*** *Electr. Power Syst. Res.,* vol. 58, no. 2, p. 89–96, 2001.

[28] M. Moazzami, M. J. Morshed and A. Fekih, ***"A new optimal unified power flow controller placement and load shedding coordination approach using the hybrid imperialist competitive algorithm-pattern search method for voltage collapse prevention in power systems,"*** *Int. J. Electr. Power Energy Syst.,* vol. 79, p. 263–274, 2016.

[29] K. Lee, H. Koizumi and K. Kurokawa, ***"Voltage control of D-UPFC between a clustered PV system and Distribution System,"*** in *Proc. IEEE Annual Power Electronics Specialists Conf*, Jeju, South Korea, June,2006.

[30] M. A. Sayed and T. Takeshita, ***"'Line loss minimization in isolated substations and multiple loop distribution systems using the UPFC,"*** *IEEE Trans. Power Electron,* vol. 29, no. 11, p. 5813–5822, 2014.

[31] S. G. Pavlos and D. H. Nikos, ***"Unified Power Flow Controllers in Smart Power Systems: Models, Methods,and Future Research,"*** *IET smart Grid ,* 2018.

[32] P. Garcia-Gonzalez and A. Garcia-Cerrada, ***"Detailed analysis and experimental results of the control system of a UPFC,"*** *IEE Proc. Gener. Transm. Distrib.*, vol. 150, no. 2, p. 147–154, 2003.

[33] A. Sonnenmoser and P. W. Lehn, ***"Line current balancing with a unified power flow controller,"*** *IEEE Trans. Power Del.,* vol. 14, no. 3, p. 1151–1157, 1999.

[34] C. D. Schauder, L. Gyugyi and M. R. Lund, ***"'Operation of the unified power flow controller under practical constraints,"*** *IEEE Trans.Power Del.,* vol. 13, no. 2, p. 630–639, 1998.

[35] I. Papic, P. Zunko, D. Povh and M. Weinhold, ***"Basic control of unified power flow controller,"*** *IEEE Trans. Power Syst.,* vol. 12, no. 4, p. 1734–1739, 1997.

[36] S. Kannan, S. Jayaram and M. M. A. Salama, ***"Real and reactive***

power coordination for a unified power flow controller," *IEEE Trans. Power Syst.,* vol. 19, no. 3, p. 1454–1461, 2004.

[37] J. Monteiro, J. F. Silva, S. F. Pinto and J. Palma, ***"'Matrix converter-based unified power-flow controllers: Advanced direct power control method,"*** *IEEE Trans. Power Del.,* vol. 26, no. 1, p. 420–430, 2001.

[38] M. Vilathgamuwa, X. Zhu and S. S. Choi, ***"A robust control method to improve the performance of aunified power flow controller,"*** *Electr. Power Syst.* , vol. 55, no. 2, p. 103–111, 2000.

[39] H. Xie, Y. H. Song, A. Yokoyama and M. Goto, ***"Integrated linear and nonlinear control of unified power flow controllers for enhancing power system stability,"*** *Electr. Power Compon. Syst.,*, vol. 31, no. 4, p. 335–347, 2003.

[40] H. Fujita, H. Akagi and Y. Watanabe, ***"Dynamic control and performance of a unified power flow controller for stabilizing an AC transmission system,"*** *IEEE Trans. Power Electron,* vol. 21, no. 4, p. 1013–1020, 2006.

[41] K. Saleh and N. Hantouli, ***"A photovoltaic integrated unified power quality conditioner with a 27-level inverter,"*** *TELKOMNIKA,* vol. 6, p. pp.101~10x, December 2019.

[42] S. Bhattacharya and D. Divan, ***"Synchronous frame based controller implementation for a hybrid series active filter system,"*** in *IEEE Industry Applications Conference Thirtieth IAS Annual Meeting,* USA, 1995.

[43] TRANSFOMAX TRANSFORMER SA, ***"TRANSFORMER TEST REPORT,"*** Turkey, 2020.

[44] R. Mageshvaran, I. J. Raglend, V. Yuvaraj, P. Rizwankhan, T. Vijayakumar and Sudheera, ***"Implementation of Non-Traditional Optimization Techniques (PSO, CPSO, HDE) for the Optimal Load Flow Solution,"*** in *TENCON2008- 2008 IEEE Region 10 Conference*, 19-21 November 2008.

[45] O. . I. Elgerd, **Electric Energy Systems Theory: An Introduction**, 2 ed., Mc-Graw-Hill, 2012.

[46] N. Sato and W. F. Tinney, ***"Techniques for Exploiting the Sparsity or the Network Admittance Matrix,"*** *IEEE Transactions on Power Apparatus and Systems,* vol. 82, pp. 944-950, 1963.

[47] B. Aroop, B. Satyajit and H. Sanjib, ***"Power Flow Analysis on IEEE 57 bus System Using Mathlab,"*** *International Journal of Engineering Research & Technology (IJERT),* vol. 3, 2014.

[48] KACO, ***"KACO-newenergy,***" 2020. [Online]. Available: https://kaco-newenergy.com/downloads/.

Appendix 1

Electrical Equipment Locations

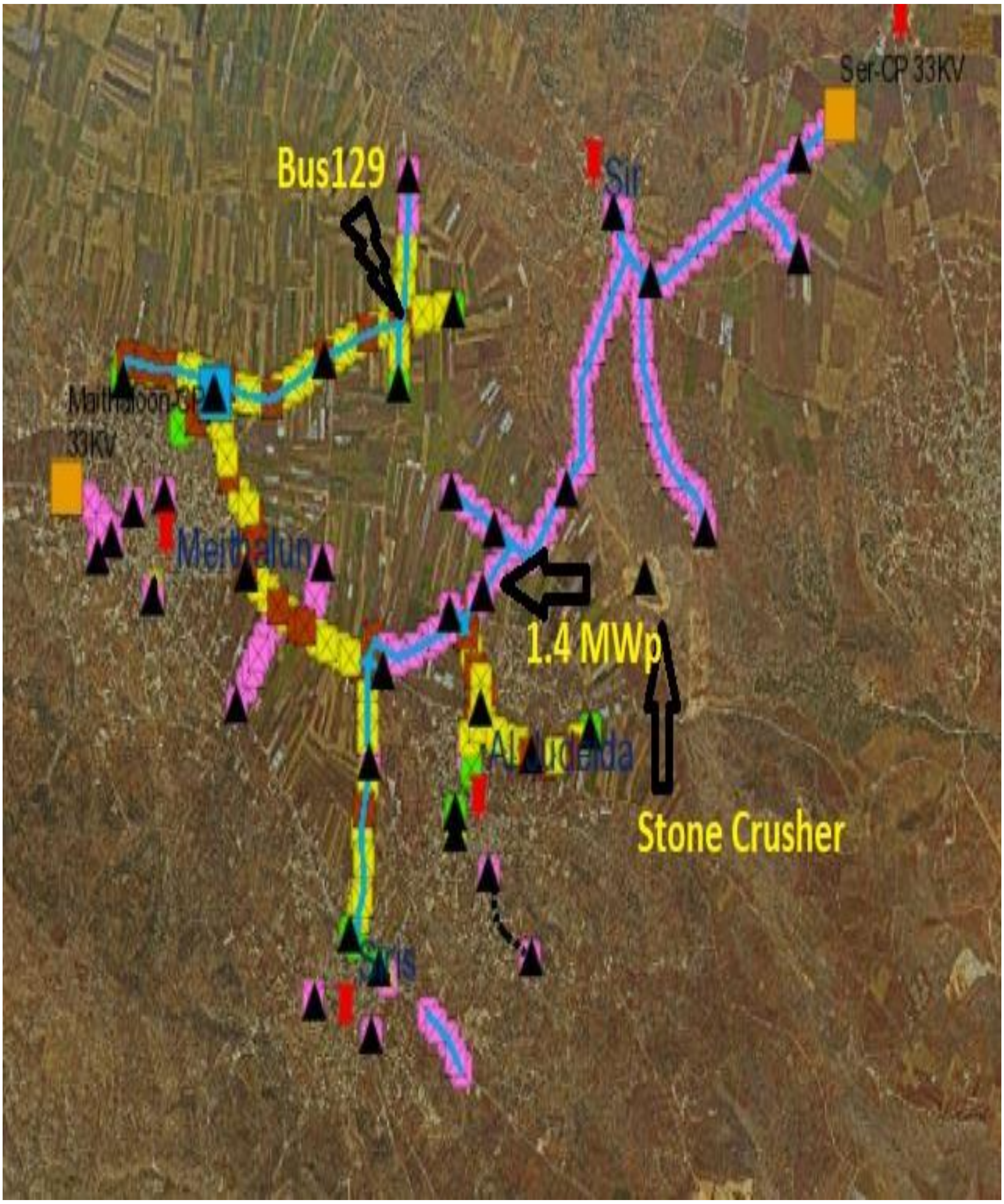

Appendix 2

Detailed Data for Cables and OHL

Cable ID	Cable Type	Length	DC Resistance per phase R'(20°C) in Ohm/km	Reactance X' in Ohm/km	Cable Resistance Ohm	Cable Reactance Ohm
JT0008-JT0001	ACSR 70	460	0.413	0.331	0.18998	0.15226
JT0001-JT0642	3*(1*50mm),36 KV,CU	440	0.387	0.203786	0.17028	0.08966584
JD0001-JT0641	3*(1*50mm),36 KV,CU	270	0.387	0.203786	0.10449	0.05502222
JT0642-JT0643	3*(1*50mm),36 KV,CU	360	0.387	0.203786	0.13932	0.07336296
JT0643-JT0009	3*(1*50mm),36 KV,CU	410	0.387	0.203786	0.15867	0.08355226
JT0009-JT0130	ACSR 70	350	0.413	0.331	0.14455	0.11585
JT0130-JT0131	ACSR 70	60	0.413	0.331	0.02478	0.01986
JT0130-JT0129	ACSR 70	30	0.413	0.331	0.01239	0.00993
JT0131-JT0170	ACSR 95	930	0.2992	0.311	0.278256	0.28923
JT0129-JT0021	ACSR 70	1000	0.413	0.331	0.413	0.331
JT0021-JT0024	ACSR 70	320	0.413	0.331	0.13216	0.10592
JT0129-JT0141	ACSR 95	1020	0.2992	0.311	0.305184	0.31722
JT0141-JT0148	ACSR 95	680	0.2992	0.311	0.203456	0.21148
JT0148-	ACSR 95	300	0.2992	0.311	0.08976	0.0933

JT0158						
JT0148-JT0149	ACSR 95	40	0.2992	0.311	0.011968	0.01244
JT0149-JT0178	ACSR 95	750	0.2992	0.311	0.2244	0.23325
JT0149-JT0154	ACSR 95	440	0.2992	0.311	0.131648	0.13684
JT0024-JT0032	ACSR 70	650	0.413	0.331	0.26845	0.21515
JT0024-JT0033	ACSR 70	263	0.413	0.331	0.108619	0.087053
JT0033-JT0037	ACSR 70	365	0.413	0.331	0.150745	0.120815
JT0033-JT0206	ACSR 70	575	0.413	0.331	0.237475	0.190325
JT0206-JT0203	ACSR 70	130	0.413	0.331	0.05369	0.04303
JT0206-JT0104	ACSR 70	970	0.413	0.331	0.40061	0.32107
JT0104-JT0183	ACSR 70	210	0.413	0.331	0.08673	0.06951
JT0183-JT0093	ACSR 70	342	0.413	0.331	0.141246	0.113202
JT0093-JT0099	ACSR 95	585	0.2992	0.311	0.175032	0.181935
JT0093-JT0186	ACSR 70	500	0.413	0.331	0.2065	0.1655
JT0186-JT0189	ACSR 70	290	0.413	0.331	0.11977	0.09599
JT0189-JD144	ACSR 95	930	0.2992	0.311	0.278256	0.28923
JT0189-JT0064	ACSR 70	1100	0.413	0.331	0.4543	0.3641

JT0064-JT0061	ACSR 70	280	0.413	0.331	0.11564	0.09268
JT0064-JT0066	ACSR 70	180	0.413	0.331	0.07434	0.05958
JT0066-JT0083	ACSR 70	1500	0.413	0.331	0.6195	0.4965
JT0066-JT0067	ACSR 70	70	0.413	0.331	0.02891	0.02317
JT0067-JT0084	ACSR 70	980	0.413	0.331	0.40474	0.32438
JT0084-JT0210	ACSR 70	480	0.413	0.331	0.19824	0.15888
JT0084-JT0090	ACSR 70	530	0.413	0.331	0.21889	0.17543
JT0104-JT0111	ACSR 70	550	0.413	0.331	0.22715	0.18205
JT0111-JT0112	ACSR 70	85	0.413	0.331	0.035105	0.028135
JT0112-JT0121	ACSR 70	525	0.413	0.331	0.216825	0.173775
JT0121-JT0126	ACSR 70	551	0.413	0.331	0.227563	0.182381
JT0112-JT0120	ACSR 70	270	0.413	0.331	0.11151	0.08937
JT0120-JT0181	3*(1*50mm),36 KV,CU	295	0.387	0.203786	0.114165	0.06011687
JT0181-JT0180	3*(1*50mm),36 KV,CU	130	0.387	0.203786	0.05031	0.02649218
JT0180-JT0179	3*(1*50mm),36 KV,CU	480	0.387	0.203786	0.18576	0.09781728
JT0206-JT0048	ACSR 70	500	0.413	0.331	0.2065	0.1655
JT0048-JT0057	ACSR 70	940	0.413	0.331	0.38822	0.31114

JT0057-JT0058	ACSR 70	80	0.413	0.331	0.03304	0.02648
JT0057-JT0059	3*(1*50mm),36 KV,CU	200	0.387	0.203786	0.0774	0.0407572
JT0059-JT0204	3*(1*50mm),36 KV,CU	430	0.387	0.203786	0.16641	0.08762798
JT0204-JT0205	3*(1*50mm),36 KV,CU	630	0.387	0.203786	0.24381	0.12838518
JT0104-JT0100	ACSR 95	156	0.2992	0.311	0.0466752	0.048516
JT0093-JT0186	ACSR 70	500	0.413	0.331	0.2065	0.1655

Appendix 3

Transformers Name Plate Data

TR ID	Capacity	Impedance	Number of taps	Nominal Tap position	Load losses (KW)	No-load losses (KW)	No-load current (%)	Vector Croup
JD0056	630 KVA	5	5	3	5	1.15	0.429	DYN11
JD0142	630 KVA	4.5	7	4	5	1.15	0.429	DYN11
JD0144	630 KVA	4	7	5	5	1.15	0.429	DYN11
JD0138	400 KVA	5	5	2	4.2	0.78	0.44	DYN11
JD0139	400 KVA	5	5	2	4.2	0.78	0.44	DYN11
JD0052	400 KVA	4.5	5	4	4.2	0.78	0.44	DYN11
JD0005	400 KVA	4.5	5	4	4.2	0.78	0.44	DYN11
JD0007	400 KVA	4.5	5	3	4.2	0.78	0.44	DYN11
JD0008	400 KVA	4.5	5	2	4.2	0.78	0.44	DYN11
JD0003	400 KVA	4	7	4	4.2	0.78	0.44	DYN11
JD0010	400 KVA	4	7	4	4.2	0.78	0.44	DYN11
JD0019	400 KVA	4	7	4	4.2	0.78	0.44	DYN11
JD0053	400 KVA	4	6	2	4.2	0.78	0.44	DYN11
JD0020	250 KVA	5	7	4	3.2	0.52	0.44	DYN11
JD0192	250 KVA	5	7	4	3.2	0.52	0.44	DYN11
JD0013	250 KVA	4.5	7	4	3.2	0.52	0.44	DYN11
JD0191	250 KVA	4.5	7	4	3.2	0.52	0.44	DYN11
JD0001	250 kVA	4.5	5	3	3.2	0.52	0.44	DYN11
JD0002	250 KVA	4.5	5	3	3.2	0.52	0.44	DYN11
JD0054	250 KVA	4.5	5	3	3.2	0.52	0.44	DYN11

JD0141	250 KVA	4.5	5	3	3.2	0.52	0.44	DYN11
JD0180	250 kVA	4.5	5	3	3.2	0.52	0.44	DYN11
JD0009	250 KVA	4.5	3	2	3.2	0.52	0.44	DYN11
JD0012	250 KVA	4.5	3	2	3.2	0.52	0.44	DYN11
JD0011	250 KVA	4	7	3	3.2	0.52	0.44	DYN11
JD0015	250 KVA	4	7	3	3.2	0.52	0.44	DYN11

Appendix 4

Single Line Diagram (SLD) of Maithaloon Electrical Grid

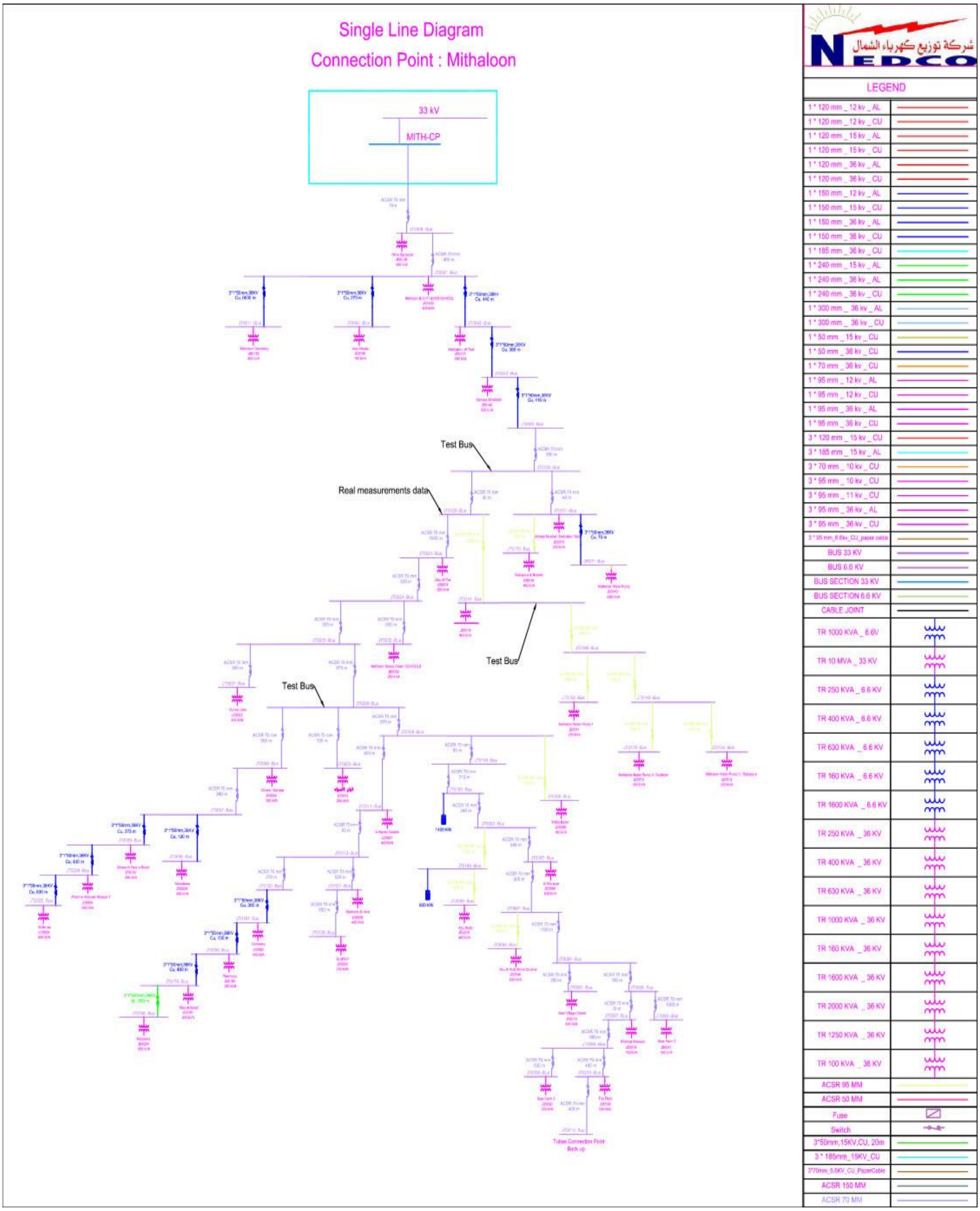

Appendix 5 : Solar Inverter 50 kWp Type Test

BUREAU VERITAS

Certificate of compliance

Applicant:	**KACO new energy GmbH** Carl-Zeiss-Straße 1 74172 Neckarsulm **Germany**
Product:	**Grid-tied photovoltaic (PV) inverter**
Model:	**KACO blueplanet 50.0 TL3 M1 WM OD IIGM** **KACO blueplanet 50.0 TL3 M1 WM OD IIGB** **KACO blueplanet 50.0 TL3 M1 WM OD IIGX** **KACO blueplanet 50.0 TL3 M1 WM OD FRGX** **KACO blueplanet 50.0 TL3 M1 WM OD IIGS**

Use in accordance with regulations:

Automatic disconnection device with three-phase mains surveillance in accordance with Engineering Recommendation G59/3 for photovoltaic systems with a three-phase parallel coupling via an inverter in the public mains supply. The automatic disconnection device is an integral part of the aforementioned inverter. This serves as a replacement for the disconnection device with isolating function that can access the distribution network provider at any time.

Applied rules and standards:

Engineering Recommendation G59/3:2014
Recommendation for the Connection of Generating Plant to the Distribution Systems of licensed Distribution Network Operators.

DIN V VDE V 0126-1-1:2006-02 (Functional safety)
Automatic disconnection device between a generator and the public low-voltage grid

The KACO blueplanet 50.0 TL3 M1 WM OD IIGM, KACO blueplanet 50.0 TL3 M1 WM OD IIGB, KACO blueplanet 50.0 TL3 M1 WM OD FRGX, KACO blueplanet 50.0 TL3 M1 WM OD IIGS and KACO blueplanet 50.0 TL3 M1 WM OD IIGX are rated >16A per phase and <= 50kW. The default values for "Small Power Stations" on the low-voltage grid were verified.

At the time of issue of this certificate the safety concept of an aforementioned representative product corresponds to the valid safety specifications for the specified use in accordance with regulations.

Report number:	**15TH0250-G59/3_2**
Certificate number:	**U18-0188**
Date of issue:	**2018-04-26**

Certification body

Holger Schaffer

DAkkS
Deutsche Akkreditierungsstelle
D-ZE-12024-01-00

Certification body of Bureau Veritas Consumer Products Services Germany GmbH
Accredited according to DIN EN ISO/IEC 17065

Annex to the G59/3 certificate of compliance No. U18-0188

Appendix 13.1 Type Testing a Generating Unit	
Extract from test report according the Engineering Recommendation G59/3	**Nr. 15TH0250**

Type Approval and declaration of compliance with the requirements of Engineering Recommendation G59/3.	
Manufacturer / applicant:	**KACO new energy GmbH** Carl-Zeiss-Straße 1 74172 Neckarsulm **Germany**
Generating Unit technology	**Grid-tied photovoltaic inverter**
Rated values	KACO blueplanet 50.0 TL3 M1 WM OD IIGM KACO blueplanet 50.0 TL3 M1 WM OD IIGB KACO blueplanet 50.0 TL3 M1 WM OD IIGX KACO blueplanet 50.0 TL3 M1 WM OD FRGX KACO blueplanet 50.0 TL3 M1 WM OD IIGS
Maximum rated capacity	50 kW
Rated voltage	400 V_{AC} (P-P) / 230 V_{AC} (3/PEN), 42-68 Hz
Firmware version	**PKT: V4.09; ARM: V5.08; CFG: V6.0572; DSP-AC: V4.09, DSP-DC: V4.02**
* The tests were performed with Firmwareversion V4.09. Changes in the Firmwareversion on position V4.x have no effect on the required electrical properties. x = could be any number or sign	
Measurement period:	**2017-09-04 to 2017-09-08**

Description of the structure of the power generation unit (Figure 1):

The input and output are protected by varistors to earth. The unit is providing EMC filtering at the output toward mains. The unit does not provide galvanic separation from input to output (transformer-less). The output is switched off redundant by the high power switching bridge and two relays in series. This assures that the opening of the output circuit will also operate in case of one error.

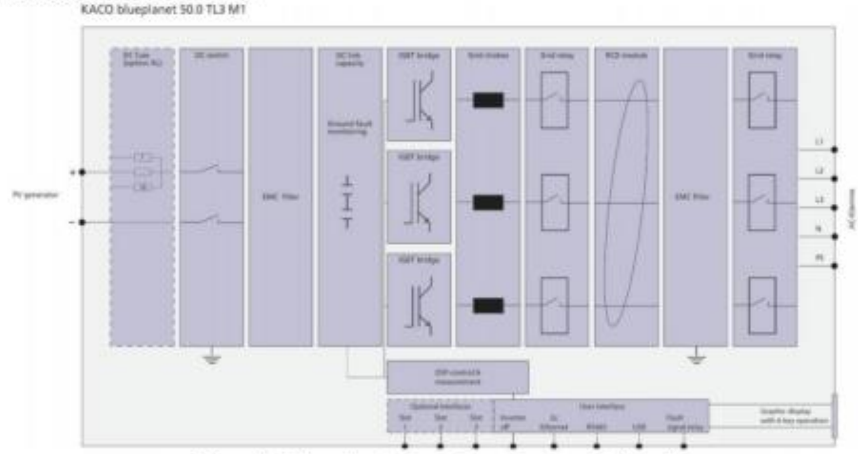

Figure 1 – Schematic structure of the power generation unit

The above stated Generating Units are tested according the requirements in the Engineering Recommendation G59/3. Any modification that affects the stated tests must be named by the manufacturer/supplier of the product to ensure that the product meets all requirements of the Engineering Recommendation G59/3.

Annex to the G59/3 certificate of compliance No. U18-0188

Appendix 13.1 Type Testing a Generating Unit

Extract from test report according the Engineering Recommendation G59/3 Nr. 15TH0250

Protection. Voltage tests.						
Phase 1						
Function	**Setting**		**Trip test**		**No trip test**	
	Voltage	**Time delay**	**Voltage**	**Time delay**	**Voltage / time**	**Confirm no trip**
U/V stage 1	200,1V	2,5s	200,3V	2,5551s	204,1V / 3,5s	No trip
U/V stage 2	184V	0,5s	184,3V	0,5559s	188V / 2,48s	No trip
					180V / 0,48s	No trip
O/V stage 1	262,2V	1,0s	261,8V	1,0561s	258,2V 2,0s	No trip
O/V stage 2	273,7V	0,5s	272,7V	0,6564s	269,7V 0,98s	No trip
					277,7V 0,48s	No trip

Protection. Voltage tests.						
Phase 2						
Function	**Setting**		**Trip test**		**No trip test**	
	Voltage	**Time delay**	**Voltage**	**Time delay**	**Voltage / time**	**Confirm no trip**
U/V stage 1	200,1V	2,5s	200,0V	2,5594	204,1V / 3,5s	No trip
U/V stage 2	184V	0,5s	184,4V	0,5589s	188V / 2,48s	No trip
					180V / 0,48s	No trip
O/V stage 1	262,2V	1,0s	262,7V	2,5589s	258,2V 2,0s	No trip
O/V stage 2	273,7V	0,5s	272,6V	0,5593s	269,7V 0,98s	No trip
					277,7V 0,48s	No trip

Annex to the G59/3 certificate of compliance No. U18-0188

Appendix 13.1 Type Testing a Generating Unit

Extract from test report according the Engineering Recommendation G59/3	Nr. 15TH0250

Protection. Voltage tests.						
Phase 3						
Function	Setting		Trip test		No trip test	
	Voltage	Time delay	Voltage	Time delay	Voltage / time	Confirm no trip
U/V stage 1	200,1V	2,5s	200,2V	2,5516s	204,1V / 3,5s	No trip
U/V stage 2	184V	0,5s	184,3V	0,5518s	188V / 2,48s	No trip
					180V / 0,48s	No trip
O/V stage 1	262,2V	1,0s	262,7V	2,5521s	258,2V 2,0s	No trip
O/V stage 2	273,7V	0,5s	272,5V	0,5515s	269,7V 0,98s	No trip
					277,7V 0,48s	No trip
Note. For Voltage tests the Voltage required to trip is the setting ±3,45V. The time delay can be measured at a larger deviation than the minimum required to operate the protection. The No trip tests need to be carried out at the setting ±4V and for the relevant times as shown in the table above to ensure that the protection will not trip in error.						

Protection. Frequency tests.						
Function	Setting		Trip test		No trip test	
	Frequency	Time delay	Frequency	Time delay	Frequency / time	Confirm no trip
U/F stage 1	47,5Hz	20s	47,49Hz	20,085s	47,7Hz / 25s	No trip
U/F stage 2	47Hz	0,5s	46,99Hz	0,582s	47,2Hz / 19,98s	No trip
					46,8Hz / 0,48s	No trip
O/F stage 1	51,5Hz	90s	51,51Hz	90,07s	51,3Hz / 95s	No trip
O/F stage 2	52Hz	0,5s	52,00Hz	0,575s	51,8Hz / 89,98s	No trip
					52,2Hz / 0,48s	No trip
Note. For Frequency Trip tests the Frequency required to trip is the setting ±0,1Hz. In order to measure the time delay a larger deviation than the minimum required to operate the projection can be used. The "No-trip tests" need to be carried out at the setting ±0,2Hz and for the relevant times as shown in the table above to ensure that the protection will not trip in error.						

Annex to the G59/3 certificate of compliance No. U18-0188

Appendix 13.1 Type Testing a Generating Unit

Extract from test report according the Engineering Recommendation G59/3 **Nr. 15TH0250**

Protection. Loss of Mains.						
Note as an alternative, inverters can be tested to BS EN 62116. The following sub set of tests should be recorded in the following table.						
Balancing load on islanded network	33% of -5% Q Test 22	66% of -5% Q Test 12	100% of -5% P Test 5	33% of +5% Q Test 31	66% of +5% Q Test 21	100% of +5% P Test 10
Trip time	211,6	210,3	601,6	235,5	229,9	363,4
Note for technologies which have a substantial shut down time this can be added to the 0,5 seconds in establishing that the trip occurred in less than 0,5s. Maximum shut down time could therefore be up to 1,0 seconds for these technologies.						
Indicate additional shut down time included in above results. (Integrated interface switch)				Type of switching equipment 1: Finder 67.23 with 35ms Type of switching equipment 2: Finder 67.23 with 35ms		
Note. All relays are direct coupled and open directly by receiving the islanding signal from the controller. Therefore the measured disconnection time on all phase is valid for three phases of the inverter.						

Annex to the G59/3 certificate of compliance No. U18-0188

Appendix 13.1 Type Testing a Generating Unit

Extract from test report according the Engineering Recommendation G59/3 **Nr. 15TH0250**

Protection. Re-connection timer.	
Test should prove that the reconnection sequence starts in no less than 20 seconds for restoration of voltage and frequency to within the stage 1 settings of table 10.5.7.1.	
Voltage	
Time delay setting	**Measured delay**
20s	81,0s
Frequency	
Time delay setting	**Measured delay**
20s	77,0s

	Checks on no reconnection when voltage or frequency is brought to just outside stage 1 limits of table 1.			
	At 266,2V	At 196,1V	At 47,4Hz	At 51,6Hz
Confirmation that the Generating Unit does not re-connect.	No reconnection	No reconnection	No reconnection	No reconnection

Protection. Frequency change, Stability test.				
	Start Frequency	**Change**	**End Frequency**	**Confirm no trip**
Positive Vector Shift	49,5Hz	+9 degrees		No trip
Negative Vector Shift	50,5Hz	- 9 degrees		No trip
Positive Frequency drift	49,5Hz	+0,19Hz/sec	51,5Hz	No trip
Negative Frequency drift	50,5Hz	-0,19Hz/sec	47,5Hz	No trip

Annex to the G59/3 certificate of compliance No. U18-0188

Appendix 13.1 Type Testing a Generating Unit

Extract from test report according the Engineering Recommendation G59/3 — Nr. 15TH0250

Power Quality. Harmonics.						
Phase 1						
Generating Unit tested to BS EN 61000-3-12						
Generating Unit rating per phase (rpp)						
	At 45-55% of rated ouput 25 kW		100% of rated output 50 kW			
Harmonic	Measured Value (MV) in Amps	Measured Value (MV) in %	Measured Value (MV) in Amps	Measured Value (MV) in %	Limit in BS EN61000-3-12 in %	
					1 phase	3 phase
2nd	0,162	0,223	0,270	0,370	8%	8%
3rd	0,151	0,207	0,112	0,154	21,6%	N/A
4th	0,089	0,122	0,101	0,139	4%	4%
5th	0,345	0,474	0,373	0,511	10,7%	10,7%
6th	0,044	0,060	0,064	0,088	2,67%	2,67%
7th	0,271	0,372	0,270	0,370	7,2%	7,2%
8th	0,026	0,036	0,039	0,054	2%	2%
9th	0,050	0,068	0,051	0,070	3,8%	N/A
10th	0,022	0,030	0,034	0,047	1,6%	1,6%
11th	0,201	0,276	0,185	0,254	3,1%	3,1%
12th	0,028	0,039	0,041	0,056	1,33%	1,33%
13th	0,195	0,267	0,187	0,257	2%	2%
14th	0,027	0,037	0,031	0,042	N/A	N/A
15th	0,028	0,038	0,034	0,047	N/A	N/A
16th	0,025	0,034	0,029	0,040	N/A	N/A
17th	0,180	0,247	0,147	0,202	N/A	N/A
18th	0,026	0,035	0,035	0,048	N/A	N/A
19th	0,201	0,276	0,171	0,235	N/A	N/A
20th	0,031	0,043	0,036	0,049	N/A	N/A
21th	0,030	0,042	0,037	0,051	N/A	N/A
22th	0,031	0,042	0,034	0,047	N/A	N/A
23th	0,208	0,286	0,146	0,201	N/A	N/A
24th	0,026	0,036	0,035	0,048	N/A	N/A
25th	0,220	0,302	0,170	0,233	N/A	N/A
26th	0,036	0,049	0,040	0,055	N/A	N/A
27th	0,035	0,048	0,046	0,063	N/A	N/A
28th	0,034	0,046	0,040	0,054	N/A	N/A
29th	0,230	0,316	0,158	0,217	N/A	N/A
30th	0,028	0,038	0,034	0,047	N/A	N/A
31th	0,231	0,317	0,147	0,201	N/A	N/A
32th	0,033	0,045	0,038	0,052	N/A	N/A
33th	0,032	0,044	0,043	0,059	N/A	N/A
34th	0,027	0,037	0,034	0,047	N/A	N/A
35th	0,194	0,267	0,112	0,154	N/A	N/A
36th	0,023	0,032	0,024	0,033	N/A	N/A
37th	0,160	0,220	0,089	0,123	N/A	N/A
38th	0,019	0,027	0,023	0,032	N/A	N/A
39th	0,021	0,029	0,029	0,040	N/A	N/A
40th	0,015	0,020	0,020	0,027	N/A	N/A
THD_{40}	2,28%		1,04%		23%	13%
PWHD	0,048%		0,006%		23%	22%

Annex to the G59/3 certificate of compliance No. U18-0188

Appendix 13.1 Type Testing a Generating Unit

Extract from test report according the Engineering Recommendation G59/3 — Nr. 15TH0250

Power Quality. Harmonics.						
Phase 2						
Generating Unit tested to BS EN 61000-3-12						
Generating Unit rating per phase (rpp)						
	At 45-55% of rated ouput 25 kW		100% of rated output 50 kW			
Harmonic	Measured Value (MV) in Amps	Measured Value (MV) in %	Measured Value (MV) in Amps	Measured Value (MV) in %	Limit in BS EN61000-3-12 in %	
					1 phase	3 phase
2nd	0,162	0,222	0,256	0,351	8%	8%
3rd	0,066	0,091	0,109	0,149	21,6%	N/A
4th	0,086	0,118	0,089	0,122	4%	4%
5th	0,336	0,461	0,365	0,499	10,7%	10,7%
6th	0,028	0,038	0,043	0,059	2,67%	2,67%
7th	0,241	0,330	0,239	0,328	7,2%	7,2%
8th	0,027	0,037	0,038	0,052	2%	2%
9th	0,040	0,055	0,051	0,070	3,8%	N/A
10th	0,022	0,031	0,033	0,045	1,6%	1,6%
11th	0,201	0,275	0,197	0,270	3,1%	3,1%
12th	0,021	0,029	0,023	0,031	1,33%	1,33%
13th	0,199	0,272	0,172	0,236	2%	2%
14th	0,023	0,031	0,029	0,040	N/A	N/A
15th	0,023	0,031	0,034	0,047	N/A	N/A
16th	0,019	0,026	0,028	0,039	N/A	N/A
17th	0,188	0,257	0,160	0,219	N/A	N/A
18th	0,030	0,041	0,027	0,036	N/A	N/A
19th	0,200	0,274	0,158	0,217	N/A	N/A
20th	0,024	0,033	0,031	0,043	N/A	N/A
21th	0,025	0,034	0,038	0,052	N/A	N/A
22th	0,023	0,031	0,030	0,041	N/A	N/A
23th	0,220	0,302	0,166	0,228	N/A	N/A
24th	0,038	0,052	0,037	0,051	N/A	N/A
25th	0,231	0,316	0,167	0,229	N/A	N/A
26th	0,027	0,037	0,035	0,048	N/A	N/A
27th	0,028	0,038	0,044	0,060	N/A	N/A
28th	0,029	0,040	0,034	0,047	N/A	N/A
29th	0,263	0,360	0,182	0,249	N/A	N/A
30th	0,039	0,054	0,039	0,054	N/A	N/A
31th	0,245	0,336	0,157	0,215	N/A	N/A
32th	0,026	0,036	0,030	0,041	N/A	N/A
33th	0,025	0,035	0,041	0,056	N/A	N/A
34th	0,025	0,034	0,027	0,037	N/A	N/A
35th	0,210	0,288	0,124	0,170	N/A	N/A
36th	0,027	0,037	0,027	0,036	N/A	N/A
37th	0,177	0,243	0,100	0,137	N/A	N/A
38th	0,018	0,024	0,020	0,027	N/A	N/A
39th	0,018	0,024	0,028	0,039	N/A	N/A
40th	0,015	0,020	0,017	0,023	N/A	N/A
THD_{40}	2,28%		1,03%		23%	13%
PWHD	0,055%		0,007%		23%	22%

Annex to the G59/3 certificate of compliance No. U18-0188

Appendix 13.1 Type Testing a Generating Unit

Extract from test report according the Engineering Recommendation G59/3 | Nr. 15TH0250

Power Quality. Harmonics.						
Phase 3						
Generating Unit tested to BS EN 61000-3-12						
Generating Unit rating per phase (rpp)						
	At 45-55% of rated ouput 25 kW		100% of rated output 50 kW			
Harmonic	Measured Value (MV) in Amps	Measured Value (MV) in %	Measured Value (MV) in Amps	Measured Value (MV) in %	Limit in BS EN61000-3-12 in %	
					1 phase	3 phase
2nd	0,270	0,370	0,162	0,223	8%	8%
3rd	0,112	0,154	0,151	0,207	21,6%	N/A
4th	0,101	0,139	0,089	0,122	4%	4%
5th	0,373	0,511	0,345	0,474	10,7%	10,7%
6th	0,064	0,088	0,044	0,060	2,67%	2,67%
7th	0,270	0,370	0,271	0,372	7,2%	7,2%
8th	0,039	0,054	0,026	0,036	2%	2%
9th	0,051	0,070	0,050	0,068	3,8%	N/A
10th	0,034	0,047	0,022	0,030	1,6%	1,6%
11th	0,185	0,254	0,201	0,276	3,1%	3,1%
12th	0,041	0,056	0,028	0,039	1,33%	1,33%
13th	0,187	0,257	0,195	0,267	2%	2%
14th	0,031	0,042	0,027	0,037	N/A	N/A
15th	0,034	0,047	0,028	0,038	N/A	N/A
16th	0,029	0,040	0,025	0,034	N/A	N/A
17th	0,147	0,202	0,180	0,247	N/A	N/A
18th	0,035	0,048	0,026	0,035	N/A	N/A
19th	0,171	0,235	0,201	0,276	N/A	N/A
20th	0,036	0,049	0,031	0,043	N/A	N/A
21th	0,037	0,051	0,030	0,042	N/A	N/A
22th	0,034	0,047	0,031	0,042	N/A	N/A
23th	0,146	0,201	0,208	0,286	N/A	N/A
24th	0,035	0,048	0,026	0,036	N/A	N/A
25th	0,170	0,233	0,220	0,302	N/A	N/A
26th	0,040	0,055	0,036	0,049	N/A	N/A
27th	0,046	0,063	0,035	0,048	N/A	N/A
28th	0,040	0,054	0,034	0,046	N/A	N/A
29th	0,158	0,217	0,230	0,316	N/A	N/A
30th	0,034	0,047	0,028	0,038	N/A	N/A
31th	0,147	0,201	0,231	0,317	N/A	N/A
32th	0,038	0,052	0,033	0,045	N/A	N/A
33th	0,043	0,059	0,032	0,044	N/A	N/A
34th	0,034	0,047	0,027	0,037	N/A	N/A
35th	0,112	0,154	0,194	0,267	N/A	N/A
36th	0,024	0,033	0,023	0,032	N/A	N/A
37th	0,089	0,123	0,160	0,220	N/A	N/A
38th	0,023	0,032	0,019	0,027	N/A	N/A
39th	0,029	0,040	0,021	0,029	N/A	N/A
40th	0,020	0,027	0,015	0,020	N/A	N/A
THD_{40}	2,28%		1,04%		23%	13%
PWHD	0,048%		0,006%		23%	22%

Annex to the G59/3 certificate of compliance No. U18-0188

Appendix 13.1 Type Testing a Generating Unit	
Extract from test report according the Engineering Recommendation G59/3	Nr. 15TH0250

Power Quality. Power factor.				
	216,2V	230V	253V	Measured at three voltage levels and at full output. Voltage to be maintained within ±1.5% of the stated level during the test.
Measured value	0,999	0,999	0,999	
Limit	>0,95	>0,95	>0,95	

Power Quality. Voltage fluctuation and Flicker.								
	Starting			Stopping			Running	
	dmax	dc	d(t)	dmax	dc	d(t)	Pst	Plt 2 hours
Measured values at test impedance	0,33%	3,3%	0,0%	0,33%	3,3%	0,0%	0,086	0,086
Limits set under BS EN 61000-3-11	4%	3,3%	3,3% 500ms	4%	3,3%	3,3% 500ms	1,0	0,65
Standard impedance	R	0,24* 0,4^	Ω	Xl	0,15* 0,25^	Ω		

Power Quality. DC injection.			
Test level power	10%	55%	100%
Recorded value	59,15 mA	71,52 mA	29,74 mA
As % of rated AC current	0,08 %	0,10%	0,04%
Limit	0,25%	0,25%	0,25%

Annex to the G59/3 certificate of compliance No. U18-0188

Appendix 13.1 Type Testing a Generating Unit

Extract from test report according the Engineering Recommendation G59/3	Nr. 15TH0250

Fault level Contribution.					
For a directly coupled SSEG			For a Inverter SSEG		
Parameter	Symbol	Value	Time after fault	Volts	Amps
Peak Short Circuit current	I_p	N/A	20ms	46,9	94,6
Initial Value of aperiodic current	A	N/A	100ms	47,0	96,8
Initial symmetrical short-circuit current*	I_k	N/A	250ms	47,2	96,7
Decaying (aperiodic) component of short circuit current*	i_{DC}	N/A	500ms	47,1	96,4
Reactance/Resistance Ratio of source*	X/R	N/A	Time to trip	0,555	In seconds
For rotating machines and linear piston machines the test should produce a 0s – 2s plot of the short circuit current as seen at the Generating Unit terminals. * Values for these parameters should be provided where the short circuit duration is sufficiently long to enable interpolation of the plot.					

Self Monitoring – Solid state switching.	N/A
It has been verified that in the event of the solid state switching device failing to disconnect the Generating Unit, the voltage on the output side of the switching device is reduced to a value below 50 volts within 0,5 seconds.	
Note. Unit do not provide solid state switching relays. In case the semiconductor bridge is switched off, then the voltage on the output drops to 0. In this case the relays on the output will also open.	

جامعة النجاح الوطنية

كلية الدراسات العليا

تصميم جهاز يعمل على تعويض تدفق وتحسين جودة الطاقة الكهربائية في شبكة الضغط المتوسط المزودة لميثلون – جنين- فلسطين

اعداد

براء ايمن دويكات

اشراف

د. كامل صالح

قدمت هذه الأطروحة استكمالا لمتطلبات الحصول على درجة الماجستير في هندسة القوى الكهربائية بكلية الدراسات العليا في جامعة النجاح الوطنية، نابلس - فلسطين

2020

تصميم جهاز يعمل على تعويض تدفق وتحسين جودة الطاقة الكهربائية في شبكة الضغط المتوسط المزودة لميثلون – جنين- فلسطين

اعداد

براء ايمن دويكات

اشراف

د. كامل صالح

الملخص

ابتدأ البحث بإنشاء نموذج محاكاة للشبكة الكهربائية المغذية لمنطقة ميثلون سيريس الجديدة وصير – جنين والقائمة ضمن منطقة امتياز شركة توزيع كهرباء الشمال – فلسطين، حيث لوحظ ان الشبكة الكهربائية تغذي العديد من الاحمال الكهربائية الغير خطية وتربط العديد من مصادر الطاقة المتجددة على خطوط الضغط المتوسط والمنخفض مما أثر الى انشاء توافقات كبيره على التيار في الشبكات الكهربائية.

في شبكات النقل والتوزيع، تؤدي التوافقيات الى احداث العديد من المشاكل مثل تشوه الفولتية، زيادة التيار مما يؤدي الى زيادة الفاقد الكهربائي والسخونة الزائدة وبالتالي فشل بعض المعدات المحولات والمكثفات والمحركات، علاوة على ذلك هذه التوافقيات تسبب في التداخل مع خطوط الاتصالات.

ولحل المشاكل المذكورة، يوجد العديد من الحلول وإحدى هذه الحلول تصميم جهاز التعويض الطاقي المتعدد الوظائف لمعالجة التوافقات ورفع مستويات الجهود في الشبكة وتقليل الفاقد الكهربائي. كما وتم ربط الجهاز في نموذج المحاكاة الذي تم انشاءه للشبكة الكهربائية حيث أحدث الجهاز نجاحا وتميزا في عمله وكانت النتائج من نموذج المحاكاة مميزة حيث تم تقليل التوافقات الى القيم المطلوبة عالميا وتقليل الخسائر الكهربائية.